ARMANDO FERNANDES DA VEIGA RODRIGUES

Transforming Iron Ore Processing – Simplifying the Comminution and Replacing Reverse Flotation with Magnetic and Gravity Separation

São Paulo
2024

ARMANDO FERNANDES DA VEIGA RODRIGUES

Corrected Version

Transforming Iron Ore Processing – Simplifying the Comminution and Replacing Reverse Flotation with Magnetic and Gravity Separation

Thesis presented to the Escola Politécnica of the Universidade de São Paulo to obtain the degree of Doctor of Science

Concentration area:
Mineral Engineering

Advisors:
Prof. Dr. Homero Delboni Jr
Prof. Dr. Kevin P. Galvin

São Paulo
2024

Este exemplar foi revisado e corrigido em relação à versão original, sob responsabilidade única do autor e com a anuência de seu orientador.

São Paulo,14 de junho de 2024

Assinatura do autor: _____

Assinatura do orientador: _____

Catalogação-na-publicação

Rodrigues, Armando Fernandes da Veiga
Transforming Iron Ore Processing – Simplifying the Comminution and Replacing Reverse Flotation with Magnetic and Gravity Separation / A. F. V. Rodrigues -- versão corr. -- São Paulo, 2024.
130 p.

Tese (Doutorado) - Escola Politécnica da Universidade de São Paulo. Departamento de Engenharia de Minas e de Petróleo.

1.Ferro (Brasil) 2.Processamento de minerais metálicos 3.Cominuição 4.Flotação de minérios 5.Reflux Classifier I.Universidade de São Paulo. Escola Politécnica. Departamento de Engenharia de Minas e de Petróleo II.t.

ACKNOWLEDGEMENTS

Firstly, I would like to thank Jesus Christ.

I also would like to acknowledge the following institutions and people for their contributions.

- Vale S. A. for sponsoring the work as well as for giving permission to publish it.

- The University of São Paulo for offering me a unique opportunity to conduct this doctorate at this worldwide known institution.

- My advisors, Prof. Homero Delboni Jr of University of São Paulo and Prof. Kevin P. Galvin of University of Newcastle for their great guidance. I sincerely appreciated their generous advice and corrections. I have learnt a lot with them.

- All colleagues of Vale for the great discussions about mineral processing.

- My father, mother, brother and all friends for providing the incentive for me to finish this doctorate.

- My daughter and my son to understand all moments that I was studying and wasn't with them.

- Lastly and not less important, I would like to thank my wife for loving and supporting me. I am eternally grateful.

GENERAL ABSTRACT

Much of the remaining iron ore resources in Brazil consist of low-grade itabirite ores. Accordingly, a typical beneficiation circuit includes three- or even four-staged crushing/screening plant, followed by grinding in a closed-circuit ball mill, desliming in hydrocyclones and final ore mineral concentration via multistage reverse flotation and thickening of the final product. With the need for decarbonisation in the iron and steelmaking industry, there is a growing demand for high grade iron ore concentrate at more than 67% Fe. In the context of declining ore grades, there is an increasing need for a more effective circuit for beneficiating the itabirite ore. A proposed flowsheet consisting of a primary crushing stage, SAG mill, primary concentration using a VPHGMS magnetic separator, and a final concentration stage using the Reflux Classifier was investigated.

This work assesses the potential suitability of autogenous (AG) and semi-autogenous (SAG) milling through an extensive pilot plant campaign carried out with itabirite iron ores and describes the findings from a comprehensive series of experiments using a Reflux Classifier demonstrating the technical feasibility of applying AG/SAG milling and the Reflux Classifier to process itabirite feeds.

The deduction of the underlying partition surface from relatively basic feed information on the Fe assays obtained as a function of the particle size provided confidence in the application of the partition surface to predict similar dense mineral separations, and stronger insights into the mechanisms responsible for the separation.

This work also demonstrated the significant reduction in energy consumption, and the potential for achieving high Fe grade of more than 67%, with high recovery, and in turn considerable process simplification. The new circuit would eliminate secondary to quaternary crushing, desliming stages, complex flotation circuits, product thickening and the flotation reagent plant. Further project assessments indicated an 8% smaller footprint, and CAPEX and OPEX reductions compared with the conventional circuit.

RESUMO GERAL

Grande parte dos recursos remanescentes de minério de ferro no Brasil consiste em minérios de itabirito de baixo teor. Assim, um circuito de beneficiamento típico inclui uma planta de britagem/peneiramento de três ou mesmo quatro estágios, seguida de moagem em moinho de bolas em circuito fechado, deslamagem em hidrociclones, concentração final do minério mineral por meio de flotação reversa em vários estágios e espessamento do produto final. Com a necessidade de descarbonização na indústria siderúrgica, há uma demanda crescente por concentrado de minério de ferro de alto teor com mais de 67% de Fe. No contexto do declínio do teor do minério, há uma necessidade crescente de um circuito mais eficaz para beneficiamento do minério de itabirito. Foi investigado um fluxograma proposto que consiste em um estágio de britagem primária, moinho SAG, concentração primária usando um separador magnético VPHGMS e um estágio de concentração final usando o Reflux Classifier.

Este trabalho avalia a adequação potencial da moagem autógena (AG) e semi-autógena (SAG) através de uma extensa campanha de planta piloto realizada com minérios de ferro itabirito e descreve os resultados de uma série abrangente de experimentos usando o Reflux Classifier demonstrando a viabilidade técnica de aplicando moagem AG/SAG e Reflux Classifier para processar o minério de itabirito.

A dedução da partição a partir de informações de alimentação relativamente básicas nos ensaios de Fe obtidos em função do tamanho das partículas proporcionou confiança na aplicação da equação para prever separações minerais e insights mais fortes sobre os mecanismos responsáveis pela separação gravimétrica.

Este trabalho demonstrou a redução significativa no consumo de energia e o potencial para alcançar um alto teor de Fe de mais de 67%, com alta recuperação O novo circuito eliminaria a britagem secundária à quaternária, estágios de deslamagem, circuitos complexos de flotação, espessamento de produto e planta de reagentes de flotação. Avaliações adicionais do projeto indicaram uma redução de 8% no footprint da usina e reduções de CAPEX e OPEX em comparação com o circuito convencional.

STRUCTURE OF THIS THESIS

This thesis presents a comprehensive investigation of the potential for applying a new iron ore processing circuit, incorporating direct investigations of the iron ore feed using AG/SAG milling, VPHGMS magnetic separator and the Reflux Classifier gravity separator as alternative technologies.

This thesis is composed of scientific articles and was organised following the sequence bellow:

- **Chapter 1: Introduction, problem presentation, hypothesis and objectives discussions.**

- **Chapter 2: Comparing strategies for grinding itabirite iron ores in autogenous and semi-autogenous pilot-scale mills.**
  Minerals Engineering 2021. 163, 106780.
  This paper describes the AG/SAG testing program.
  https://doi.org/10.1016/j.mineng.2021.106780

- **Chapter 3: Gravity separation of fine itabirite iron ore using the Reflux Classifier – Part I – Investigation of continuous steady state separations across a wide range of parameters.**
  Minerals Engineering 2023. 201, 108187
  This paper describes the Reflux Classifier testing program.
  https://doi.org/10.1016/j.mineng.2023.108187

- **Chapter 4: Gravity separation of fine itabirite iron ore using the Reflux Classifier – Part II – Establishing the underpinning partition surface**
  Minerals Engineering 2024. 210, 108641
  This paper provides a basis for applying the partition surface to a given feed to predict the separation performance.
  https://doi.org/10.1016/j.mineng.2024.108641

- **Chapter 5: Transforming Iron Ore Processing – Simplifying the Comminution and Replacing Reverse Flotation with Magnetic and Gravity Separation.**

  Minerals Engineering 2023. 199, 108112

  This paper describes tests results and research analyses of the entirely new process circuit covering the AG/SAG, VPHGMS and Reflux Classifier.

  https://doi.org/10.1016/j.mineng.2023.108112

- **Chapter 6: Conclusions of the four studies developed and the relationship with the research objectives.**

LIST OF FIGURES

LIST OF TABLES

CONTENTS

1. General Introduction

An important iron ore geological formation is the Iron Quadrangle, located in the State of Minas Gerais in Brazil. Typical lower grade iron ores are found in this region and are referred as itabirites, a metamorphic rock that consists basically of iron oxide (hematite and/or magnetite) and quartz.

Figure 1 shows an example of a typical industrial circuit flow sheet used for processing itabirite, consisting in four stages of crushing, the ore then passes through grinding and desliming to remove the ultrafine particles in preparation for flotation. Reverse cationic flotation is then used to remove the quartz. Amines are employed as quartz collectors, while gelatinized corn starch is used as an iron oxide depressant. High grade iron ore concentrates are obtained from flotation cells underflow, but at a low concentration of solids. Product thickening is therefore required ahead of the final dewatering stage.

Figure 1. Typical itabirite circuit

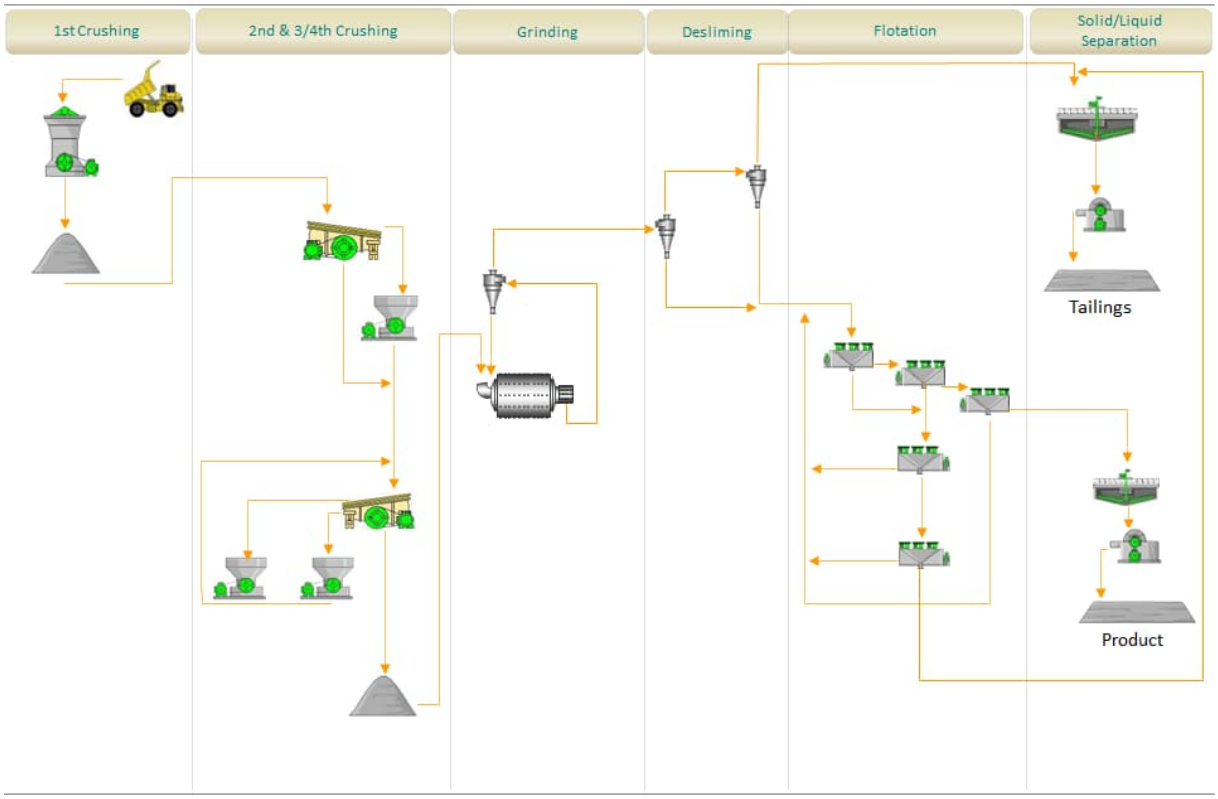

There is significant scope for simplifying the current comminution circuit flow sheets, by replacing part of the crushing and grinding operations with either fully autogenous (AG) or semi autogenous (SAG) mills. The use of these grinding technologies can lead to significant simplifications in the comminution circuit by removing altogether the secondary, tertiary and quaternary crushing stages.

Following the grinding, a single stage of magnetic separation in combination with a Reflux Classifier could be used to deliver the final concentrate. In this case there would be no need for the current two desliming stages, which usually involves hundreds of cyclones. The removal of flotation would exclude the use of chemicals, flotation cells, and product thickeners. Figure 2 shows the proposed novel itabirite processing circuit, consisting of a primary crushing stage, SAG milling, primary concentration using a VPHGMS magnetic separator, and a final concentration stage using the Reflux Classifier gravity separator.

Figure 2. Proposed novel itabirite circuit

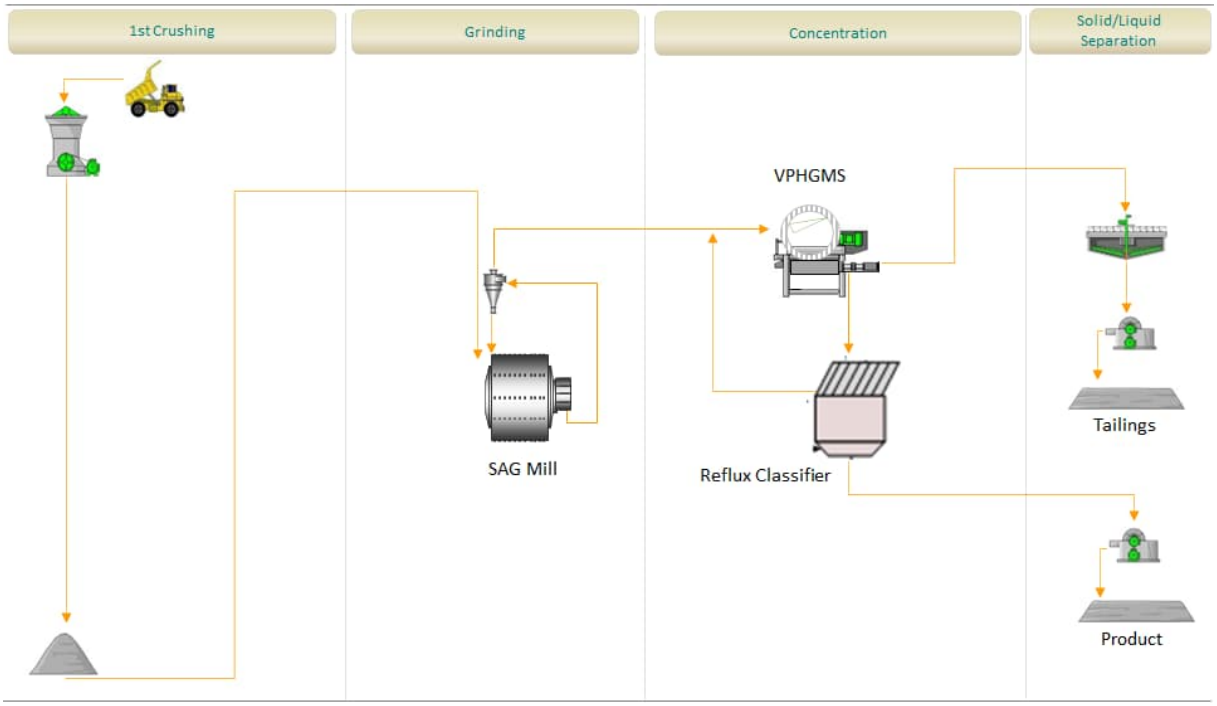

This study provides a comprehensive investigation of grinding carried out in a pilot-scale SAG/AG plant conducted with itabirite at different configurations and conditions. The study also provides an investigation of the gravity separation of the fine iron ore feed achieved by the Reflux Classifier, covering the effects of changes in the volumetric feed rate, bed density set point, feed pulp density, fluidization velocity, channel spacing and then the partition surface model was tested. A total of 21 SAG/AG pilot tests and 14 Reflux Classifier pilot tests were conducted.

In order to investigate new synergy between two physical separation technologies, a sample obtained from an existing industrial processing plant was tested in the VPHGMS magnetic separator, whose concentrate was further processed using the Reflux Classifier to achieve an even higher grade. This is the first investigation of the potential for applying this new circuit (Figure 2), incorporating direct investigations of the iron ore feed using these alternative technologies.

1.1. Hypothesis

- AG/SAG milling is a technically feasible alternative from the standpoint of energy efficiency, for grinding itabirites.

- Gravity separation can be used to replace reverse flotation, resulting in a significant reduction in the complexity, cost, and environmental impact of the beneficiation circuit.

- Applying the partition surface equation to a given feed predicts the separation performance.

- The novel and disruptive circuit, using SAG mill, VPHGMS and Reflux Classifier produces high grade pellet feed.

- The proposed itabirite processing circuit reduces the CAPEX and OPEX and increase the NPV compared with the conventional circuit.

1.2. Objectives

- Analyse the applicability of semi-autogenous and fully-autogenous grinding for itabirite ores from Brazil through pilot-scale milling tests.

- Examine the suitability of the Reflux Classifier for processing fine itabirite iron ore through pilot-scale concentration tests.

- Deduce the underlying partition surface from relatively basic feed information on the Fe assays obtained as a function of the particle size.

- Investigate the potential for applying a much simpler itabirite iron ore processing circuit, using SAG, VPHGMS and the Reflux Classifier.

2. Comparing strategies for grinding itabirite iron ores in autogenous and semi-autogenous pilot-scale mills[1]

[1]Rodrigues, A.F.V., Delboni Jr., H., Powell, M.S., Tavares, L.M., 2021. Miner. Eng. 163, 106780 https://doi.org/10.1016/j.mineng.2021.106780

2.1. Abstract

High grade iron ore resources are becoming depleted in Brazil, with relatively low-grade ores requiring more intensive comminution for proper liberation of iron minerals, followed by upgrading. Comminution circuits that have been frequently used in the Brazilian iron ore industry in preparation of high-grade iron ores consist of multiple crushing stages followed by ball milling and are known for being highly complex and capital-intensive installations. This work assesses the potential suitability of autogenous (AG) and semi-autogenous (SAG) milling through an extensive pilot plant campaign carried out with itabirite iron ores. The effects of ore type, feed size distribution, circuit configuration (open or closed-circuit and two-stage or single-stage), mode of grinding (AG or SAG), ball load, use of pebble crushing as well as of full secondary pre-crushing have been investigated. The results demonstrate both the technical feasibility and energy efficiency of such an alternative for itabirite comminution circuits.

2.2. Introduction

High-grade iron ores from Brazil were frequently processed via multistage crushing/screening followed by magnetic separation and flotation. Progressive depletion of high-grade iron ore reserves resulted in the need to process the lower grade iron ores. Typical lower grade iron ores are represented by itabirites, which are metamorphic banded-iron formations (Hagemann et al., 2016), and consist basically of iron oxide (predominantly hematite), with quartz as the main gangue mineral. Such dilution of the ore fed to the plant has demanded the inclusion of grinding stages to

liberate the valuable iron oxides from the gangue, typically to sizes below about 0.15 mm (Rodrigues, 2014; França et al., 2020).

Circuits that are currently in operation dealing with the low-grade itabirite ores rely typically on four crushing stages, followed by grinding in ball mills and concentration by flotation. This size reduction strategy requires several pieces of equipment, both for processing and handling the ore in several parallel lines for the case of high capacity plants, resulting in significant operating and capital costs (Segura-Salazar et al., 2018). Adoption of autogenous or semi-autogenous grinding (AG/SAG) would lead to a significant simplification alternative to such plants.

Within the scope of AG/SAG grinding, several approaches can be used in size reduction. For instance, the mill may be operated in the absence of steel grinding media (AG) or with steel balls (SAG) (Gupta and Yan, 2016). In the case of SAG operation, different ball fillings can be used (Napier-Munn et al., 1996). Circuits can operate in open circuit or in closed circuit with a classifier. Further, either SAG or AG mills can be operated in a stand-alone mode (single-stage) or coupled to a ball mill in FAB or SAB configurations (Gupta and Yan, 2016). The size distribution of the fresh feed as well as the ball size distribution are also known to have important effects in the process (Napier-Munn et al., 1996). Finally, more recently, the full secondary pre-crushing of the fresh feed to the mill has also been considered a valid alternative to improve throughput of SAG mills (Siddal and Putland, 2007).

Their low competence, with drop weight A*b indices of over 100, has led to some doubts regarding the suitability of itabirite ores to AG/SAG milling. However, the presence of different types of itabirites with different levels of competence results in a wide variability of competence in this type of ores (Rodrigues, 2014; França et al., 2020), which may provide sufficient competent material to build up a suitable rock charge in the mill, thus allowing successful AG/SAG milling. An example is magnetite iron ore with a bulk A*b of over 100, but an A*b of 37 for the waste silica content that is successfully milled in AG mode in Sweden by LKAB mines (Bueno et al., 2011a).

In spite of the important advances in modelling and simulation of autogenous and semi-autogenous grinding made in recent decades (Napier-Munn et al., 1996; Morrell, 2004), risks exist in designing a circuit adopting AG/SAG mills for low-grade itabirite iron ores from bench-scale information. This is especially due to the multi-component nature of the ores, as addressed in modelling and test work of Bueno et al. (2011b, 2012). As such, pilot-plant testing remains a valid method to gain insights into the use of this alternative in size reduction for ores with which only limited experience exists with the technology. The present work investigates several variables that influence the performance of AG/SAG grinding through experiments conducted at a pilot-scale. Different ore types, feed size distributions, modes of operation (open/closed circuit, AG/SAG, single/two-stage), ball loads and size distributions, as well as the use of secondary pre-crushing or pebble crushing have been investigated, with the aim of assessing the effect of the various variables as well as the technical feasibility of processing such low-grade ores in AG/SAG mills.

2.3. Experimental

2.3.1. Ore samples

Samples of four ore types were collected from the Run-of-Mine product of three Brazilian mines operated by Vale and located in the Iron Quadrangle of the state of Minas Gerais: Galinheiro (GAL), Sapecado (SAP) and Jangada (JAN). In the case of Galinheiro mine, two samples were collected, named GAL-IC and GAL-IF, the former presenting a coarser particle size distribution and, supposedly, also a more compact itabirite, than the latter which is known as friable. Figure 3 shows images of typical itabirites at the mine sites, thus demonstrating the widely different competences of the ore types. Samples containing a total of 625 tons were collected for both bench-scale and pilot plant tests.

Figure 3. Images of itabirites at the mine site during sample collection (modified from Rodrigues, 2014)

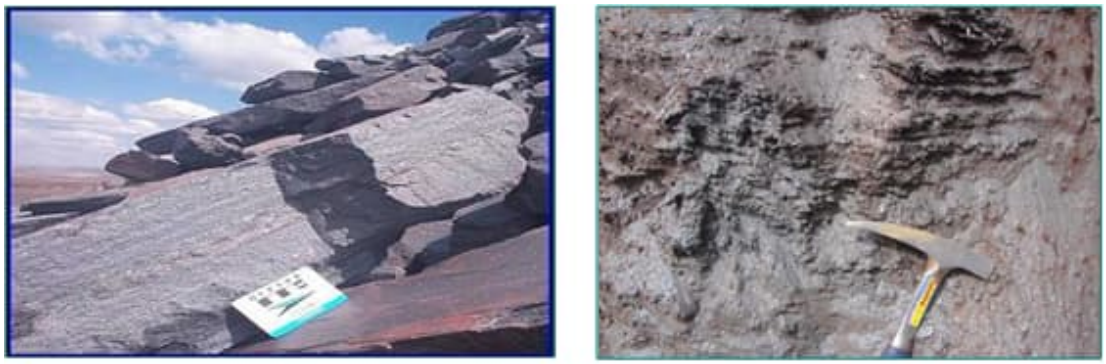

2.3.2. Bench-scale tests

Comminution properties for all samples were determined according to the Bond ball mill work index (BWi), Bond crushability work index (CWi), JK Drop Weight Tests (DWT) and JK Abrasion testing (Napier-Munn et al. 1996). The BWi was determined following the standard test, using a closing sieve of 150 µm.

The DWT consists of dropping a weight under gravity to crush individual particles placed on a steel anvil (Napier-Munn et al., 1996). Important parameters extracted from the DWT are the tn values where t is defined as the percentage passing each nth fraction of the original particle size. The value of tn that is more often used is t10 which can be described as the percentage passing in one tenth of the original particle size. The breakage index (t10) is related to the specific comminution energy as follows:

$$t_{10} = A\,(1 - e^{-b\,\mathrm{Ecs}}) \qquad (1)$$

where Ecs is specific comminution energy (kWh/t), t10 is the percentage passing 1/10th of the initial mean particle size tested and A and b are ore impact breakage parameters. The product A*b is regarded as an index of the amenability of the ore to breakage by impact.

2.3.3. Pilot-scale tests

The pilot plant process equipment consisted of a 1.83 m diameter by 0.61 m length SAG/AG mill, a pebble crusher, two spiral classifiers and a 0.91 m diameter by 1.22 m length ball mill. Two circuit configurations were adopted in pilot plant testing as shown in Figure 4. For the single-stage (SS) configuration the AG/SAG mill operated in a closed circuit with a spiral classifier, so that the product was nominally below 0.4 mm. The two-stage configuration included AG/SAG milling with optional pebble crushing followed by ball milling, the latter in a closed mode with a spiral (screw) classifier. The coupling of the SAG or AG mill with ball milling is known as SAB (C) or FAB (C) circuit respectively, where C denotes the use or not of pebble crushing. A total of 21 SAG/AG tests, four of which included ball milling, were conducted at different configurations and conditions. Figure 5 shows the pilot-scale AG/SAG mill configurations, and Table 1 summarizes the apertures of grates, pebble ports and trommel used in the tests. It is worth mentioning that there were no open pebble ports in most tests.

Figure 4. Circuit configurations adopted in the pilot-scale tests

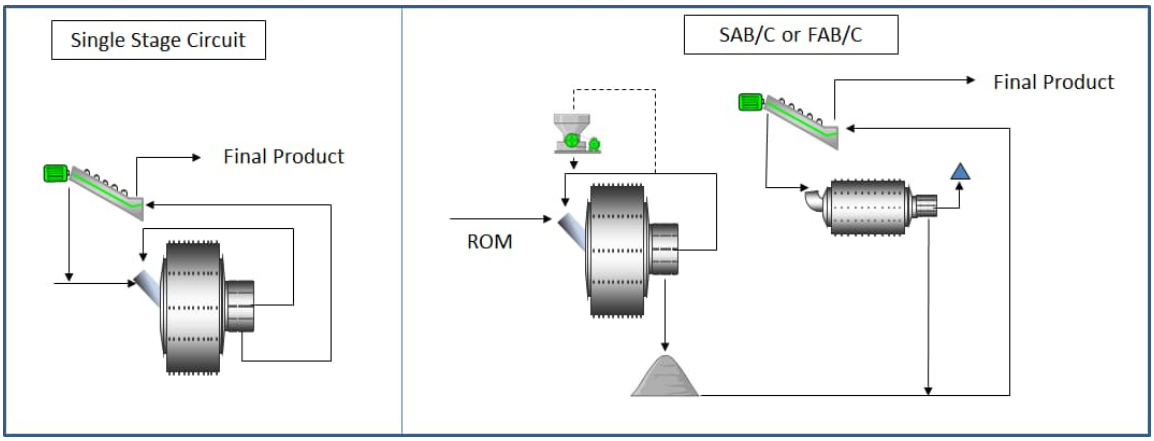

Figure 5. Overview of the pilot SAG mill, with the spiral classifier on the left (Rodrigues, 2014)

Table 1. Apertures of grates, pebble ports and trommel

Feature	Aperture (mm)
Grate	12–14
Pebble ports	63.5 x 63.5
Trommel	12.7

The ball size distribution used in the SAG mill tests is presented in Table 2. The one designated as “standard” was used in nearly all SAG tests, whereas the one identified as “finer” was used for a particular test involving the JAN sample.

Table 2. Ball size distributions used in the SAG mill tests (percent in weight)

Ball size	% retained	
(mm)	Standard	Finer
101.6	50	12
88.9	32	17
76.2	18	18
63.5	-	24
50.8	-	29

The system adopted for feeding the AG/SAG mill consisted initially in screening the ROM feed size distributions, separating into five individual size fractions: -203+152 mm; -152+76.2 mm; -76.2+25.4 mm; -25.4+12.7 mm and -12.7 mm. The weight of each size fraction was calculated in order to reconstitute 100 kg sub-samples according to a predefined size distribution. The sub-samples containing 100 kg were prepared using wheelbarrows and a platform scale. The contents of each wheelbarrow were then discharged onto the ground for shovelling on the SAG/AG mill fresh feed conveyor belt. The rate of ore addition was dictated by the need to maintain the mill at a constant total weight, which was measured by the loadcell mountings and shown on a large display in the pilot plant area. In order to shorten the period required to stabilise the mill, the desired weight of ore was loaded into the mill prior to each test. This procedure was successful in maintaining the mill charge volume within a narrow range for all tests. Mill power was measured during the tests and the mean power during steady-state operation recorded.

Stability of the circuit operation was assessed by monitoring variables such as mill feed rate and power draw. After a period of steady-state operation, ranging from 2 to 7 hours, sampling started. In order to reduce the stabilization period for some tests, a blend of new and conditioned charge from previous tests with the same ore was loaded into the mill at start-up. Sampling increments were collected throughout the duration of the test for each stream selected. At the end of each test the entire mill charge was emptied and both the ball and the rock charges were carefully screened. All data from the tests were mass-balanced. Percentage of solids in the feed to the AG/SAG mill was maintained at 78 ± 2% (w/w) in all tests.

Different feed size distributions were prepared. Besides the Run-of-Mine (ROM) size distribution, which emulated the product of primary crushing, in the case of JAN, a finer size distribution was prepared for testing, whereas in the case of GAL-IC, a coarser size distribution was prepared, by controlling the proportions of the different size fractions contained in the tested sample. This was carried out in order to isolate the effects of feed size distribution and ore competence in the tests. In addition, in the case of JAN, an additional feed was prepared, emulating the application of secondary

crushing of the feed, so that the sample contained a top size of 102 mm, which contrasts with the 203 mm of the primary crusher product.

More detail on the experimental procedures may be found in the thesis of Rodrigues (2014).

2.4. Results and Discussion

2.4.1. Feed ore characteristics

Table 3 presents the chemical assays, which confirm that grades were reasonably low in comparison to richer Brazilian iron ores, being in the range from 42 to 50% Fe. Figure 6 shows the particle size distribution of the Run-of-Mine samples, as well as additional feeds prepared for the pilot-scale tests. The Figure 6 shows that the ROM size distributions varied significantly for the different ores, with GAL-IF, GAL-IC and SAP presenting bimodal size distributions, shown by the ‘steps’ in the size distribution, with a significant proportion of already fine material contained in the feed, in the range of 40 – 60% finer than 150 µm. On the other hand, JAN sample presented a smoother size distribution which is more typical of the feed to SAG mills in hard rock applications (Napier-Munn et al., 1996).

Table 3. Sample assays

Sample	Fe (%)	SiO_2 (%)
GAL–IF	47.4	29.5
GAL–IC	42.2	37.9
SAP	46.4	33.1
JAN	49.8	26.4

Figure 6. Particle size distributions (PSD) of the samples of the feed to the pilot-scale tests. Solid lines represent the “as received” samples, whereas the dashed lines represent size distributions that were prepared for particular pilot-scale tests

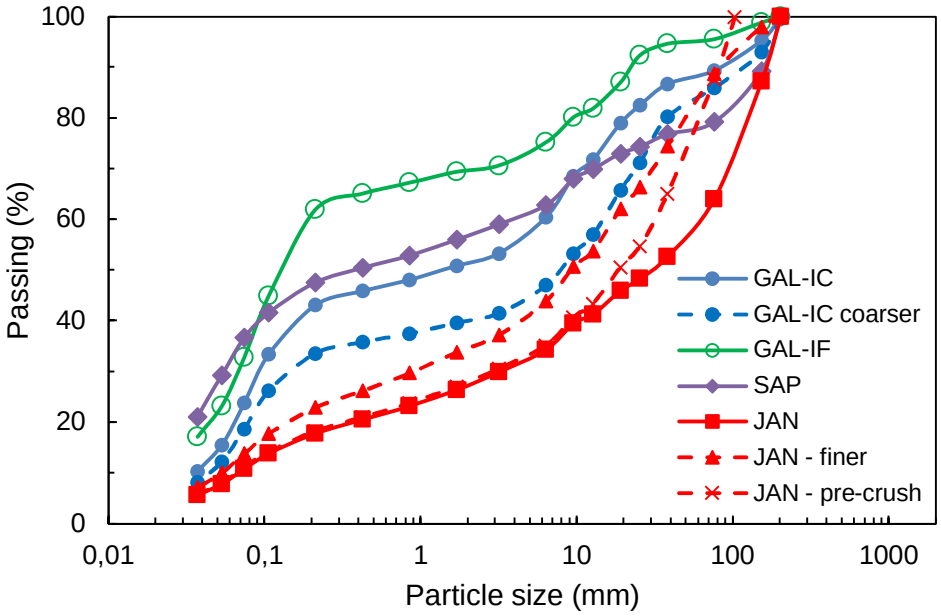

Table 4 summarizes results of the bench scale tests. Values of A*b and ta for the ores studied are also strongly correlated, as commonly observed for other ores (Napier-Munn et al., 1996; Tavares and Silveira, 2008). Apart from JAN, all other samples may be classified as very soft, when values of the A*b breakage index are considered (Napier-Munn et al., 1996). Also, values of crushing work index (CWi) increased inversely with the A*b breakage index, as commonly observed (Napier-Munn et al., 1996; Tavares and Silveira, 2008).

In order to demonstrate the exceptionally low competence of these ores in comparison to those usually subjected to SAG/AG milling, data from Table 4 has been plotted in the diagram proposed by Bueno and Lane (2011), which originally consisted of sets of A*b (DWT) and BWi from 134 SAG/AG pilot plant tested samples. Figure 7 compares the original results from that work to the results of the four itabirite samples, indicating that the latter are much softer than any of the former as described in the figure.

Table 4. Summary of bench scale test results

Sample	JK Abrasion t_a	JK DWT			Bond crushing CWi (kWh/t)	Bond Ball mill BWi (kWh/t)*
		A	b	A*b		
GAL-IF	4.21	63.1	5.86	370	4.1	6.5
GAL-IC	3.42	58.8	4.51	265	6.4	6.2
SAP	2.04	56.7	3.06	174	9.6	7.7
JAN	0.55	38.8	1.40	54.2	15.5	10.8

* Calculated for 150 µm

Figure 7. Values of BWi and A*b from 134 tests in pilot-scale AG/SAG mill (Bueno and Lane, 2011) showing the region of Itabirite ore samples from the present work is off the scales of the data base of ores.

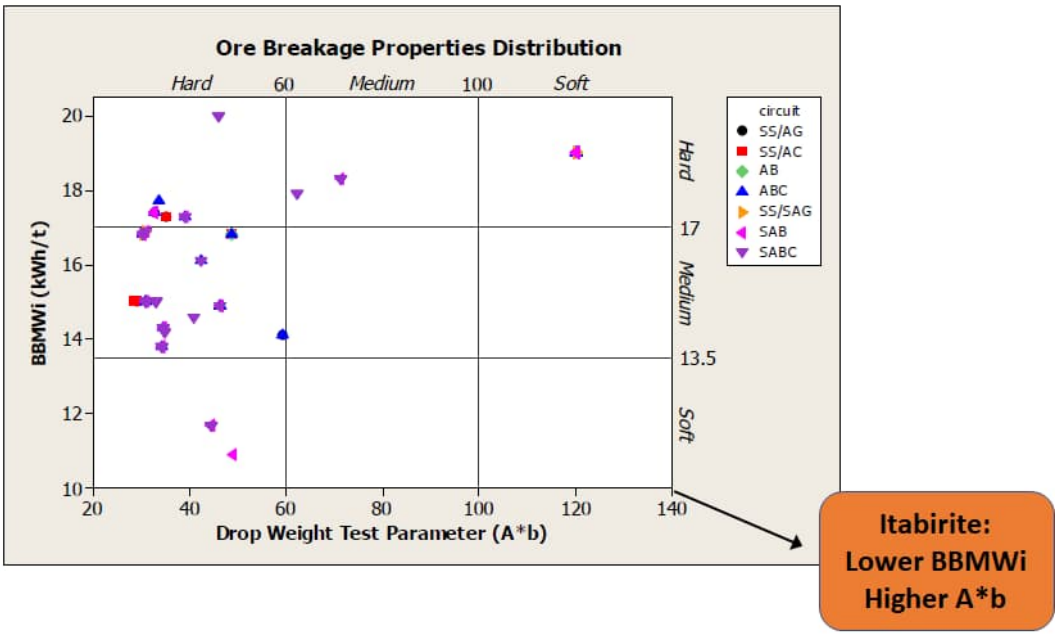

2.4.2. Pilot-scale trial results

2.4.2.1. Effect of ore type

Typical results from the tests are presented in Figure 8, which shows the size distributions of the various product streams measured in a particular test. It is evident that in closed-circuit operation the return of the oversize (coarse product) from the

screw classifier is responsible for a less bimodal feed size distribution to the mill relative to the fresh feed, shown by the smother size distribution.

Figure 8. Size distributions from SAG test with GAL-IC in closed-circuit mode

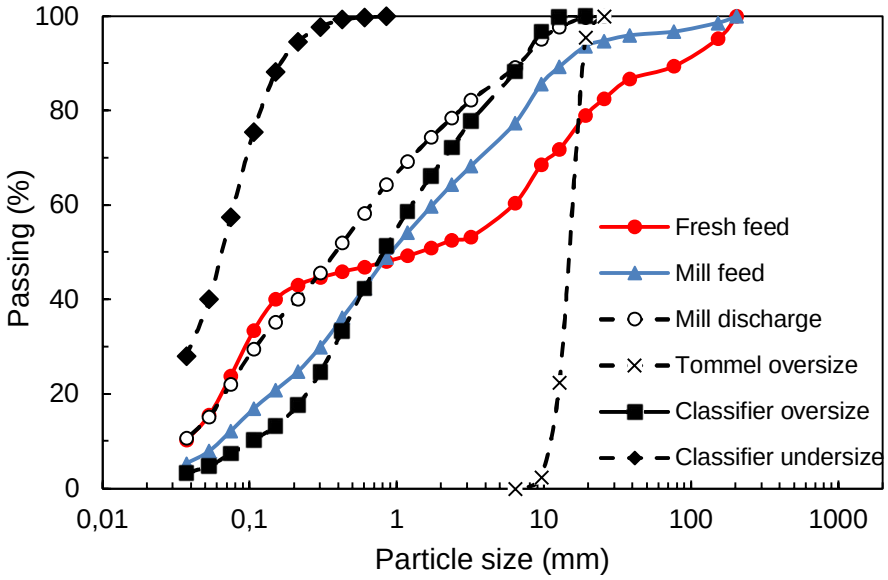

Table 5 presents results from tests for the four itabirite ore types that are the object of the present work. The tests have been conducted under the same conditions, namely in single-stage (SS) SAG mode, with 4% ball charge, with the mill total filling varying from 21.4 to 26.6%, and the mill operating in closed circuit with the spiral classifier. It shows that product fineness was relatively consistent, whereas feed rates and specific energies varied an order of magnitude from the test with the softest (GAL-IF) to the toughest (JAN) ore sample. Given this variation, which is partially due to the significant differences in feed size distribution (Figure 6), results from the tests have been analysed on the basis of two indices, namely the size-specific energy and the fSAG. First, the size-specific energy (SSE) (Ballantyne et al., 2015) is given by

$$SSE = \frac{100 * SE}{\%\ <\ 75\ \mu\text{m in product} - \%\ <\ 75\ \mu\text{m in feed}} \quad (2)$$

where SE is the specific milling energy, given in kWh/t.

The SSE was used throughout the present work to assess the AG/SAG milling tests, being a useful index of grindability. In addition, results have also been analysed on the basis of the fSAG (Siddall et al., 1996; Bueno and Lane 2011), which is given by

$$fSAG = \frac{\text{SAG circuit specific energy}}{\text{Bond crushing-ball milling circuit specific energy}} \quad (3)$$

where the SAG circuit specific energy is given by the sum of the energy in the SAG/AG pilot mill, added to the ball mill and the crusher specific energies (when applicable). Whereas the ball mill energy was measured in the pilot plant, the crusher energy (either secondary or pebble) was estimated on the basis of the Bond model and the Bond crushing work index (Table 4) (Bueno and Lane, 2011). The crushing-ball milling circuit specific energy was estimated on the basis of the Bond equation and the relevant Bond work indices (Table 4), with the crushing energy given from the SAG/AG F_{80} to a nominal product with P_{80} of 8.0 mm being added to the ball mill energy from F_{80} of 8.0 mm to the actual P_{80} of the pilot test, given either by the SAG/AG or the ball mill, depending on the circuit configuration (Figure 4). No correction factors were used in the Bond equation, so that these may be regarded only as a rough estimate, valid for comparative purposes.

Table 5 shows that GAL-IF and SAP demanded the lowest energy per tonne of fine (–75 µm) material, GAL-IC demanded about 1 kWh/t more, whereas JAN demanded more than four times that amount to produce the same tonnage of fine material. These results are in qualitative agreement with results from both A*b of the JKDWT and ta values from the JK abrasion test (Table 4). The value of fSAG was significantly lower for the tests with the three softer materials, suggesting that the energy demanded in size reduction using the SAG mill would be significantly lower than that estimated for the traditional crushing-ball milling circuit when used in the same task. The value of fSAG above one in the case of JAN demonstrates the challenge in the SAG mill operating with such a tough ore.

Table 5. Effect of feed ore in closed-circuit single-stage (SS) SAG operation

Sample	Feed		Product		Fresh feed rate (t/h)	Specific energy (kWh/t)	SSE (kWh/t –75 µm)	fSAG (-)
	–75 µm (%)	F_{80} (µm)	–75 µm (%)	P_{80} (µm)				
GAL-IF	32.8	9,449	55.5	128	8.39	1.41	6.2	0.28
GAL-IC	23.8	20,708	57.5	121	5.48	2.49	7.4	0.48
SAP	36.7	80,798	77.6	82	5.40	2.61	6.4	0.31
JAN	10.8	125,637	70.9	95	0.93	13.60	22.6	1.22

2.4.2.2. Effect of feed size distribution and mode of circuit operation

Due to the large variations in particle size distribution (PSD) of samples, it was decided to prepare additional PSDs for selected samples (Figure 6) in order to assess the influence of feed size distribution on SAG milling. Table 6 summarizes the results for tests conducted in two different configurations, that is, open and closed circuit, for GAL-IC and JAN ores.

It is observed that the throughput increased as the PSD of the feed became finer in all tests. In the case of GAL-IC sample the SAG mill open circuit throughput obtained for the coarser PSD was 38% lower than the figure observed for the finer PSD. Accordingly, the throughput reduction resulted in 17% increase in SSE, from 6.5 to 7.6 kWh/t–75 µm. The same occurred with the JAN sample i.e. the SAG mill circuit throughput obtained for the coarser PSD was 30% lower than the figure observed for the finer PSD. Accordingly, in this case the throughput reduction resulted in 13% increase in SSE. All these results were obtained for SAG milling open circuit configuration. The finer feed size distribution for the GAL-IC ore resulted in almost halving the fSAG index, thus demonstrating an improved advantage in comparison to the traditional crushing-ball milling circuit.

Table 6 also shows the SAG milling results obtained for samples GAL-IC but in this case in closed-circuit configuration. Here too the SAG mill circuit throughput was reduced as PSD was changed from fine to a coarser sample. The reduction was thus 25% which is smaller than the 38% figure obtained for the open circuit configuration. Interestingly, the change in SSE and fSAG were also smaller than for the open circuit, indicating that the variation of the feed PSD has a higher influence in open-circuit than in closed-circuit operation for the ore in question.

A comparison between open and closed-circuit operation is also possible by examining Table 6 for GAL-IC. Evidently, closed-circuit operation resulted in significant reduction in circuit throughput, while producing much greater proportion of fines in the product. Comparisons normalizing the results on the basis of fineness of the product suggest that the SSE either increased marginally (GAL-IC fine sample) ore was unaffected by mode of operation (GAL-IC coarse sample).

Table 6. Effect of feed size distribution and type of circuit in single-stage SAG milling (open/closed)

Sample	Circuit	Feed		Product		Fresh feed rate (t/h)	SSE (kWh/t – 75 µm)	fSAG (-)
		–75 µm (%)	F_{80} (µm)	–75 µm (%)	P_{80} (µm)			
JAN fine	Open	13.8	44,216	40.1	1,570	2.09	23.4	2.45
JAN		10.8	125,637	40.6	1,308	1.46	26.9	2.60
GAL-IC	Open	23.8	20,708	41.7	714	11.87	6.5	0.61
Coarser		18.7	37,777	43.3	985	7.34	7.6	1.12
GAL-IC	Closed	23.8	20,708	57.5	121	5.48	7.4	0.48
Coarser		18.7	37,777	62.1	108	4.13	7.7	0.59

Figure 9 shows photographs taken from the charge upon crash-stopping the SAG mill. The relatively dry charge obtained for the mill when operating in open circuit contrasts with the slurry pooling conditions observed for the closed circuit (single-stage) operation. The presence of the slurry pool could have been a result of a small delay in stopping the recirculating flow or/and the pulp flowrate exceeded the capacity of the

mill to remove the pulp. The incapacity of the mill to remove the pulp would have been responsible, at least in part, for the higher SSE in the closed-circuit operation. Thus, the design of grate profile and pulp lifters must be carefully addressed in the case of single-stage industrial operations.

Figure 9. Typical mill loads as observed in pilot scale tests: open circuit (left) and closed-circuit (right) SAG operation (modified from Rodrigues, 2014)

2.4.2.3. Effect of mode of mill operation (SAG or AG) and ball load

Additional tests were carried out to compare SAG and AG milling, the former with 4% steel ball load. The comparative tests comprised both operation in open and closed circuit, as well as in single- and two-stage configurations. In this case the coarser PSDs from GAL-IC and JAN were used, together with a GAL-IF as a third sample. Tables 7 and 8 show the summary of the results.

Table 7 and Table 8 show that AG operation resulted in lower throughput than SAG milling. The largest reduction in throughput in AG milling (45%) was observed for the softest ore (GAL-IF) operating in closed circuit, which could be explained by the inability of the ore to perform as autogenous grinding media, given its fineness (Figure 6) and low competence (Table 4). This was also the ore associated with the largest increase in SSE. This points to the need to blend in a more competent component if

this were to be milled autogenously, as successfully trialled for an incompetent ore by Powell et al (2019). With the exception of JAN (Table 8), AG operation resulted in much larger production of fines (Table 7) than SAG milling and has the added benefit of not requiring the use of steel grinding media. In single-stage operation the fSAG increased from SAG to AG mode, further confirming the smaller attractiveness of the autogenous mode of operation in terms of energy demand.

Table 7. Effect of AG/SAG mode for selected samples

Sample	Circuit	Feed		Product		Fresh feed rate (t/h)	SSE (kWh/t – 75 µm)	fSAG (-)
		–75 µm (%)	F_{80} (µm)	–75 µm (%)	P_{80} (µm)			
GAL-IC	SAG	18.7	37,777	43.3	985	7.34	7.6	1.12
	AG	18.7	37,777	48.6	374	4.65	9.4	0.97
	SAG*	18.7	37,777	62.1	108	4.13	7.7	0.59
	AG*	18.7	37,777	68.4	94	3.00	8.9	0.73
GAL-IF	SAG*	32.8	9,449	55.5	128	8.39	6.2	0.28
	AG*	32.8	9,449	67.0	99	4.60	8.0	0.47

* Single-stage (SS) operation

The influence of ball load on SAG milling performance was also evaluated. Table 8 shows the summary of open-circuit SAG milling tests for JAN ore with 0%, 4% and 16% ball charge. It shows the increase, although modest, of mill throughput with ball load. It also shows that operation with the 4% ball load led to the most energy-efficient operation, as evidenced by the lower SSE and fSAG values, thus demonstrating that the modest increase in capacity using higher ball loads for this particular ore occurs at the expense of significant reduction in energy efficiency.

Table 8. Effect of ball load for JAN sample in open-circuit grinding

% Balls	Feed		Product		Fresh feed rate (t/h)	Specific energy (kWh/t)	SSE (kWh/t – 75 µm)	fSAG (-)
	–75 µm (%)	F_{80} (µm)	–75 µm (%)	P_{80} (µm)				
0	10.8	125,637	41.0	1,152	1.21	8.61	28.5	2.63
4	10.8	125,637	40.6	1,308	1.46	8.00	26.8	2.60
16	10.8	125,637	36.3	1,703	1.52	9.28	36.4	3.43

2.4.2.4. Effect of number of grinding stages

Operation of the AG/SAG mill in single-stage and two-stage mode was then compared, both in closed-circuit operation. The two-stage circuit was configured as SAG/AG grinding followed by ball milling (SAB or FAB) (Figure 4). These comparisons have been made for GAL-IC with a coarser PSD sample (Figure 6) and results are summarized in Table 9.

Two-stage circuits presented consistently higher throughput than single-stage, which is not a surprise, given the higher installed power. Indeed, SAB mill circuit throughput was 78% greater than the figure observed for single-stage SAG milling. Besides the throughput increase, SSE and fSAG demonstrate the lower energy efficiency of the two-stage circuits, which is associated to the large power demanded in ball milling. The same occurred with AG milling i.e. AB mill circuit throughput was 53% greater than the figure observed for AGSS milling. Here too, all grinding parameters showed a reduction in the efficiency of the two-stage circuits.

The amount of material finer than 10µm in the product, namely slimes, is one of the critical issues when dealing with Itabirite grinding. Prior to flotation the ore needs to be deslimed, since the presence of such fines would negatively impact flotation performance. Comparing the two-stage to the single-stage circuits, no clear pattern was identified in terms of generation of this material. This demonstrates that slimes

generation would not be a relevant criterion for selection either circuit confirmation, at least for the ore in question.

Table 9. Effect of double/single stage in closed-circuit grinding of sample GAL-IC*

Primary/ Secondary mill	Final Product			Fresh feed rate (t/h)	Specific energy (kWh/t)		SSE (kWh/t –75 µm)	fSAG (-)
	P_{80} (µm)	75 µm (%)	10 µm (%)		SAG/AG	Ball mill		
SAG/Ball	102	63.0	6.4	7.34	1.87	3.56	12.3	0.93
SAG/ -	108	62.1	6.7	4.13	3.34	-	7.7	0.59
AG/Ball	97	67.2	7.9	4.65	2.81	3.58	13.2	1.07
AG/ -	94	68.4	7.4	3.00	4.44	-	8.9	0.73

* Fresh feed: F_{80} of 37,777 µm, 18.7% –75 µm and 1.2% – 10 µm

2.4.2.5. Effect of pebble crushing

The effect of using a pebble crusher was also evaluated. Table 10 shows the results obtained in a test carried out with a combination of pebble ports and pebble crusher as opposed to a test with no pebble crushing, both using JAN sample. It shows that the use of pebble crushing was responsible for an increase in SAG mill circuit throughput by 18% in comparison to the figure observed for the circuit with no pebble crushing. Pebble crushing had the additional benefit of reducing the SSE by 7%, i.e. from 26.9 kWh/t–75 µm to 25.1 kWh/t–75 µm. However, energy consumed in pebble crushing was not included in calculation of SSE. On the other hand, estimates of fSAG, which incorporated the crushing energy consumption, attested to the energy benefit, however modest, of use of the pebble crusher.

Table 10. Effect of pebble crushing for sample JAN* for mill operating in open-circuit SAG mode

Pebble crushing	Product		Fresh feed rate (t/h)	Circulating load (%)**	Specific energy (kWh/t)		SSE (kWh/t – 75 µm)	fSAG (-)
	P_{80} (µm)	–75 µm (%)			SAG	Crusher ***		
With	1,645	36.8	1.73	10.83	6.52	0.06	25.1	2.39
Without	1,308	40.6	1.46	6.04	8.00	-	26.9	2.60

* Fresh feed: F_{80} of 125,637 µm and 10.8% –75 µm

** Ratio of trommel oversize divided by trommel undersize flowrates

** Calculated pebble crusher specific energy with Bond crusher Wi and multiplied by the percentage of circulating load

2.4.2.6. Effect of secondary crushing

An alternative recently used to increase throughput in SAG mill circuits has been to include a secondary crushing stage in the circuit, therefore resulting in a finer fresh feed to the SAG mill (Siddal and Putland, 2007). A sample with a truncated PSD was prepared to assess the response of the circuit grinding JAN sample of such an alternative, already shown in Figure 6. The summary of test results is shown in Table 11, which indicates that the SAG mill circuit throughput decreased by 18% for the truncated feed (secondary crushing) as compared with the original PSD. No substantial change was observed in SSE, whereas the fSAG increased 53%. This substantial increase in fSAG may be explained by the reduction in autogenous grinding media and increase in proportion of critical size in the mill, a deleterious effect that has been associated with feeding fully crushed secondary crushing material to the SAG mill (Powell et al., 2015).

Table 11. Effect of secondary crushing in SAG milling of JAN in open circuit

Secondary crushing	Feed			Product		Fresh feed rate (t/h)	Specific energy (kWh/t)		SSE (kWh/t –75 µm)	fSAG
	Top size (mm)	F_{80} (µm)	–75 µm (%)	P_{80} (µm)	–75 µm (%)		SAG	Crusher *		
Without	203	126,637	10.8	1.308	40.6	1.46	8.00	-	26.8	2.60
With	102	51,550	11.1	1.535	52.4	1.19	11.10	0.25	26.9	3.99

* Estimated using Bond CWi

2.4.2.7. Effect of ball size distribution

One of the key operating aspects of AG/SAG single-stage configuration is the circulating load, which tends to be relatively high due to the high reduction ratio required for this kind of circuit, demanding handling and classifying high flowrates. As very high circulating loads are deleterious to the circuit performance a SAG mill test with a modified ball charge was designed to assess such issue. Table 2 compares the two ball size distributions used in testing SAG milling. The one referred as “standard” was used throughout the entire campaign, while the one identified as “finer” was prepared specifically for the test whose results are listed in Table 12. In both cases the JAN sample was used in tests in single-stage SAG circuit configuration (SAGSS).

Table 12 indicates that the SAG circuit throughput for finer ball size distribution test decreased by 2% as compared to standard ball size distribution test. The exceedingly high circulating load of over 800% was successfully decreased to nearly half, for the finer ball size distribution test, but the benefit would need to be balanced against the 10% increase in SSE and a 9% increase in fSAG.

Table 12. Effect of ball size distribution of JAN* in closed-circuit single-stage grinding

Ball size (Table 2)	Product		Fresh feed rate (t/h)	Specific energy (kWh/t)	Circulating load (%)	SSE (kWh/t –75 µm)	fSAG (-)
	P_{80} (µm)	–75 µm (%)					
Standard	90	72.8	0.95	12.8	836	20.6	1.12
Finer	95	70.9	0.93	13.6	476	22.6	1.22

* Fresh feed: F_{80} of 125,637 µm and 10.8% –75 µm

2.5. Conclusions

A wide range of SAG and AG milling tests were conducted, with circuit configurations covering single and two stage, with and without pebble and pre-crushing, in order to assess the viability of grinding low grade itabirite ores in these circuits compared to the current approach of multistage crushing and ball milling.

The relative efficiencies of the alternative circuits were assessed using the size specific energy (SSE) measured at 75 µm. The fSAG parameter was also used as an alternative measure to provide a rough comparison to expected crushing-milling production values, where values below one indicate a greater efficiency than expected.

The following conclusions were derived from the extensive pilot plant campaign with three different itabirite ores:

- For SAG mill open circuit configuration, coarser feed size distributions resulted in significant reductions in circuit throughput, accompanied by a systematic increase in SSE and fSAG;
- Comparisons with SAG mill closed circuit configuration showed the same trends in throughput and energy efficiency with coarser feed sizes observed for open circuit mode, but the magnitude of changes was smaller;

- SAG milling allows significantly higher circuit throughput compared to AG milling, ranging from 25% to 83% depending upon circuit configuration (open/closed) and grinding mode (AG/SAG). The energy efficiency of AG milling was lower, however, this should be balanced against the benefit of AG milling not requiring the use of steel grinding media;
- AG milling produces a finer product;
- It is possible that in autogenous mode the more competent components, richer in silicates, were ground far finer – due to the greater abrasion component in autogenous milling, leading to the unexpected rise in SSE. Unfortunately, component-by-size data was not generated by which this hypothesis can be tested. It is recommended that this is assessed in future work, as finer grinding of the silicates is not a favorable outcome, from both an energy and recovery perspective.
- Single stage AG/SAG milling required significantly less energy than two-stage circuits;
- Pebble crushing increases throughput and energy efficiency when incorporated in the circuit for the tougher itabirite ore tested;
- Increased SAG mill ball charge from 4 to 16% resulted in only a modest increase in circuit throughput, but a significant reduction in energy efficiency, demonstrating that a high SAG mill ball load is unfavourable for these ores;
- A truncated feed, mimicking secondary crushing of the SAG feed, was detrimental to the operation, resulting in reduction in both circuit throughput and efficiency;
- Finer ball charge size distribution was beneficial for single stage SAG mill operation, being responsible for 43% reduction in the circulating load in milling, with only a 2% reduction in circuit throughput.
- Based on energy efficiency in terms of fSAG values, values lower than one achieved for three of the softer ores (GAL-IC, GAL-IF and SAP) demonstrate, however roughly, the attractiveness of AG/SAG milling in comparison to multiple stages of crushing following ball milling. The opposite conclusion could be drawn from the tests involving the tougher ore (JAN), since values of fSAG were all higher than one, so that the attractiveness of AG/SAG milling could only be

potentially justified on the basis of other criteria, such as circuit simplicity and CAPEx.

In summary, the results of this comprehensive set of pilot test work show that AG/SAG milling is technically feasible and generally an attractive alternative from the standpoint of energy efficiency, for grinding itabirites. Among the circuit configurations/variables studied, the closed single-stage tests were the most attractive in terms of grinding efficiency. However, evidence of slurry pooling, associated with the substantial proportion of fines in the feed, suggest that great care must be exercised on mill discharge design when deploying this circuit configuration at industrial scale.

3. Gravity separation of fine itabirite iron ore using the Reflux Classifier – Part I – Investigation of continuous steady state separations across a wide range of parameters[2]

[2]Rodrigues, A.F.V., Delboni Junior., H., Rodrigues, O.M.S., Zhou, J., Galvin, K.P., 2023. Miner. Eng. 201, 108187, https://doi.org/10.1016/j.mineng.2023.108187

3.1. Abstract

High grade iron ore resources are becoming depleted in Brazil, with relatively low-grade ores requiring more intensive concentration to achieve a premium product. Accordingly, a typical industrial itabirite concentration circuit includes desliming in hydrocyclones and concentration via reverse flotation, product thickening and filtration, with the slimes sent to tailings thickeners, and onto tailings storage facilities. This work examined the potential for applying a vastly simpler approach, a single stage of gravity separation using the Reflux Classifier. Here the classified feed, 90% finer than 0.150 mm, is sent directly to the Reflux Classifier, leading immediately to a high-grade concentrate at high solids concentration.

Part I describes the findings from a comprehensive series of experiments covering the effects of bed density set point, feed pulp density, throughput, fluidisation water rate and lamella channel spacing. The main program, based on an ore with 8% goethite and 45% hematite, achieved a feed upgrade from 37% to 65.6+/-0.4% iron and iron recovery of 72.9+/-0.4% at 9 t/m^2/h. A second feed with 1% goethite and 57% hematite was upgraded from 40% to 66.3+/-0.4% iron at an iron recovery of 84.7+/-0.5% at 10 t/m^2/h. (The grade of pure hematite is 69.9% iron). It was essential to run the Reflux Classifier at a sufficient volumetric rate to achieve shear induced inertial lift of the coarse silica within the closely spaced inclined channels, to reject the gangue minerals from the high-grade product. The results demonstrate the technical feasibility of applying the Reflux Classifier to upgrade itabirite feeds.

3.2. Introduction

The iron and steel industry contributes approximately 8% of global carbon dioxide emissions (Holappa, 2020). With the growing commitment to achieving net zero emissions of carbon dioxide by the year 2050, there is an imperative to establish a way forward for decarbonizing the industry. A key enabler is the development of more advanced methods of mineral beneficiation to increase the grade of the iron ore (Galvin and Iveson, 2022).

Itabirites, which are typical of the lower grade iron ores, are metamorphic banded-iron formations (Hagemann et al., 2016), consisting of iron oxide (predominantly hematite), with quartz as the main gangue mineral. The processing of the itabirite commences with multi-staged crushing, then grinding, classification and desliming stages, reverse quartz flotation, dewatering of the concentrate, slimes and tailings (Filippov et al., 2014). This conventional circuit requires size distributions finer than 150 µm to achieve adequate liberation (Rodrigues. 2014; França et al., 2020). These flowsheets can upgrade an ore from a typical level of ~36% Fe to 67% Fe, but are capital intensive (Segura-Salazar et al., 2021) and lead to significant losses of fine iron ore to the tailings due to the need for the desliming.

The performance of the flotation process decreases with increasing particle size due to the tendency for coarse particle detachment in flotation (Dai et al., 2000; Fornasiero and Filippov, 2017; Lima et al., 2020). The flotation also suffers from losses of ultrafine hematite due to entrainment with the quartz, and from a failure to float ultrafine quartz (Lima et al., 2012. 2016; Filippov et al., 2021) due to the low collision probability between the particles and the bubbles (Fornasiero and Filippov, 2017).

The purpose of the present paper is to examine the potential for applying a much simpler, single stage, gravity separation of the itabirite feed, utilising a Reflux Classifier. Strong performance on fine iron ore has been obtained previously over the size range from 150 µm down to 45 µm using a relatively wide inclined channel spacing of 6 mm (Amariei et al, 2014). The itabirite ore presents a major challenge to gravity separation.

Following the grinding, typically 80% of the particle mass is finer than 150 µm and typically 15-20% finer than 20 µm. The gravity separation needs to achieve an iron recovery that exceeds the recovery from the reverse flotation circuit at a solids throughput higher than for reverse flotation (typically 4 t/m^2/h), targeting hematite down to about 10 µm. Moreover, the goal is to target a product grade of at least 65% iron, and ideally up to 68% iron (pure hematite is 69.9% iron).

The Reflux Classifier would receive the feed directly from the initial classifier at a pulp density of ~ 26 wt% solids. There would be no need for desliming as required for the preparation of the feed for reverse flotation. This means all the feed is directed to the Reflux Classifier, ideally producing a high-grade concentrate at high solids concentration. This approach offers the potential for removing the desliming cyclones, the reverse flotation, magnetic separators, and the product thickener. There is also no need for flotation chemicals.

The Reflux Classifier consists of a series of inclined channels above an upward current fluidized bed (Galvin, 2021). When the feed enters the system, most of the flow conveys upwards through the system of inclined channels while the faster settling particles segregate downwards towards the lower fluidized bed. Within the inclined channels the denser particles segregate towards the upwards facing inclined surfaces, forming a sediment that slides downwards (Galvin, 2021). Lower density particles experience shear induced lift, exposing those particles to the higher upwards velocities within the inclined channels, conveying those particles upwards. Fluidization water supports the formation of a lower fluidized bed, while also delivering strong desliming. Pressure transducers are used to quantify the suspension density in the lower fluidized bed. The control valve opens when the measured suspension density exceeds the value of the set point.

The inclined channels have a perpendicular spacing, z, which, for a given superficial flow velocity, governs the shear rates within the flow field of the inclined channels, and hence the hydrodynamic lift force that acts on the particles. In previous work conducted primarily on coal, a channel spacing of 6 mm was used, sufficient to deliver the lift force necessary to convey relatively coarse particles of low-density coal upwards through

the inclined channels. Amariei et al (2014) used the 6 mm channel spacing for fine iron ore feeds, however the effectiveness was limited to a relatively narrow size range. More recently, with an increasing focus on dense minerals, a channel spacing of z=3 mm has been used to deliver the much larger lift force necessary to convey relatively coarse particles of silica and other gangue minerals to the overflow, while extending the recovery of the higher density particles in the underflow product to include finer particles.

The present work examines the upgrading of itabirite ores using even more closely spaced channels with z = 1.8 mm. These closely spaced channels should in principle lead to stronger rejection of the coarse silicates while also increasing the capture of the ultrafine hematite below 20 µm. These two benefits should increase the potential for replacing the existing beneficiation circuits described above with a vastly simpler single stage gravity device.

The obvious concern with utilising closely spaced channels is whether there is an increased potential for blockages to develop. It is important to appreciate there is a considerable difference between a planar channel and conduit. The planar channel delivers a critical additional degree of freedom, which allows particles to readily develop trajectories around other particles. Thus, the tendency for blockage is counter-intuitive, indeed exceedingly low. Moreover, the higher shear rates produce a cleaning effect within the channels, preventing any compaction of sediment. In general, the tendency for particle blockage is negligible, though it is appropriate that oversize protections be applied to circuits.

This study provides a comprehensive investigation of the gravity separation of the fine iron ore feed achieved by the Reflux Classifier, covering the effects of changes in the volumetric feed rate, bed density set point, feed pulp density, fluidization velocity, and channel spacing. In a subsequent Part II of this study, these data sets are investigated theoretically, applying a partition surface to a binary hematite-silica representation of the feed as a generalized model to predict the grade and recovery. It is noted the binary components incorporate minor adjustments in their compositions to include features in the mineralogy.

3.3. Experimental

3.3.1. Ore samples

Samples from two itabirite mines were collected at industrial plants operated by Vale and located in the Iron Quadrangle of the state of Minas Gerais, Brazil. Figure 10 shows the point from which a 700 kg Sample A was obtained. In this case, the fines formed naturally through the breakage of the ore to pass ~0.15 mm. Sample B was processed further as shown in Figure 11, using wet grinding of the ore to pass ~0.15 mm.

Figure 10. Industrial itabirite plant sampling point – Sample A

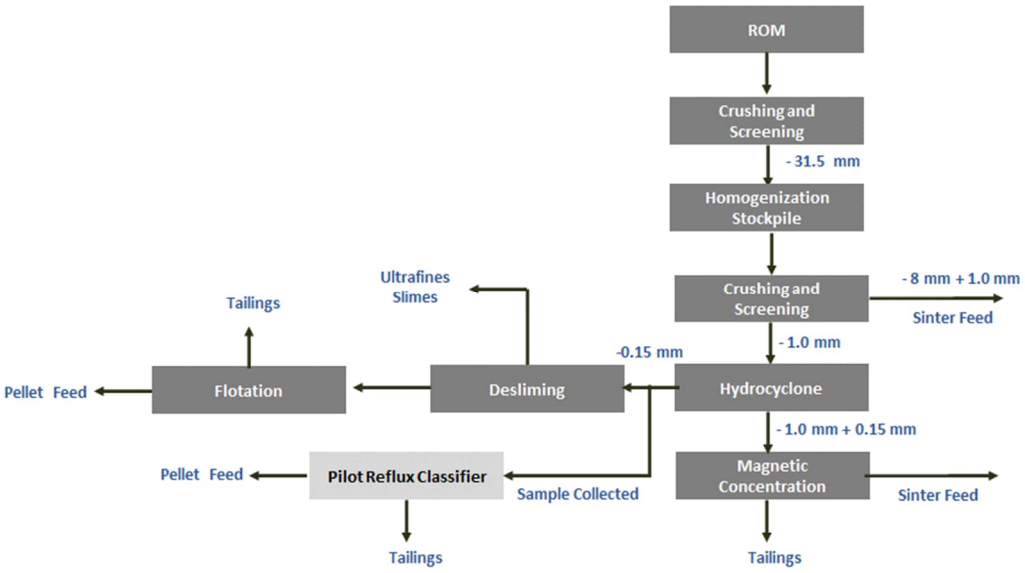

Figure 11. Industrial itabirite plant sampling point – Sample B

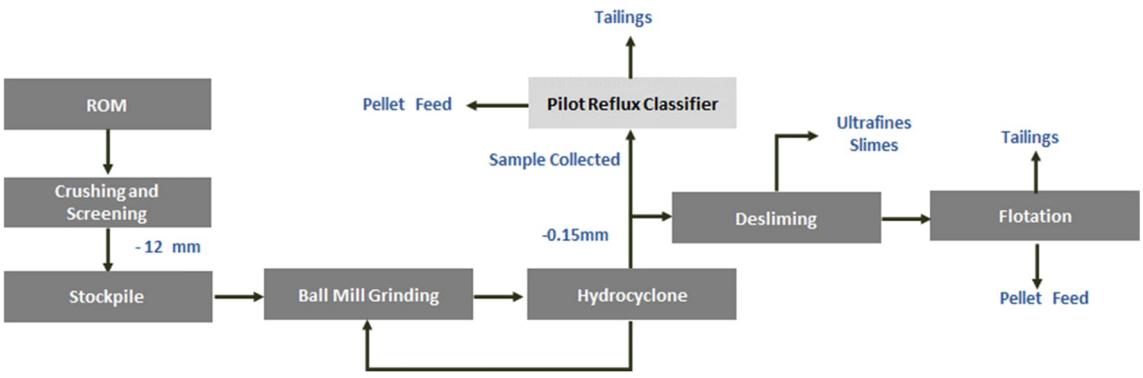

3.3.2. Feed ore characteristics

Table 13 presents the nominal chemical assays as a function of the particle size showing the relatively low iron grade, less than the richer Brazilian ores. It is also evident the coarser particles are rich in silica and hence the iron concentrates much more in the finer sizes. Table 14 shows the mineralogy, by optical microscopy, the dominant minerals being hematite and quartz. Figure 12 shows the complete particle size distribution of the two samples including the significant proportion of ultrafine particles below 10 µm. All assays were obtained using XRF. Optical mineralogy was undertaken using a polarization microscope. It is noted these samples were taken as aliquots at the mine prior to the experimental work so are included primarily for illustrative purposes.

Table 13. Nominal chemical assays by size

Size (mm)	Mass (%)	Fe (%)	SiO_2 (%)	P (%)	Al_2O_3 (%)	Mn (%)	LOI (%)
Sample A							
+0.150	12.7	18.9	72.2	0.017	0.26	0.053	0.44
-0.150 +0.045	53.6	32.2	52.8	0.017	0.31	0.040	0.46
-0.045+0	33.8	53.1	18.4	0.072	2.85	0.370	2.43
Overall	100.0	37.3	43.3	0.041	1.31	0.194	1.40
Sample B							
+0.150	14.2	4.5	92.6	0.010	0.28	0.016	0.22
-0.150 +0.045	38.3	34.0	50.7	0.010	0.22	0.016	0.13
-0.045+0	47.5	57.2	17.0	0.011	0.45	0.023	0.24
Overall	100.0	40.9	40.7	0.010	0.34	0.019	0.20

Table 14. Nominal mineralogy

Hematite (%)	Magnetite (%)	Goethite (%)	Quartz (%)	Manganese Oxides (%)	Gibbsite (%)	Others (%)	Quartz Liberation (%)
Sample A							
45.13	3.09	7.94	43.0	0.28	0.53	0.00	100
Sample B							
56.76	0.00	1.04	41.4	0.02	0.02	0.73	99

Figure 12. Nominal particle size distributions of the two samples.

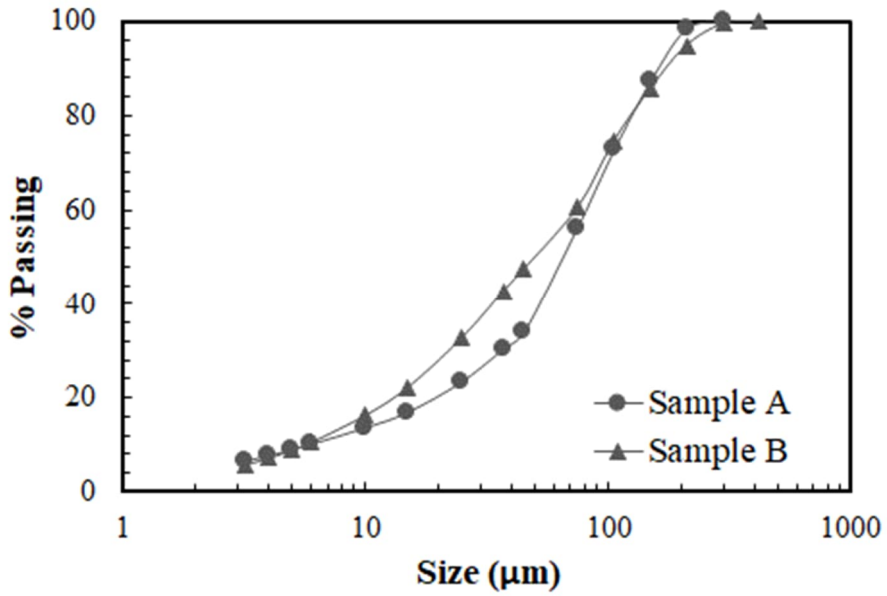

3.3.3. Methodology

A laboratory scale Reflux Classifier, with horizontal cross-section 0.1 m x 0.1 m, vertical height of 1 m, and inclined section containing parallel channels of 1 m is shown in Figure 13. Fluidization water was distributed through 16 holes, each 0.8 mm in diameter. The experimental program utilised a system of inclined channels with perpendicular spacing of 1.8 mm, with some additional experiments conducted using the wider channel spacing of 3.0 mm. This is the first comprehensive study of a Reflux Classifier operated using a 1.8 mm channel spacing.

Figure 13. Reflux Classifier (a) schematic representation (b) image of laboratory system.

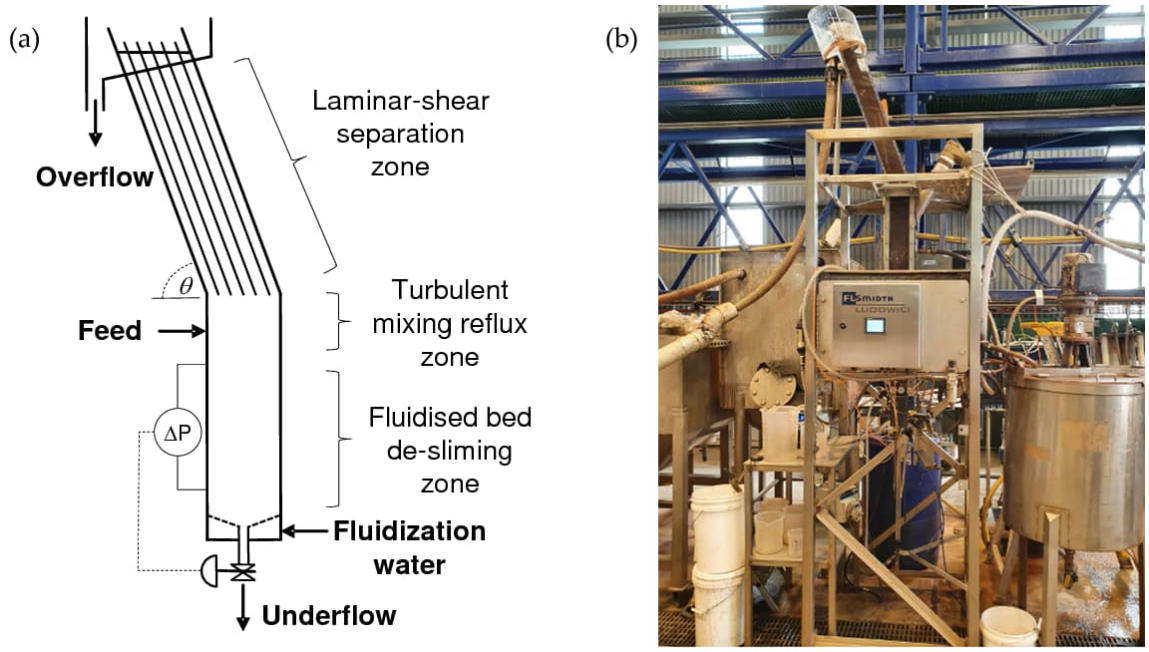

The authors have provided a Supplementary Data Source with this paper outlining the approach used to ensure high quality, and accurate data were produced in this study. The Supplementary provides additional data sets and expands on the analysis of the errors described later in the paper. The system adopted for feeding the Reflux Classifier (RC) commenced with a preparation phase. The entire sample was added to a 1300 Litre feed tank, water was added to adjust the pulp density, then the entire sample was discharged into 20 Litre buckets. The buckets were numbered and randomly sorted via a random number generator, and then stacked ahead of the experimental facility as shown in Figure 14. Then, a much smaller 300 Litre feed tank was used to supply the feed to the Reflux Classifier, the level maintained by adding the random sequence of buckets to the tank. The feed tank operated with a stirrer, a set of baffles, and a circulation flow was generated out of the bottom of the tank and back into the tank using a centrifugal pump. A peristaltic feed pump operated off this circulation line to supply the feed to the Reflux Classifier.

The method of feed preparation and delivery was successful in maintaining the assays and particle size distribution across a given experiment and across the entire

campaign. Steady state samples of the underflow product, and overflow reject were collected simultaneously over the same period, followed by a sample of the feed. These were weighed, dried, and subjected to desliming, and dry sieving. Sample assays were secured from an external commercial laboratory. All data from the experiments were subjected to mass balance reconciliation (Galvin et al, 1995). A Simplex Search Technique, guided by an objective function, was used to optimise the overall material balance. The objective function is formed from the errors generated during the mass balancing, given by the weighted sum of the errors squared. The weighting is given by the inverse of the estimated variance in the experimental value. Based on the analysis of 13 feed samples, sieve analysis is assumed to carry a standard deviation of 10% of the experimental value while assays are assumed to carry a standard deviation of 1%. Ultimately it is the internal consistency in the data that matters. This procedure delivered high level agreement between the raw experimental values and the mass balanced data as shown later.

Figure 14. Randomly sorted buckets of the feed slurry prepared prior to an experiment.

3.3.4. Laboratory-scale experiments – Sample A, B

The present work offered an opportunity to undertake a systematic approach to traverse the phase space of this system, guided by established fundamental principles. Thus, in most of the experiments undertaken in this study only a single parameter was changed at a time, thus allowing the direct effect of that change to be evaluated. The

experimental methodology described in the previous section had the effect of eliminating much of the feed variability that plagues many experiments of this kind (Crompton et al, 2022; Starrett and Galvin, 2023), ensuring the provision of very consistent experimental data. During the experimental campaign, building on the knowledge developed from former experiments, more than one change was introduced at a time into a single experiment to capture multiple benefits. Ultimately, the program of work provided a substantial data set and in turn a direct insight into the complexities of the particle transport in the Reflux Classifier.

The feed used for the main campaign was Sample A, reconstituted at the end of each experiment. Table 15 summarizes the conditions applied. For example, the first three experiments involved volumetric feed flow rates of 2, 6, and 4 Litres per minute. The channel spacing was 1.8 mm, the density set point 2000 kg/m^3, feed pulp density 26%, and fluidization rate 0.14 L/min (except for Run 1 which used 0.12 L/min). The nominal solids throughputs are listed showing a range from 5 to 14 t/m^2/h.

Table 15. Summary of conditions used in the experimental program on Sample A.

Run No.	Channel spacing (mm)	Set point (kg/m^3)	Feed rate (L/min)	Throughput ($t/m^2/h$)	Pulp density (w/w%)	Fluidisation rate (L/min)
1	1.8	2000	2	5	26	0.12
2			6	10	26	0.14
3			4	7	26	
4		2200	5	9	27	
5		2100		9	27	
6		1900		9	27	
7		2000		14	36	
8				6	16	
9				9	27	0.17
10				9	27	0.20
11	3.0			10	27	0.14
12			8	9	16	
13	1.8			9	17	

In the following three experiments the density set point was varied, covering 1900, 2100, and 2200 kg/m^3, while the feed flow rate was fixed at 5 L/min. Again, the channel spacing was fixed at 1.8 mm, the feed pulp density fixed at 27% solids (close to the target of 26%), and the fluidization rate remained at 0.14 L/min. The feed pulp density was then varied in the next two experiments, set at 36 wt% solids and then 16 wt% solids, with the density set point at 2000 kg/m^3. All other settings remained fixed. In the next two experiments the fluidization rate was increased beyond the level deemed ideal, known as the minimum fluidization rate, to 0.17 L/min and then 0.20 L/min, while the feed pulp density returned to 27 wt% solids.

In the next two experiments the inclined channel spacing was increased to 3.0 mm. The density set point was fixed at 2000 kg/m^3 and the fluidization rate set at 0.14 L/min. The first of these experiments used a feed flow rate of 5 L/min, with the feed pulp

density set at 27 wt% solids. In the following experiment the feed rate was increased to 8 L/min to produce a higher shear rate. However, the feed pulp density was reduced to 16 wt% solids, a decision based on knowledge acquired during the program of work. In the final experiment the channel spacing was returned to 1.8 mm, however the feed rate was increased to 8 L/min, with the feed pulp density again set at the lower level, this time 17 wt% solids.

The density of the feed particles used in these experiments was measured using pycnometry. The average density across 13 experiments was 3531 kg/m^3 and the standard deviation was 13 kg/m^3, a variation of just 0.4%.

Finally, it is noted that one additional experiment was conducted on Sample B, adopting virtually the same conditions as those used in Run 2 for Sample A. Here, the fluidization rate used for Sample B was raised to 0.2 L/min due to the denser and hence faster settlings particles.

3.3.5. Rheology of the Slimes

The rheology of the suspension medium was measured to investigate the above hypothesis that the suspension viscosity increased significantly as the feed pulp density increased. The overflow reject sample from Run 13 was wet screened at 20 µm. The material in the size-range from 0-20 µm was then dried, and the density of the particles measured using pycnometry. A series of samples of different pulp density and hence solids volume fraction was prepared, and, for each, the suspension viscosity measured as a function of the shear rate.

3.4. Results and Discussion

3.4.1. Effect of feed throughput on separation performance

The Reflux Classifier offers a significant throughput advantage over more conventional fluidized bed separators, estimated to be up to 50-fold when targeting the recovery of particles with a density of 4000 kg/m^3 down to a particle size of 10 µm. Galvin (2021) provides the detailed basis behind this estimation. In order to be competitive with the

reverse flotation it was necessary to secure a successful separation at a solids throughput of at least 5 t/m^2/h. Thus, the initial series of experiments focussed on the effects of changes in the volumetric flowrate at the fixed feed pulp density of 26 wt% solids, covering a solids throughput range of 5-10 t/m^2/h. The operating conditions involved a fixed lamella channel spacing of 1.8 mm, density set point of 2000 kg/m^3, and fluidization rate of 0.14 L/min (Run 1 was set at 0.12 L/min). The vessel cross-sectional area was always 0.01 m^2.

Table 16 provides a summary of the overall results obtained for the first three experiments. Interestingly, the product grade improved significantly with increases in the volumetric flow rate, reaching an iron grade of 64.6% in Run 2, however the iron recovery decreased to 73.2%. Table 17 shows the balanced data set for Run 2 conducted at the highest solids throughput of 10 t/m^2/h. Note the raw data, given in Table 18, are very consistent with the balanced values, confirming the value of the experimental method described earlier. Based on an error analysis at the end of this paper, it is estimated the uncertainty in the grade and recovery are both +/-0.4%. There is strong confidence therefore in the reliability of this key result.

Table 16. Effect of throughput on separation performance

Run	Feed rate (L/min)	Throughput (t/m^2/h)	Feed Grade (%Fe)	(SiO_2)	Product Grade (%Fe)	(SiO_2)	Reject Grade (%Fe)	(SiO_2)	Yield (%)	Iron Recovery (%)
1	2.0	4.7	36.5	44.6	45.1	32.8	16.0	72.9	70.5	87.0
3	4.0	7.3	36.4	44.8	59.7	12.0	14.4	75.8	48.6	79.7
2	6.0	10.0	37.2	43.7	64.6	4.9	17.2	71.9	42.1	73.2

Table 17. Balanced data set for Run 2 – throughput 10 t/m^2/h

	Feed		Product		Reject	
Sieve size (mm)	Mass (%)	Grade (%Fe)	Mass (%)	Grade (%Fe)	Mass (%)	Grade (%Fe)
0.250	0.4	18.5	0.5	28.7	0.3	5.3
0.180	4.2	17.2	4.0	40.0	4.4	2.1
0.150	6.9	19.4	5.8	51.0	7.8	2.1
0.125	6.6	19.8	4.8	59.3	7.9	2.1
0.090	20.3	25.2	17.1	65.6	22.7	3.0
0.063	16.2	35.0	18.1	68.5	14.9	5.2
0.045	14.2	47.3	20.7	68.8	9.5	13.1
0.038	6.1	52.5	8.9	69.1	4.0	25.3
0.020	10.1	57.4	13.9	68.4	7.3	42.0
-0.020	15.1	48.5	6.2	57.0	21.5	46.7
Overall	100	37.2	100	64.6	100	17.2

Table 18. Raw data set for Run 2 – throughput 10 t/m^2/h

	Feed		Product		Reject	
Sieve size (mm)	Mass (%)	Grade (%Fe)	Mass (%)	Grade (%Fe)	Mass (%)	Grade (%Fe)
0.250	0.3	18.5	0.6	28.8	0.3	5.3
0.180	4.1	17.2	4.0	39.9	4.4	2.1
0.150	6.9	19.4	5.3	51.0	8.1	2.1
0.125	6.3	19.8	4.8	59.2	7.6	2.1
0.090	21.1	25.3	13.3	65.2	25.7	3.0
0.063	16.6	34.9	19.9	68.5	13.1	5.2
0.045	13.7	47.3	21.5	68.8	9.0	13.1
0.038	5.7	52.5	9.6	69.1	3.9	25.3
0.020	9.8	57.0	15.0	68.7	6.8	42.1
-0.020	15.5	48.7	6.1	56.8	21.2	46.6
Overall	100	36.9	100	65.3	100	17.2

Figure 15 shows the iron and silica grades in the underflow product stream as a function of the particle size. Although the iron grade declines significantly at particle sizes larger than about 100 µm, there is relatively little solids in the coarser size fractions, hence the overall grade remains high. The silica grade is initially very low, but climbs significantly beyond a particle size of 100 µm.

Figure 15. Effect of throughput on separation performance - iron (a) and silica (b) grades versus particle size in the underflow (UF) product.

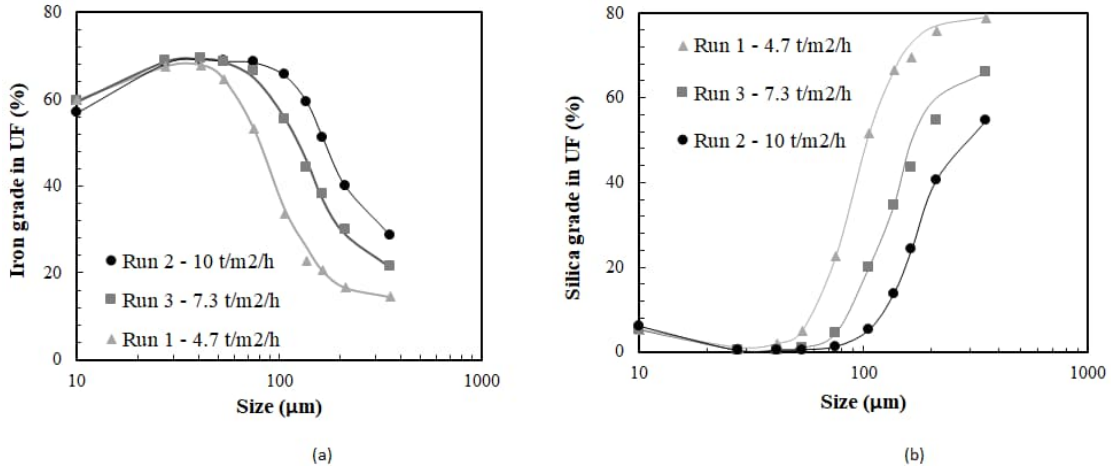

The partitioning of the silica to the underflow product is shown as a function of the particle size in Figure 16. These data show the very strong effect of the feed flow rate and hence solids throughput on the probability of the coarser silica particles reporting to the underflow product. At the highest feed flow rate, the partition numbers are significantly lower, making the iron grade of the product significantly higher. This finding is consistent with the mechanism of a shear induced inertial lift force within the inclined channels that causes the coarse silica to physically lift from the upward facing surfaces and in turn convey to the overflow.

Figure 16. Effect of the throughput on the silica partition to the underflow (UF) product. It is evident the highest throughput leads to the lowest partitioning of the silica to the product.

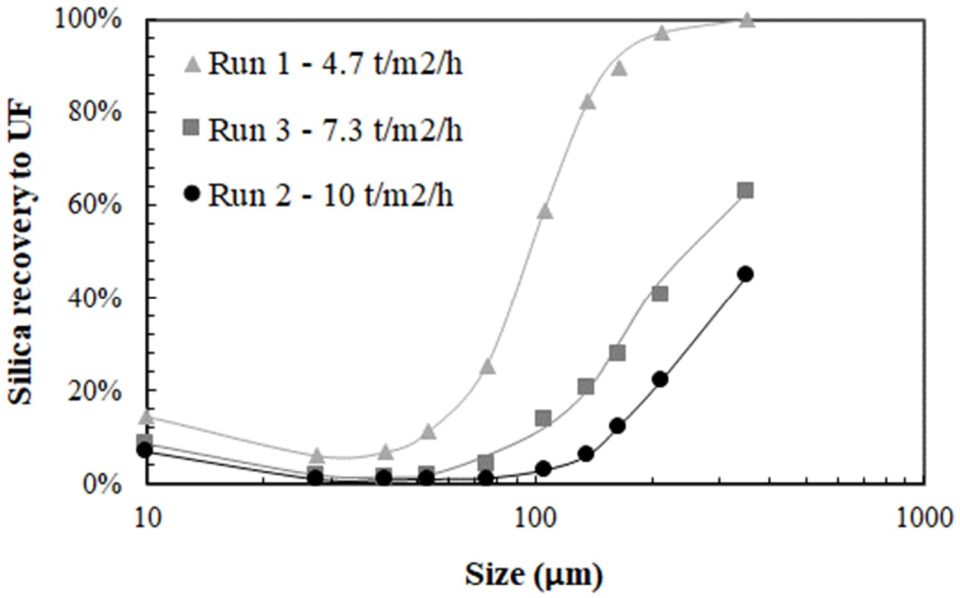

3.4.2. Effect of bed density set point

For a given set of operating conditions, the primary control variable is the density set point. The interpretation of the measured signal is important. Here pressure transducers were located at elevations above the fluidization distributor of 60 and 440 mm as shown in Figure 13A. The transducers measure the weight loading of the suspension above each probe, hence the difference is the weight loading of the suspension between the probes. If there is a distinct fluidized bed level located between the probes, then part of the reading will relate to the low concentration zone above the bed and the rest to the suspension within the bed. Solids that are supported mechanically off the base of the vessel and not by the fluid are not recognised by the pressure transducers. So, the bed must be sufficiently fluidized for the reading to have meaning, a condition which is therefore essential to the control of the system.

For a well liberated feed, the suspension density is arguably just a measure of the height of the fluidized bed when the bed level is located between the elevation of the

probes. The extent to which the bed density can be increased is governed by the level of coarse silica that ends up in the bed. If the silica content is excessive, then it becomes difficult to reach a high suspension density. In this case the bed level will tend to increase, limiting the underflow discharge to achieve the set point. In general, a lower density set point promotes a higher yield to underflow, hence a higher recovery, but a lower grade.

Table 19 summarizes the results obtained using the three density set points ranging from 2200 kg/m^3 down to 1900 kg/m^3. These experiments used a fixed inclined channel spacing of 1.8mm, keeping the feed rate fixed at 5 L/min, the pulp density at 27 wt% solids, and the fluidization rate at 0.14 L/min. The feed solids throughput was 9 t/m^2/h. At this stage of the work, the benefits of a higher volumetric feed rate of 6 L/min were not known.

Table 19. Effect of bed density set point on separation performance

Run	Set Point	Feed Grade		Product Grade		Reject Grade		Yield	Iron Recovery
	(kg/m^3)	(%Fe)	(%SiO_2)	(%Fe)	(%SiO_2)	(%Fe)	(%SiO_2)	(%)	(%)
4	2200	36.0	44.3	60.7	11.9	19.3	66.0	40.1	67.8
5	2100	36.9	43.7	60.4	12.6	19.0	67.4	43.2	70.7
6	1900	36.3	43.9	58.1	14.3	16.8	70.3	47.2	75.6

Run 4, operated at a set point of 2200 kg/m^3, produced the highest product grade of 60.7% and lowest iron recovery of 67.8%. This result is therefore compared with the findings from Run 2 which previously had the highest product grade of iron of 64.6% at an iron recovery of 73.2%. The significantly higher set point used here of 2200 kg/m^3 has likely resulted in the lower iron recovery, restricting the underflow discharge to target the high bed density set point. In fact, the average iron recovery produced for set points of 1900 and 2100 kg/m^3 (70.7%, 75.6%) is close to the result obtained for Run 2 (73.2%) operated at the intermediate density set point of 2000 kg/m^3.

Interestingly the highest iron grade of 60.7% is significantly lower than the grade of 64.6% obtained in Run 2 despite the use of a significantly higher set point density in

Run 4. Runs 4-6 involved a volumetric feed rate of 5 L/min. Run 2 involved the higher volumetric feed rate of 6 L/min. At this stage of the experimental program, it was not apparent that this modest increase in the volumetric feed rate to 6 L/min was important, hence most of the work continued at the lower feed rate of 5 L/min. While its possible a statistical design might have identified the optimal separation with fewer experiments, the systematic series of experiments offered strong clarity relating cause and effect.

The shear induced inertial lift is higher at 6 L/min than for the experiments conducted at lower volumetric feed rates. Physical lift is a critical phenomenon (Galvin and Liu, 2011; King and Leighton, 1997). Once the lift force exceeds the net weight of the particle in the fluid, in the normal direction to the incline, physical lift occurs. But no lift occurs if the lift force does not reach this level. When physical lift occurs, the particles migrate to more central positions within the inclined channels where the local fluid velocities are substantially higher. These particles then convey upwards as part of the overflow reject stream. In this series of experiments the feed flow rate of 5 L/min was not sufficient to convey some of the coarse particles hence the product grades decreased significantly in comparison to Run 2 which had a feed flow rate of 6 L/min.

Figure 17 shows the partitioning of the iron to the underflow product as a function of the particle size. The results obtained at the two lowest density set points of 1900 and 2100 kg/m^3 are indicative of the Run 2 recoveries obtained using the intermediate density set point of 2000 kg/m^3, which involved a higher feed flow rate of 6 L/min. Figure 18 compares the size partition curves for the silica from Run 2 at 2000 kg/m^3 and 10 t/m^2/h with the experiment here at a set point of 2200 kg/m^3 and 9 t/m^2/h. As noted, the former experiment achieved an iron grade of 64.6% and the latter 60.7%. These results appear to confirm the importance of the hydrodynamics in the inclined channels, and that the slightly higher volumetric flow rate conveys the coarse silica to the overflow reject stream, thus increasing the iron grade in the underflow product stream.

Figure 17. Effect of bed density set point on the iron partition to the underflow (UF) product.

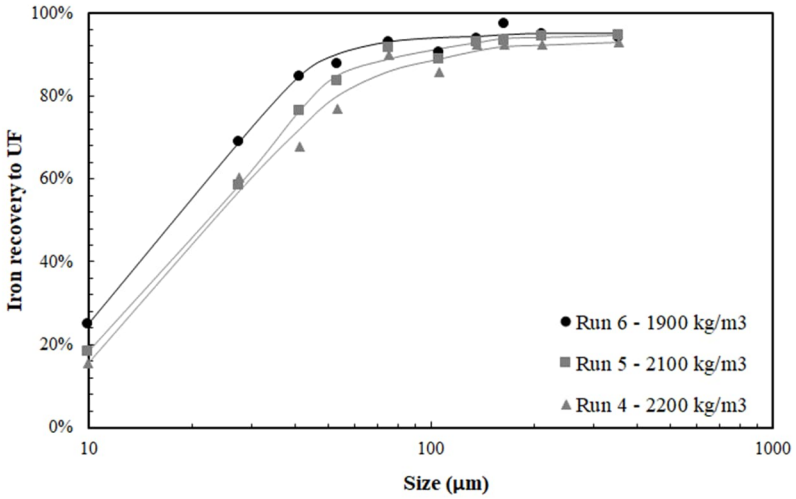

Figure 18. Effects of bed density set point and feed throughput on the silica partition to the underflow (UF) product. The higher volumetric rate of Run 2 (6 L/min) compared to Run 4 (5 L/min) led to less silica recovery in the underflow.

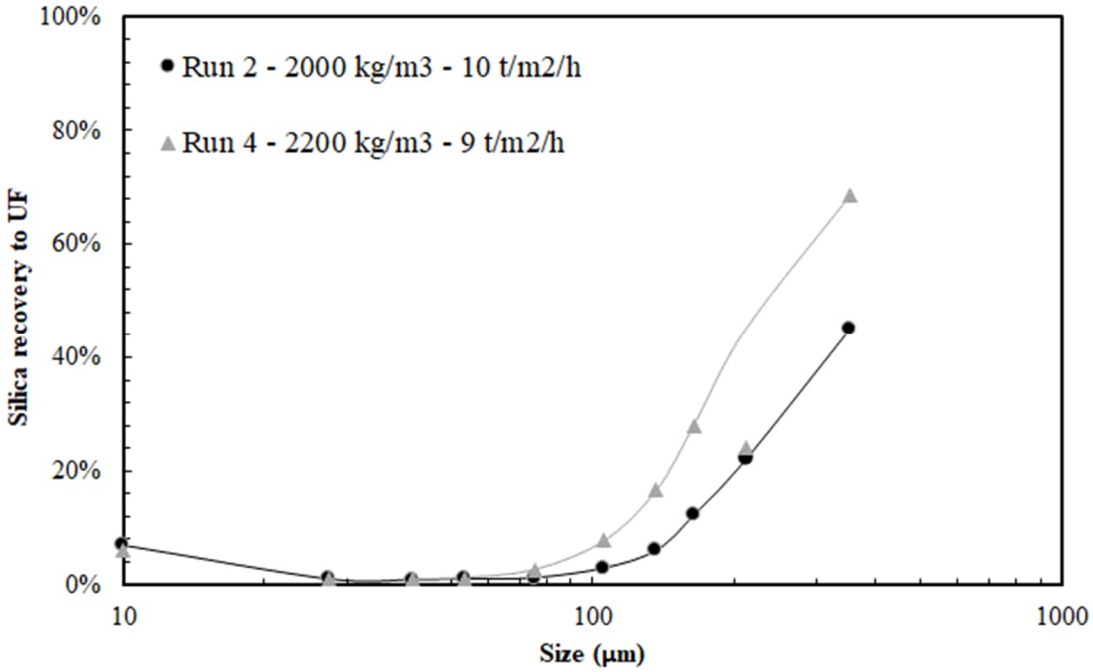

3.4.3. Effect of fluidization water rate

The fluidization rate must be set at a level sufficient to support the weight of the particles within the fluidized bed. This requirement is essential simply from a process control perspective, to ensure the physical state of the steady state system is characterised uniquely by the measured suspension density. It is also important to ensure the bed can act as a zone for sorting particles, permitting the upwards displacement of the relatively low-density particles from the bed, the so-called inversion phenomenon reported by previous researchers (Moritomi et al., 1982; Moritomi et al., 1986). The quiescent nature of the fluidized bed acts as a buffer, permitting ultrafine low-grade slimes to permeate out of the bed, improving product grade and subsequent dewatering. The fluidization rate was first set at 0.12 L/min, but later shifted to 0.14 L/min.

This section considers the effects of utilising an excessive fluidization rate on separation performance. This work involved a fixed lamella channel spacing of 1.8mm, bed density set point of 2000 kg/m^3, volumetric feed rate of 5 L/min, and feed pulp density of 27 wt% solids. The solids throughput was again 9 t/m^2/h. The use of excessive fluidization water causes an expansion of the bed to lower concentrations, and hence the need for the bed height to increase when targeting the density set point. This bed expansion can invite coarse silica to join the bed, leading to poorer product grade. The most significant effect, however, is the loss of ultrafine particles of hematite. While these may well be captured by the inclined channels, and hence returned to the lower zone, the high fluidization rate ultimately creates a barrier to their transport into the underflow product stream. Table 20 shows that as the fluidization rate increases the iron recovery decreases. In Run 2 the iron recovery (at a higher feed rate of 6 L/min) was 73.2%. Here the recovery decreased to 71.4% for a fluidization rate of 0.17 L/min, and to 66.8% at a fluidization rate of 0.20 L/min.

Table 20. Effect of fluidization rate on the separation performance

Run	Fluidization water rate (L/min)	Feed Grade (%Fe)	(SiO_2)	Product Grade (%Fe)	(SiO_2)	Reject Grade (%Fe)	(SiO_2)	Yield (%)	Iron Recovery (%)
9	0.17	37.3	43.6	61.3	9.7	18.8	69.6	43.4	71.4
10	0.20	37.1	43.8	61.4	9.6	20.7	67.0	40.4	66.8

3.4.4. Effect of the feed pulp density on separation performance

The feed pulp density used in this study was set at the nominal level expected in the industrial setting, at about 26 to 27 wt% solids. For a given volumetric feed rate, it is in principle possible to achieve a much higher solids throughput, with acceptable recovery, by increasing the feed pulp density. Thus, the first of these experiments involved the higher feed pulp density of 36%. The conditions of the experiments listed in Table 21 involved a channel spacing of 1.8 mm, set point 2000 kg/m^3, volumetric feed rate of 5 L/min, and fluidization rate of 0.14 L/min. It is evident that the iron recovery achieved using the high feed pulp density of 36% was very low at 48.2%. The conclusion drawn from this work is that the viscosity of the feed suspension increases with the feed pulp density. In previous work, Carpenter et al (2019) undertook a systematic study on the effects of suspension viscosity, showing the considerable impact on particle recovery. In that work significantly higher recoveries were achieved by halving the feed pulp density while doubling the volumetric feed rate.

In order to investigate the effect of viscosity further, Run 8 was conducted at the lower feed pulp density of 16%, producing a very high iron recovery of 81%. This case indicates a pulp density of 16% is almost sufficient to “switch off” the effects of elevated viscosity. This issue is examined later through direct measurement of the suspension viscosity at different concentrations. Interestingly, the product grade decreased significantly to 54.3%. This result suggests the silica partitioning to the underflow increased because of the reduction in the suspension viscosity. Moreover, the result suggested there could be significant benefits from increasing the volumetric feed rate

to improve the shear induced inertial lift, while also increasing the solids throughput, and most importantly improving the product grade.

Table 21. Effect of feed pulp density on separation performance

Run	Pulp Density (w/w %)	Throughput ($t/m^2/h$)	Feed Grade (%Fe)	(SiO_2)	Product Grade (%Fe)	(SiO_2)	Reject Grade (%Fe)	(SiO_2)	Yield (%)	Iron Recovery (%)
7	36	14	36.8	44.2	61.2	9.8	26.8	58.3	29.0	48.2
8	16	6	35.5	46.1	54.3	19.7	14.3	75.9	53.1	81.0

3.4.5. Effect of increasing the volumetric feed rate at low feed pulp density

The initial three experiments conducted in this study showed the profound effect of increasing the volumetric feed rate from 2 to 4 to 6 L/min. The separation performance improved as the volumetric feed rate increased. Subsequent work conducted at 5 L/min consistently produced a performance below that observed at 6 L/min. The iron grades at the lower volumetric feed rate of 5 L/min never reached 62%, but at 6 L/min the grade reached 64.6%. A second key observation in this work is that a reduction in the feed pulp density leads to improved performance, most likely due to the reduction in the suspension viscosity. In this section experiments were conducted using a volumetric feed rate of 8 L/min, with the feed pulp density reduced to 16-17 wt% solids. In both cases the solids throughput was 9 $t/m^2/h$. The density set point was set at 2000 kg/m^3, and fluidization rate at 0.14 L/min. The first of these experiments was conducted using an inclined channel spacing of 3.0 mm. The iron grade increased to 65.1%, the highest so far in the study, and the iron recovery reached 71.7%. In the next experiment the inclined channel spacing was reduced to 1.8 mm. This experiment produced the best overall performance from the study, an iron grade of 65.6% and iron recovery of 72.9%. These grades were better than that from Run 2 (lower grade of 64.6%, recovery marginally higher at 73.2%).

These research findings reveal a robust scenario where a viscosity problem can be addressed by reducing the feed pulp density while increasing the volumetric feed rate

to compensate for any loss in the solids throughput. The primary limitation in securing a higher-grade product is the tendency for the coarse silica to partition to the underflow product.

3.4.6. Effect of the inclined channel spacing

In this section the performance of the Reflux Classifier operated with a channel spacing of 3.0 mm, with the feed flow rate reduced to the standard 5 L/min, was investigated. Here the feed pulp density was set at the usual 27 wt% solids, density set point at 2000 kg/m^3, and fluidization rate at 0.14 L/min. Table 22 provides a summary of the results. The conditions led to a lower iron recovery of 65.7% due to the reduction in the capture efficiency of the ultrafine particles due to the wider channels. The return to the higher feed pulp density and hence suspension viscosity also impacted negatively on the iron recovery. However, the product grade reached a level of 63.6%. This was surprising given the shear rate within the inclined channels would have been lower due to the 3.0 mm wide channel spacing and the lower volumetric feed rate of 5 L/min. The higher suspension viscosity associated with the feed pulp density of 27% probably assisted with the inertial lift, and in turn the conveying of the coarse silica up through the inclined channels.

It is worth noting that the performance of the Reflux Classifier with the wider channel spacing of 3.0 mm was relatively close to that observed for the channel spacing of 1.8 mm in Run 2. If the level of coarse silica could be reduced, the wider channel system would prove highly effective in beneficiating the itabirite resource.

Table 22. Effects of channel spacing on separation performance

Run	Pulp Density (wt %)	Channel Spacing (mm)	Flow Rate (L/min)	Throughput ($t/m^2/h$)	Product Grade (%Fe)	Product Grade ($\%SiO_2$)	Reject Grade (%Fe)	Reject Grade ($\%SiO_2$)	Yield (%)	Iron Recovery (%)
2	26	1.8	6	10	64.6	4.9	17.2	71.9	42.1	73.2
11	27	3.0	5	10	63.6	6.6	19.9	67.6	37.5	65.7
12	16	3.0	8	9	65.1	4.5	17.3	71.4	40.1	71.7
13	17	1.8	8	9	65.6	3.8	17.0	73.1	41.1	72.9

3.4.7. Reflux Classifier Experiment on Sample B

Table 23 presents the test conditions used for Sample B. The experimental conditions selected for this experiment were virtually the same as those used in Run 2 for Sample A. Sample B permitted the use of a higher fluidization rate, with less sensitivity to losses, probably due to the higher proportion of hematite. Sample A was clearly more sensitive to a higher fluidization rate, perhaps due to the significant presence of the goethite. Table 24 provides a summary of the results following mass balance reconciliation showing a remarkably high iron grade of 66.3% and high iron recovery of 84.7%.

The experimental results produced for Sample B are best compared with those obtained in Run 2 for sample A. Firstly the product grade for Sample A was 64.6% and for Sample B 66.3% while the recoveries were 73.2% and 84.7% respectively. Sample A has a significant level of goethite (mineral density ~ 4.3 t/m^3), and 45% hematite (mineral density up to 5.3 t/m^3) as shown in Table 14. Sample B had only 1% goethite, and 57% hematite. It is probable that the high proportion of hematite in Sample B led to the stronger iron recovery especially at the finer sizes as shown in Figure 19. Interestingly, Figure 10 also shows the partition of the silica to the underflow product was almost the same for the two experiments.

Table 23. Experimental conditions used for Sample B

Channel spacing (mm)	Set Point (kg/m^3)	Fluidization (L/min)	Throughput ($t/m^2/h$)	Flow Rate (L/min)	Pulp Density (%)
1.8	2000	0.2	10	6	24

Table 24. Summary of experimental results obtained for sample B

Feed Grade		Product Grade		Reject Grade		Yield	Iron Recovery
(%Fe)	(%SiO_2)	(%Fe)	(%SiO_2)	(%Fe)	(%SiO_2)	(%)	(%)
41.4	39.0	66.3	4.4	13.4	77.7	52.9	84.7

Figure 19. Comparison between Sample A-Run 2 and the Sample B separation. (a) Iron recovery versus particle size and (b) partition of silica to the underflow product versus particle size.

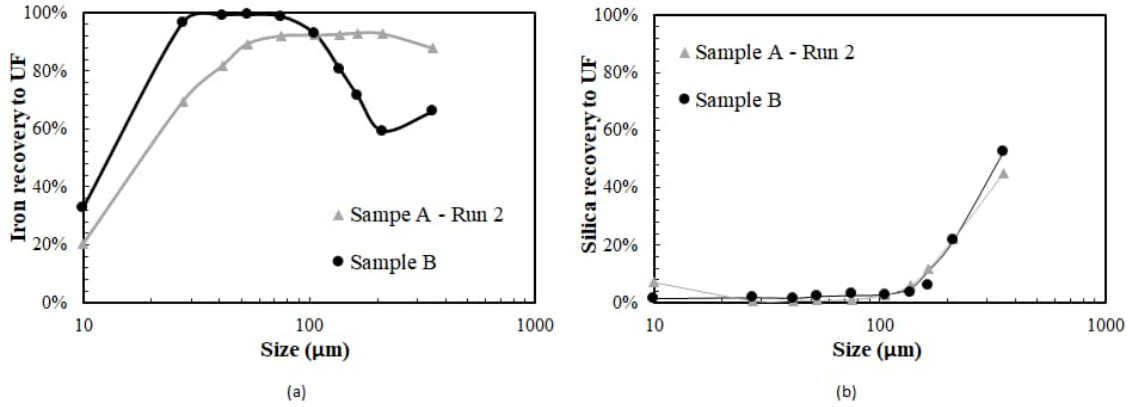

Figure 20 shows the particle size distribution of the feed, product and reject from the experiment conducted on Sample B. The overflow reject is much coarser than the underflow product, showing the Reflux Classifier was very efficient in removing the coarse quartz contained in the feed (Table 13). However, it is also evident there are losses of ultrafines in the overflow containing iron, something that is inevitable in gravity separation. Table 25 shows the balanced data set for the Sample B separation showing the losses of ultrafine iron in the overflow. The raw data set is shown in Table 26.

Figure 20. Particle size distributions of the feed, product, and reject streams for the Sample B separation.

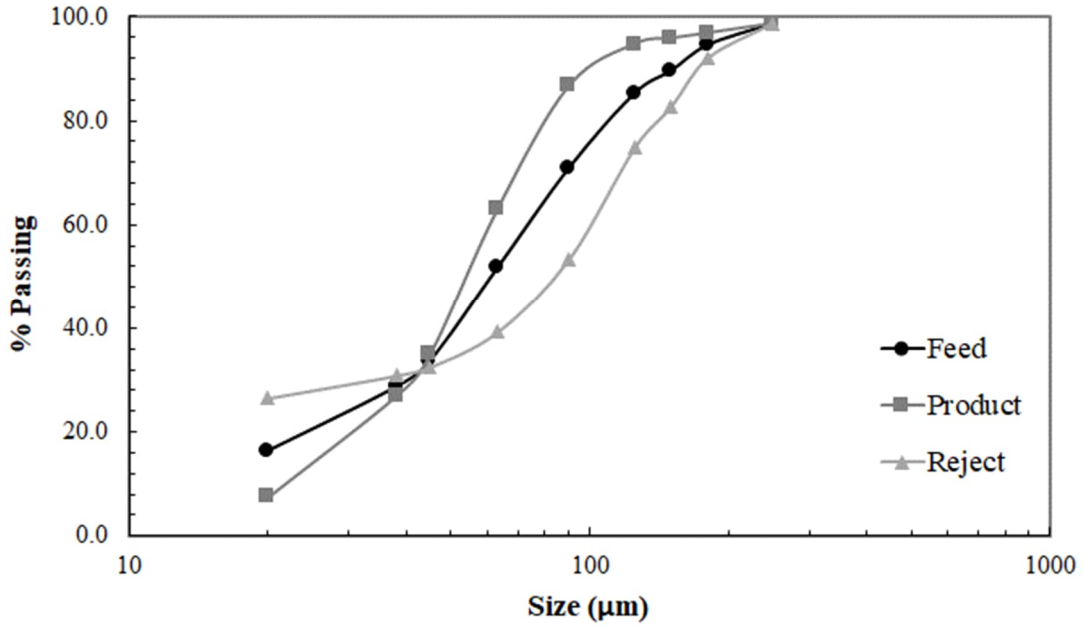

Table 25. Balanced data set for Sample B separation

Sieve size (mm)	Feed Mass (%)	Feed Grade (%Fe)	Product Mass (%)	Product Grade (%Fe)	Reject Mass (%)	Reject Grade (%Fe)
0.25	1.3	1.4	1.4	1.8	1.3	1.0
0.18	4.1	2.4	1.8	6.0	6.7	1.2
0.15	4.9	4.7	1.0	31.3	9.3	1.5
0.13	4.3	8.9	1.1	52.4	7.9	2.0
0.09	14.3	20.6	8.0	64.8	21.4	2.1
0.06	19.1	45.5	23.6	69.1	14.1	1.4
0.05	18.0	57.7	28.1	69.5	6.7	2.0
0.04	5.1	59.2	8.1	69.5	1.7	3.4
0.02	12.4	60.1	19.5	69.6	4.4	12.2
-0.02	16.4	49.7	7.4	68.1	26.5	44.0
Overall	100.0	41.4	100.0	66.3	100.0	13.4

Table 26. Raw data set for Sample B separation.

Sieve size (mm)	Feed Mass (%)	Feed Grade (%Fe)	Product Mass (%)	Product Grade (%Fe)	Reject Mass (%)	Reject Grade (%Fe)
0.25	1.4	1.5	1.3	1.7	1.3	1.0
0.18	4.5	2.4	1.5	6.0	6.7	1.2
0.15	5.2	4.7	0.8	31.2	9.5	1.5
0.13	4.2	8.9	0.9	52.2	8.8	2.0
0.09	12.8	20.7	6.5	64.6	21.1	2.1
0.06	20.0	45.8	20.9	69.0	13.0	1.4
0.05	17.0	57.8	31.1	69.7	6.3	2.0
0.04	5.3	59.0	8.5	70.0	1.5	3.4
0.02	12.1	60.1	21.2	69.8	4.2	12.2
-0.02	17.5	50.0	7.2	68.1	27.5	44.1
Overall	100.0	39.9	100.0	67.1	100.0	13.4

3.4.8. Rheology of the Slimes

Shear rates of 6U/z are produced at the planar surface of the inclined channels, where U is the channel superficial velocity based on the overflow rate, and z the channel spacing (Galvin and Liu, 2011). The shear rates within the inclined channels were calculated and used to guide the selection of the conditions in the rheometer. The suspension viscosities were therefore determined as a function of the solids concentration at specific shear rates of 33 s^{-1} (based on Run 12 with 3 mm channels), 45 s^{-1} (based on Run 2), and 63 s^{-1} (based on Run 13).

Figure 21 shows the slimes viscosity on a log scale as a function of the solids volume fraction across a broad range of concentration for the three shear rates. The strong exponential relationship is clear. Figure 22 presents the same data in a more relevant form, with the slimes viscosity on a linear scale as a function of the pulp density, covering the smaller range of concentration used in this work. Run 7 had a feed pulp density of 36 wt% solids and overflow pulp density of 29 wt% solids thus the viscosity

of the suspension likely exceeded 9 mPas. Run 2 had a feed pulp density of 26 wt% solids and overflow pulp density of 17 wt% solids thus the viscosity was much lower, and likely exceeded 2 mPas. Run 13 had a feed pulp density of 17 wt% solids and overflow pulp density of 11% solids thus the viscosity likely exceeded about 1 mPas, the viscosity of water. These data show the effects of the suspension viscosity were largely eliminated by reducing the feed pulp density down to ~ 17 wt% solids. The data also helps to explain the poor iron recovery in Run 7 at the highest feed pulp density of 36 wt% solids.

Figure 21. The viscosity of the suspension containing the slimes shown as a function of the solids volume fraction, with a clear exponential dependence on the concentration.

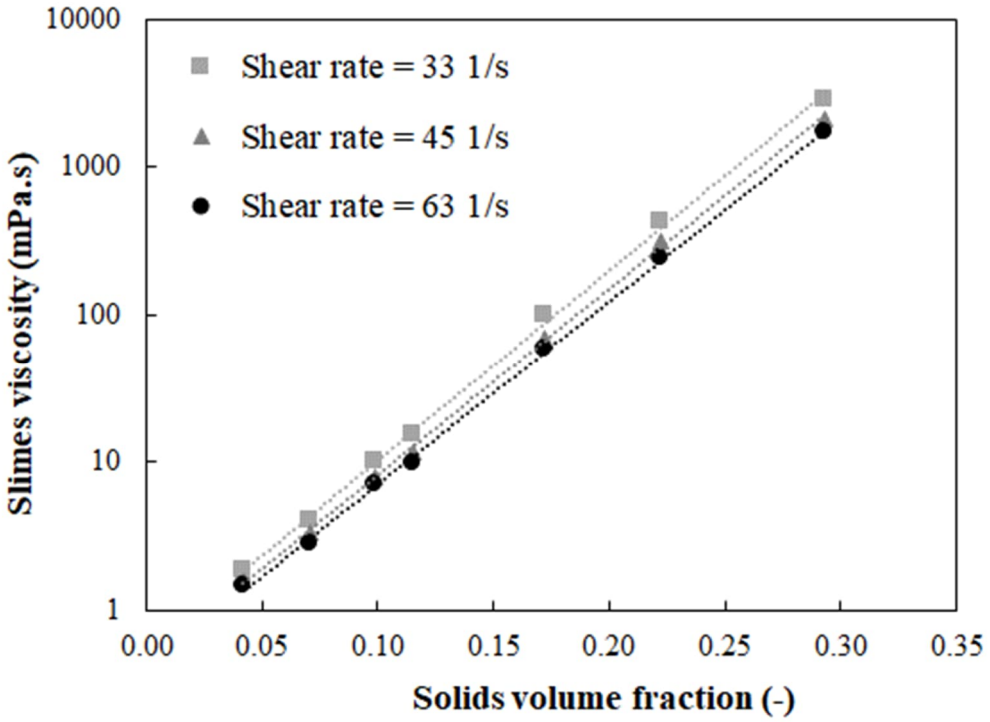

Figure 22. Slimes viscosity of the 0-20 µm particles as a function of the pulp density for three shear rates.

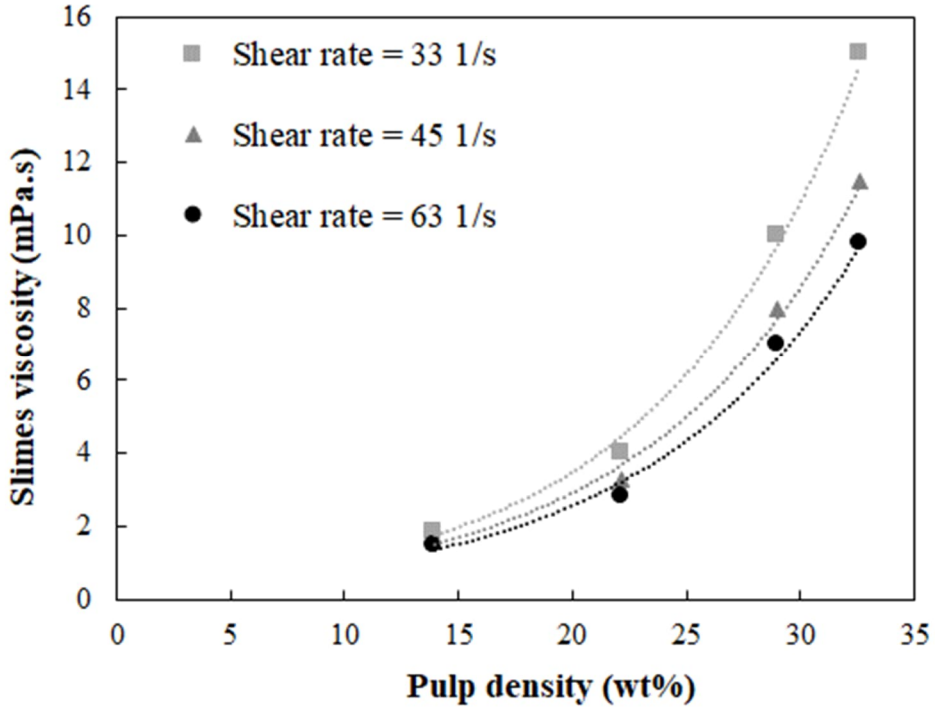

3.4.9. Error Analysis

The direct comparison of the balanced and raw data sets reveals very strong steady state consistency, and in turn very low mass balance errors across this work. The average error in the assays between Table 17 and Table 18 and between Table 13 and Table 14 is 0.6% of the assay value, neglecting outliers including errors of zero. Thus, the highest grades in this work were 65.6+/-0.4% for Sample A and 66.3+/-0.4% for Sample B. Using this uncertainty in the assays, and the two product formulae for recovery, a Monte Carlo analysis produced an estimated error in the recovery of 0.6% of the recovery value. Thus, the corresponding recoveries for Samples A and B were 72.9+/-0.4% and 84.7+/-0.5% respectively. As noted previously, this precision is attributed to the experimental method used to deliver the feed.

This research involved a systematic program of experiments aimed at developing an understanding of the underlying, albeit complex, physical processes involved in the

hydrodynamic transport of the particles through the Reflux Classifier. Highly consistent data sets were generated, ideal for validating future models. Part II of this study uses the data set to assess the extent to which the data conform to a generic partition surface. It is evident the feed is largely of a binary nature, meaning the separation performance could be assessed using the partition surface covering the low-density quartz and the high-density hematite, modified slightly to reflect the mineralogy. By using this data set to validate the partition surface it will be possible for practitioners to readily predict the potential grade-recovery relationship for very different feeds.

3.5. Conclusions

This paper provides a comprehensive and detailed investigation of the gravity separation of a dense mineral feed in a Reflux Classifier. The experimental conditions covered different density set points, feed pulp densities, throughputs, fluidization water rates and lamella channel spacings. The work showed the clear potential of a single stage gravity separator in upgrading dense minerals down towards a lower nominal particle size of 10 µm. This means that gravity separation could be used to replace reverse flotation, resulting in a significant reduction in the complexity, cost, and environmental impact of the beneficiation circuit. Although the bed density set point provides an effective measure of control, other factors are arguably more important, especially those that impact on the hydrodynamics within the inclined channels.

The feed iron grade was upgraded from 37% to 65.6% at a recovery of 72.9%. Note that pure hematite has an iron grade of 69.9%. The loss in recovery is attributed to the slow settling of the relatively fine particles and to the presence of goethite in the iron ore. The solids throughput achieved was 9 $t/m^2/h$, notably higher than achieved by reverse flotation (typically 4 $t/m^2/h$). A separate feed, Sample B, containing much less goethite, was also processed in the Reflux Classifier, achieving an iron grade of 66.3% and iron recovery of 84.7%. This work demonstrated the importance of maintaining a sufficient volumetric feed rate to promote shear induced inertial lift of the coarse gangue silica within the inclined channels. These conditions are needed to convey these particles into the overflow reject stream. Interestingly, the separation performance improved as the throughput was increased.

Benefits were also observed by reducing the feed pulp density, most likely due to the corresponding reduction in the suspension viscosity. In fact, the poorest performance was obtained at a higher feed pulp density of 36 wt% while the best performance was observed at the lower feed pulp density of ~17 wt%. The best overall results were obtained by increasing the volumetric feed rate to 8 L/min and lowering the feed pulp density to 17 wt% solids.

The fluidization rate must be set at a rate sufficient to suspend the particles in the lower bed. This work showed that excessive fluidization caused a strong decline in the iron recovery. Finally, although most of this work involved an inclined channel spacing of 1.8 mm, and it was concluded that this spacing gave the best performance, the separations observed using a channel spacing of 3.0 mm were more than satisfactory. Moreover, any reduction in the level of coarse silica in the feed would deliver a step change improvement in product grade.

3.6. Appendix A

Supplementary material Supplementary data to this article can be found online at https://doi.org/10.1016/j.mineng.2023.108187.

4. Gravity separation of fine itabirite iron ore using the Reflux Classifier – Part II – Establishing the underpinning partition surface[3]

[3]Rodrigues, A.F.d.V., Delboni Junior., H., Zhou, J., Galvin, K.P., 2024. Miner. Eng. 210, 108641, https://doi.org/10.1016/j.mineng.2024.108641

4.1. Abstract

This work assessed the potential of a single stage Reflux Classifier to upgrade itabirite iron ore to high grade at satisfactory recovery. Part I reported on the detailed findings of the experimental program and the physical transport of the particles through the system. A key purpose of the present paper was to deduce the underlying partition surface from relatively basic feed information on the Fe assays obtained as a function of the particle size. Conversion of the feed data into a simple binary description based on the density of hematite and density of silicates was used. This approach then provided a basis for applying the partition surface to a given feed to predict the separation performance. Data from the experiments were compared to values predicted from the partition surface. A least squares objective function was used to implicitly deduce the parameters governing the partition surface, notably the key exponent n and the Écarté Probable, E_p. Across 12 of the experiments, the exponent, n, governing the partition surface was found to be 0.26+/-0.02. This result was in very good agreement with the value of 0.28 determined previously. The second key parameter, the E_p, was also determined for each of the experiments. The lowest E_p, found to be 365 kg/m^3 for a low slimes viscosity, was also in good agreement with the result reported previously for a deslimed feed. This work provides confidence in the application of the partition surface to predict similar dense mineral separations, and stronger insights into the mechanisms responsible for the separation.

4.2. Introduction

Beneficiation of the fine itabirite iron ores of Brazil is achieved by reverse flotation of the quartz gangue, operated through a sequence of rougher and cleaner flotation stages, typically achieving a processing rate of 4 t/(m^2h). The feed to the reverse flotation must first undergo a desliming stage, involving hundreds of cyclones, to remove silica slimes finer than about 20 mm, given these slimes reduce the flotation efficiency (Lima et al, 2012; 2020). Ultrafine iron ore is therefore lost in the desliming stage, and by entrainment during the reverse flotation. The iron ore product from the reverse flotation, released via the underflow of the cells, is then sent to the product thickener to achieve a sufficient pulp density ahead of the final dewatering.

In Part I the feasibility of a vastly simpler method of beneficiation was investigated (Rodrigues et al, 2023). In principle, the Reflux Classifier offers the potential to achieve the required product grade in a single stage separation (Amariei, 2014), without the need for the desliming stage, reverse flotation stages, and product thickening (Rodrigues et al, 2023). There is now increasing interest in achieving very high grade, ideally as high as 67% Fe, to support direct reduction using hydrogen, and to support blending. Moreover, with minimum fluidization at a solids volume fraction more than 0.40, the corresponding solids concentration in the lower bed and by inference in the underflow exceeds 70wt% solids.

The Reflux Classifier, shown schematically in Figure 23, consists of a series of inclined channels above an upward current fluidized bed (Galvin, 2021). When the feed enters the system, most of the flow passes up through the system of inclined channels while the faster settling particles segregate downwards towards the lower fluidized bed. Within the inclined channels the denser particles form a sediment that slides downwards, joining the underflow, while the less dense particles are conveyed upwards towards the overflow. Fluidization water permeates up through the lower fluidized bed. Pressure transducers are used to quantify the suspension density in the lower bed, in turn controlling the discharge of underflow product.

Figure 23. Schematic representation of the Reflux Classifier showing feed entry, overflow tailings, and underflow product via the off-take pump. Laboratory systems use the patented underflow buffer arrangement below the Reflux Classifier to minimize the non-linear effects of the control valve on discharge from a small-scale laboratory system.

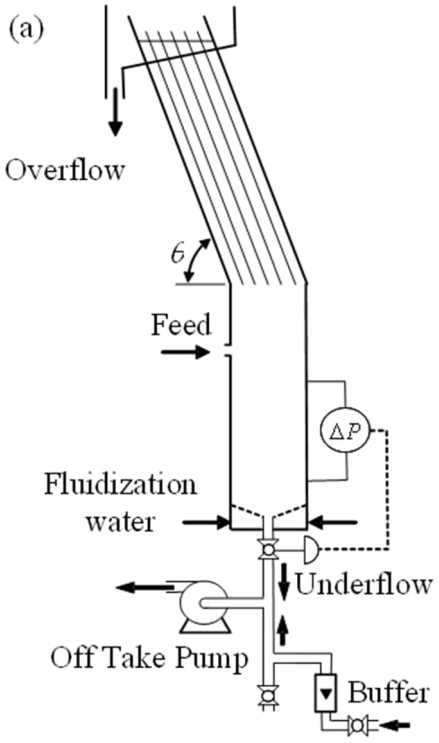

The experimental conditions used in Part I covered different density set points, feed pulp densities, throughputs, fluidization water rates and lamella channel spacings of 1.8 and 3.0 mm. A broad range of separation performance was observed, leading to two key results. Firstly, it was concluded that the product grade improved by promoting shear induced inertial lift (King and Leighton, 1997) of the coarser silica within the inclined channels, achieved by increasing the volumetric feed rate. Secondly, it was concluded the suspension viscosity impacted on the particle segregation. Hence the best performance was achieved by a combined change of lowering the feed pulp density and increasing the volumetric feed rate. The feed iron grade was increased from 37% to 65.6% at a recovery of 72.9% and solids throughput of 9 t/(m^2h). The analysis in Part I, however, was largely qualitative.

Clearly, it is not practical to undertake an extensive program of research like that conducted in Part I on every feed of interest. The best approach to assessing different feeds is to firstly quantify the size and density distribution and apply that information to the partition surface of the separator, and in turn quantify the expected final product grade and recovery. It is often difficult securing the detailed size and density distribution. It is common practice in minerals processing, however, to undertake a sieve analysis of the feed, and determine the relevant assays for each size fraction. For well liberated feeds such as these itabirite iron ores, it may be possible to convert these basic data into a simple binary representation of the feed.

Galvin et al (2020) previously reported on the partition surface of a Reflux Classifier, based on data for a chromite feed ranging in particle size from 300 mm down to zero, with nominal desliming at 38 mm. Detailed sink-float analysis was used to obtain the underlying partition surface. Equation 1 provides an expression for describing the value of the separation density, D50, as a function of the particle size, S. That is,

$$\frac{(D_{50} - D_w)}{(D_o - D_w)} = \left(\frac{S}{S_o}\right)^{-n} \tag{4}$$

Dw is the density of the fluid medium, water, D_o an adjustable reference density, So a reference particle size set at 300 mm, and n, an exponent value. The underpinning physics is assumed to involve a simple scaling law between the buoyant density, (D_{50}-D_w), and the particle size, S, raised to the power, -n. With D_w and n fixed, we need just one additional parameter value to define the entire relationship. To introduce physical meaning into that additional parameter we have configured Equation 1 in terms of two parameters that carry dimensions. Thus, we have introduced the reference density, D_o, which becomes the adjustable parameter, and have set the additional parameter, S_o, to 300 mm.

For channels with a perpendicular spacing z=3 mm they obtained n=0.28. They also reported a value for the Ecarte Probable, E_p=325 kg/m^3. Interestingly, for the closely spaced channels, z=3mm, the value of the E_p was reasonably constant, independent of the particle size. The Whiten Equation (Scott and Napier-Munn, 1992) provided a

formal description of the partition surface for particles of a given density, D, based on the value of the D_{50} from Equation 4. That is,

$$P = \frac{1}{1 + \exp\left(\ln(3)\frac{(D_{50} - D)}{E_{\mathrm{p}}}\right)} \tag{5}$$

where P is the fraction of the particles of a given density, D, and size, S, reporting to the underflow. It is noted that this former work covered relatively few experiments, and limited validation.

The objective of Part II of this work is to investigate the underpinning partition surface model for the separations produced in Part I. The basic information on the feed supplied to the Reflux Classifier is converted into a binary form for the minerals, hematite, and silica, with the assumption the mineral species are well liberated. Table 28 from Part I shows the feed it liberated. As shown later in Table 29, the raw data generated from the underflow product stream has a grade ~69 wt% Fe in the primary size fractions, from 0.020 to 0.90 mm. Pure hematite has a grade of 69.9 wt% Fe. These data, and the high Fe recoveries support the assumption of a well liberated feed.

The partition surface described above has three unknown parameters, which are arguably orthogonal: the adjustable parameter, D_o, used to raise, and lower the partition surface, the exponent value, n, and the value of the E_p. In this paper, these values are computed objectively using the Solver routine in Microsoft Excel subject to the need to achieve a strong agreement with the experimental data of Part I. The key data used in the objective function includes the fractional grades and recoveries (for each size fraction) and the overall product head grade and recovery.

This analysis seeks to reveal the extent of variation in the value of n in Equation 4, and importantly how the E_p varies over a wide range of operating conditions, especially through changes in the volumetric feed rate, and the feed weight % solids (which influences the suspension viscosity). This depth of insight covering separations down

to particle sizes as fine as 10 microns has not previously been obtained. The findings should underpin the application of the partition surface model for new feeds.

4.3. Establishing Feed as a Binary Mixture

A key goal of this study is to utilise basic data on the dense mineral assay as a function of the particle size covering the feed, product and reject flow streams to quantify the partition surface. In the minerals industry it is recognised that it is very difficult and expensive to secure the so-called washability data. Washability data involves a sink-float analysis across the density range, and across the full particle size range. A key question here is whether there are alternative ways to construct the feed washability data, and in turn quantify the underpinning partition surface from the assay data.

The itabirite ore is known to liberate strongly into a nearly pure hematite component and low-density gangue component mainly comprising silica. This section outlines the deconvolution of the feed data into a simple binary description of the feed, quantified in terms of the particle density. This approach then provides a basis for applying the generalized partition surface to the feed guided by the separation performance. Data from the experiments can then be used to deduce the partition surface.

Table 27 shows the theoretical approach used to construct the feed for use in the assessment of the experimental data in this study. The first column lists the geometrical mean particle size. For example, 28 mm is the geometric mean of the upper and lower sieve sizes of 38 and 20 mm. The exception is the finest particle size of 10 mm, which is an arithmetic mean of 20 and 0 mm. The grey section of the Table denotes the standard description of the feed based on the Fe wt% assay for each size fraction, showing an overall cumulative Fe grade of 36.9 wt. %. Using a feed mass basis of 100 kg, the mass of Fe_2O_3 is calculated directly, and then summed to give the total of 52.80 kg. The next column shows the mass % Fe_2O_3. The balance is largely silica, described as the Light component. Those values are calculated by difference to give a total Light mass of 47.20 kg. The mass % Light is then listed. These data form the basis of the partition surface modelling.

Table 27. Binary Feed Calculations for Run 13. Note 1.0 kg Fe equals 1.430 kg Fe_2O_3

Geometric Mean Size (mm)	Feed Mass (%)	Cum. Mass (%)	Grade Fe (wt. %)	Cum. Grade Fe (wt. %)	Mass Fe_2O_3 (kg)	Mass Fe_2O_3 (%)	Mass Light (kg)	Mass Light (%)
0.354	0.5	0.5	15.3	15.3	0.10	0.19	0.35	0.75
0.212	4.5	5.0	15.8	15.8	1.02	1.93	3.48	7.38
0.164	5.4	10.3	17.9	16.8	1.37	2.60	4.01	8.49
0.137	9.0	19.4	20.2	18.4	2.60	4.93	6.43	13.62
0.106	22.3	41.6	24.8	21.8	7.91	14.99	14.37	30.44
0.075	20.9	62.5	40.3	28.0	12.02	22.77	8.86	18.76
0.053	11.8	74.3	52.4	31.9	8.79	16.66	2.96	6.26
0.041	3.3	77.6	55.6	32.9	2.63	4.98	0.68	1.44
0.028	6.1	83.7	57.7	34.7	5.06	9.58	1.07	2.27
0.010	16.3	100.0	48.5	36.9	11.29	21.39	5.00	10.59
	100.0				52.80	100.00	47.20	100.00

4.4. Experimental

Table 28 lists the experimental program reported on in Part I for feed A. In most of the experiments the inclined channel spacing was 1.8 mm, the density set point 2000 kg/m^3, volumetric feed rate 5 L/min, feed pulp density 26 or 27% solids, and fluidization rate 0.14 L/min. It is noted the vessel cross-sectional area was 0.1mx0.1m, hence the standard volumetric feed flux of 5 L/min corresponds to a volume flux of 30 $m^3/(m^2.h)$. It is evident that in most of the experiments just one parameter was varied at a time, hence cause and effect were readily interpreted. The initial phase focussed on changes in the volumetric feed rate, from 2, to 4, to 6 L/min. Then the effect of the set point density was varied, followed by the feed pulp density, the fluidization rate, then the channel spacing, and finally combinations of changes were introduced.

Our group has introduced a new method for feeding a mineral separator in the laboratory which, if followed, leads to a significant reduction in feed variability and strong internal consistency across multiple experiments (Crompton et al, 2022; Starrett and Galvin, 2023). The principles of the new method, which were outlined briefly in Part I, lead to high quality data, such that the balanced data set is numerically very close in value to the raw data set. Briefly, the method involves discharging a well-mixed

feed suspension of about 1500 Litres into approximately 100 part-filled 20 Litre buckets, then applying a random sequence to those buckets. A relatively small feed tank with a capacity of ~ 300 Litres is then used to feed the separator. The volume of this feed tank is maintained by adding the contents of the buckets in the randomised sequence until the experiment is completed. With less uncertainty in the data, it is possible to secure much more knowledge from a single experiment.

Table 28. Summary of conditions used in the experimental program on Sample A in Part I. (*Pulp densities for Runs 1 and 9 have been reviewed and adjusted due to minor rounding errors in Part I; Run 1 value of 26 increased to 27 and Run 9 value of 27 decreased to 26 wt%)

Run No.	**Channel spacing** (mm)	**Set point** (kg/m^3)	**Feed rate** (L/min)	**Throughput** ($t/h/m^2$)	**Pulp density** (wt%)	**Fluidization rate** (L/min)
1	1.8	2000	2	5	27*	0.12
2			6	10	26	0.14
3			4	7	26	
4		2200	5	9	27	
5		2100		9	27	
6		1900		9	27	
7		2000		14	36	
8				6	16	
9				9	26*	0.17
10				9	27	0.20
11	3.0			10	27	0.14
12			8	9	16	
13	1.8			9	17	

4.5. Results and Discussion

4.5.1. Run 13 – A Case Study

The experiments in Part I produced new knowledge, firstly showing that a higher volumetric feed rate improved the product grade by increasing the shear induced inertial lift, secondly that dilution helped to improve the recovery of the iron ore in the underflow by effectively removing the effects of suspension viscosity, and that the more closely spaced inclined channels of 1.8 mm improved the grade and recovery by increasing the lift force and the effective sedimentation area respectively. Run 13 was effectively the culmination of all these factors. Thus, results from Run 13 are based on the best set of operating conditions used in the Part I study and are therefore presented first.

Table 29 shows the raw data set and Table 30 the mass balanced data set. It is evident there is strong consistency in these sets confirming the strong adherence of the raw data to steady state material balance. The feed entered the Reflux Classifier with an Fe wt% grade of 36.5% (balanced value 36.9%), producing an overall Fe wt% product grade of 65.9% (balanced value 65.6%), and overall Fe wt% reject grade of 16.6% (balanced value of 17%). These overall values correspond to a balanced Fe recovery of 72.9%.

In order to ensure the highest possible internal consistency in the analysis, the evaluation of the experiments was based on the balanced data sets. Table 31 shows the partition surface analysis applied to the balanced feed data set given by Table 27. Firstly, the D_{50} is determined as a function of the particle size using Equation 4, with S_o=300 mm, D_o=3019 kg/m^3, and n=0.27. It is noted that either So or Do can be varied, but not both. Here So=300 mm is fixed for all cases. The other two parameters were used as search variables in the Solver Routine in Microsoft Excel, discussed later. Interestingly, the value of n=0.27 is very close in value to the result obtained by Galvin et al (2020) for a chromite ore. The second parameter, Do, is used to either raise or lower the partition surface, like the way the set point density of the Reflux Classifier is

raised or lowered to vary the grade and recovery. It is noted however that these two quantities are not directly related.

Table 29. Raw data for Run 13

Feed				Product			Reject		
Size (mm)	Mass (%)	Grade (%Fe)	Cumulative (%Fe)	Mass (%)	Grade (%Fe)	Cumulative (%Fe)	Mass (%)	Grade (%Fe)	Cumulative (%Fe)
0.354	0.5	16.4	16.4	0.6	21.8	21.8	0.3	3.1	3.1
0.212	4.6	15.8	15.9	4.2	37.6	35.7	4.6	1.4	1.5
0.164	5.8	17.9	16.9	4.0	51.6	43.0	6.2	1.4	1.5
0.137	9.2	20.2	18.4	6.1	62.1	50.9	11.2	1.5	1.5
0.106	22.9	25.0	21.9	14.8	67.2	59.0	28.4	2.6	2.1
0.075	20.3	40.1	27.8	32.0	69.2	64.3	13.1	5.7	2.9
0.053	11.5	52.2	31.5	20.3	69.7	65.6	5.8	14.5	3.8
0.041	3.3	55.7	32.5	5.4	68.9	65.8	1.8	25.1	4.4
0.028	6.2	57.5	34.4	9.0	69.4	66.2	4.0	41.3	6.3
0.010	15.7	48.2	36.5	3.6	58.3	65.9	24.7	47.9	16.6

Table 30. Balanced Data for Run 13

Feed				Product			Reject		
Size (mm)	Mass (%)	*Grade* (%Fe)	Cum. Grade (%Fe)	Mass (%)	Grade (%Fe)	Cum. Grade (%Fe)	Mass (%)	Grade (%Fe)	Cum. Grade (%Fe)
0.354	0.5	15.3	15.3	0.7	22.8	22.8	0.3	3.2	3.2
0.212	4.5	15.8	15.8	4.4	37.6	35.6	4.6	1.4	1.5
0.164	5.4	17.9	16.8	4.3	51.6	43.0	6.1	1.4	1.5
0.137	9.0	20.2	18.4	6.7	62.3	51.1	10.6	1.5	1.5
0.106	22.3	24.8	21.8	18.6	67.5	59.9	24.9	2.6	2.1
0.075	20.9	40.3	28.0	27.7	69.1	64.0	16.1	5.7	3.0
0.053	11.8	52.4	31.9	19.7	69.5	65.3	6.2	14.5	4.1
0.041	3.3	55.6	32.9	5.6	69.0	65.6	1.7	25.2	4.6
0.028	6.1	57.7	34.7	8.8	69.2	65.9	4.3	41.3	6.7
0.010	16.3	48.5	36.9	3.6	58.3	65.6	25.2	47.5	17.0

The density values assumed for the heavy and light components were 5100 and 2675 kg/m^3 respectively. The value for the light species is higher than for pure quartz to allow

for impurity from the iron oxide as noted later. Table 31 lists the calculated partition numbers (%) obtained using Equation 5, based on the D_{50} values derived from Equation 4. Equation 5 requires one additional search variable, namely the E_p. The value of the E_p was found to be 365 kg/m^3, of similar magnitude to the numerical value of 325 kg/m^3 reported by Galvin et al (2020). These three values, D_o=3019 kg/m^3, n=0.27, E_p=365 kg/m^3 led to a minimum in the value of the objective function used in the Solver Routine, which is defined later. The function was formed from the errors in the grades and recovery values for each particle size fraction, and the errors in the overall head grade of the product, and the overall Fe recovery.

Figure 24 shows the calculated partition number (%) as a function of the particle size for the heavy and light components, based on the values reported in Table 31. It is evident the partition number for the Fe_2O_3, density 5100 kg/m^3, is 99.9% for the 354 mm particles, and that the partition number declines monotonically, remaining relatively high at 98.7% for particles of 106 mm, 69.5% for particles of 28 mm, declining sharply to 5.9% at 10 mm. For the silica species, the corresponding partition numbers are 31.6, 4.8, 0.2%, and 0% for particles 354, 106, 28, and 10 mm. Based on a feed of 100 mass units, the mass of Fe_2O_3 reporting to the product is obtained by multiplying the mass values in Table 27 by these probabilities. The same approach is used to compute the mass of SiO_2 reporting to the product.

Figure 24. Model partition number as a function of the particle size for the heavy (Fe_2O_3) and Light components (eg SiO_2). It is evident a high proportion of the heavy Fe_2O_3 component is recovered, while a much lower proportion of the Light component is recovered, primarily at coarser sizes.

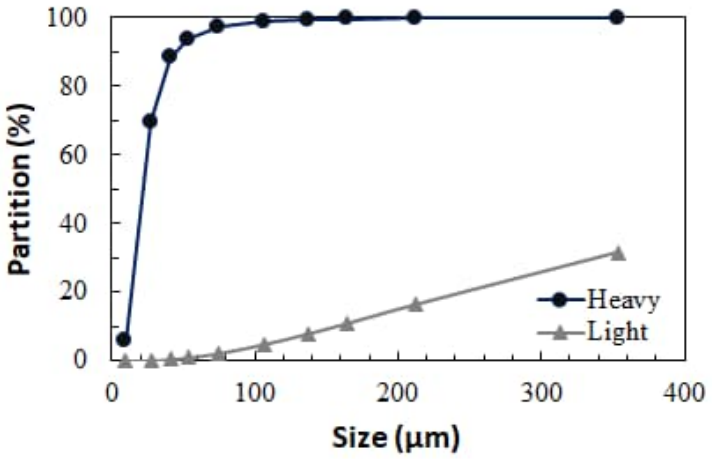

The model used in this study incorporated one correction for the Fe_2O_3 unliberated from the silicates. It was assumed universally in the model that the silicates that reported to the overflow carried a mass portion of 1.6% Fe_2O_3. This singular correction to the model, which was incorporated as part of the error minimization using the Solver routine, was necessary to address the fact that the silicates were not fully liberated, especially for the coarser sizes. For example (using more significant figures), at 212 mm the mass of Fe_2O_3 in the feed, shown in Table 27, is 1.0165 kg, or 1.02 kg to two decimal places. The partition number to two decimal places is 99.66% so the mass of Fe_2O_3 to the product underflow is 1.0130 kg. The mass of the Light species in the feed, shown in Table 27, is 3.483 kg. The partition number to the underflow is 16.45%, hence the mass to the underflow is 0.573 kg. The loss of Fe_2O_3 to the overflow via the Light species is 0.016x(3.483-0.573)=0.0466 kg. Thus, the corrected Mass* of Fe_2O_3 to the underflow is 1.0130-0.0466=0.966 kg (ie 0.97 kg). The Light species reporting to the underflow is 0.57 kg. This corrected value of Fe_2O_3 is then summed with the mass of the Light species reporting to the underflow to obtain the total product underflow mass of 1.54 kg for that size fraction. The approach, while not exact, provides for a very

simple and realistic correction for lower Fe_2O_3 recovery at the coarser sizes. An exact calculation would require the introduction and consideration of a mixed particle species.

The right-hand panel of Table 31 shows the model calculations for the product from Run 13. These should be compared directly with the middle panel of Table 30 which lists the balanced data set for the product. It is evident the model produced a cumulative product Fe grade of 65.6 wt%, identical to that shown in Table 30. This agreement simply reflects the objective function which drove this error to near zero. A stronger measure of the model performance can be seen in the corresponding mass % and Fe % values for each of the size fractions in Table 30 and Table 31. The agreement is strong.

Table 31. Underflow product obtained using the partition surface and feed data from Table 27.

Size	Model	Density		Partition		Mass	Mass*	Mass		Mass	Grade		Cum.
	D_{50}	Fe_2O_3	Light	Fe_2O_3	Light	Fe_2O_3	Fe_2O_3	Light	Total		Fe_2O_3	Fe	Fe
(mm)		(Kg/m^3)		(%)		(Kg)				(%)			
0.354	2932	5100	2675	99.9	31.6	0.10	0.09	0.11	0.21	0.50	45.8	32.1	32.1
0.212	3215	5100	2675	99.7	16.5	1.01	0.97	0.57	1.54	3.74	62.8	43.9	42.5
0.164	3372	5100	2675	99.4	10.9	1.37	1.31	0.44	1.75	4.25	74.9	52.4	47.4
0.137	3491	5100	2675	99.2	7.9	2.58	2.49	0.51	2.99	7.28	83.0	58.1	52.3
0.106	3667	5100	2675	98.7	4.8	7.81	7.59	0.69	8.28	20.13	91.6	64.1	58.9
0.075	3924	5100	2675	97.2	2.3	11.68	11.54	0.20	11.75	28.57	98.3	68.7	63.3
0.053	4208	5100	2675	93.6	1.0	8.23	8.18	0.03	8.21	19.98	99.6	69.7	64.8
0.041	4433	5100	2675	88.1	0.5	2.32	2.31	0.00	2.31	5.62	99.9	69.8	65.1
0.028	4827	5100	2675	69.5	0.2	3.51	3.50	0.00	3.50	8.51	100.0	69.9	65.5
0.010	6021	5100	2675	5.9	0.0	0.67	0.59	0.00	0.59	1.42	100.0	69.9	65.6

Figure 25 shows the product Fe grade as a function of the particle size and Figure 26 shows the Fe recovery as a function of the particle size. The error analysis was reported previously in Part I (Rodrigues et al, 2023). In this paper the error analysis is taken to a deeper level, based on the uncertainty in the E_p as described later. Based on the full mass balance, the overall Fe recovery was found to be 73 % and overall product grade 65.6%. In general, the grade obtained in the size range from 0 to 20 mm, characterised by the arithmetic average value of 10 mm, was consistently lower

than the model prediction. Ultrafine slimes and clays are efficiently removed from the product by the fluidization, but clearly not all the low-grade slimes are rejected. The partition surface will tend to predict a negligible presence of the low density ultrafines, but there is a finite presence of the hematite, hence the model predicts a high grade. There is also a modest discrepancy between the model and the experimental data at the coarsest size, but this is of little consequence given the exceedingly small mass presence of such particles in the feed. In general, the agreement between the model and the data sets derived from the experimental data were similar across the 13 runs. Appendix A shows the agreement achieved.

Figure 25. Comparison between the iron grade and the particle size showing the discrete experimental values (open triangles) and the partition surface model (black squares and red curve).

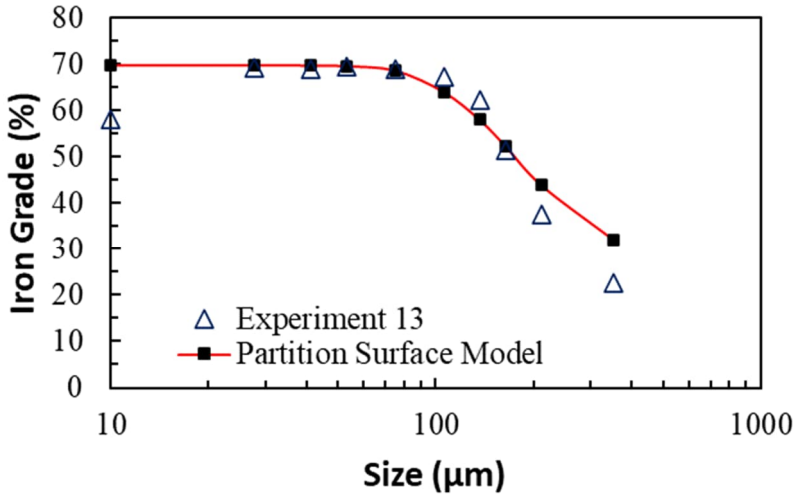

Figure 26. Comparison between the iron recovery and the particle size showing the discrete experimental values (open triangles) and the partition surface model (black squares and red curve).

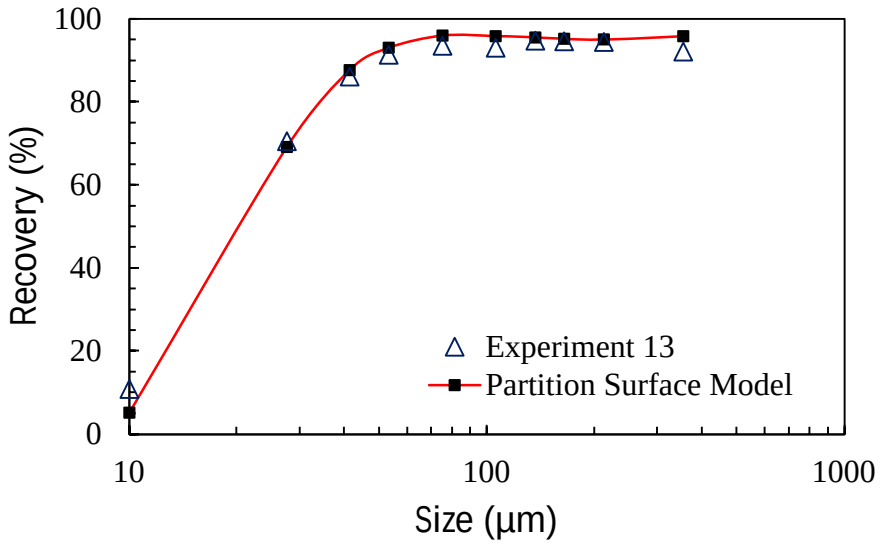

4.5.2. Application of the Partition Surface to 13 Separations

The remainder of this paper is focused on the full complement of experiments reported for this feed in Part I of the study. In all cases, as noted previously, it is assumed that additional Fe_2O_3 is lost to the overflow reject stream at the rate of 1.6% of the silica that partitions to the reject overflow. This is a simple approach, given the model remains binary in nature. However, the silica particles are effectively composites. It is of interest to determine whether these separations are also consistent with an exponent value of n=0.28 in Equation 4. Moreover, it is of interest to examine how the inferred E_p, derived from the use of the Microsoft Solver routine, varies with the experimental conditions. Will the fitted E_p show consistency and continuity across the broad range of conditions, or will the E_p carry significant levels of random noise arising from inconsistencies in the data and from the fitting of that data? This is a key question that addresses the internal reliability of the entire study. Reliable values of the E_p should further improve our physical understanding of the particle transport mechanisms in the Reflux Classifier.

The Solver routine in Microsoft Excel was used to quantify the partition surface for 13 different experiments. The objective function, F, for a given experiment is given by,

$$F = W_1 x\left(G_{ep} - G_{mp}\right)^2 + W_2 x\left(R_{ep} - R_{mp}\right)^2 + \sum(G_{ei} - G_{mi})^2 + \sum(R_{ei} - R_{mi})^2 \quad (6)$$

The first term involves the square of the error in the head grade of the product, where G_{ep} is the experimental product grade, and G_{mp} is the model product grade. The second term involves the square of the error in the product recovery, where R_{ep} is the experimental product recovery, and R_{mp} the model product recovery. These two terms have weightings of W_1=1000 and W_2=100 applied respectively, set to ensure a negligible grade-recovery error for an experiment. The final term is a summation of the squares of the errors in the grades and recovery for each particle size i. Here Gei is the experimental grade for size i, G_{mi} is the model grade for size i, Rei is the experimental recovery for size i, and R_{mi} is the model recovery for size i. Appendix A shows the agreement between the model and the experimental data for the 13 experiments.

As already noted, values for D_o and n in Equation 4, and the value of the E_p in Equation 5 were used as search variables. Equation 4 was used to obtain the D_{50} as a function of the particle size, S. In turn the D_{50} and the E_p were used in Equation 2 to obtain the partition number. The value of D, based on the density value given for the heavy component (5100 kg/m^3), was used to obtain the partition number for the heavy component. Similarly, the value of D, based on the density value for the light component (2675 kg/m^3), was used to obtain the partition number for the light component.

Table 32 shows the findings of this analysis for the 13 experiments. Interestingly, based on Runs 2-13, the value of n was almost constant at n=0.26 +/- 0.02, very close to the value of n=0.28 obtained by Galvin et al (2020). Each of these experiments was evaluated independently, yet produced almost the same value for the exponent, n. These results provide significant confidence in the value of this exponent. The larger value obtained for Run 1 corresponds to a relatively low feed rate, and in turn a

separation that is affected more strongly by particle size, more akin to a simple desliming of the feed.

Different values of the E_p were produced depending on the operating conditions. It is the significance of those differences that we now examine. This model is based on three distinct parameters, each of which operates orthogonally. The value of n governs how the D_{50} varies with particle size, while the E_p governs the separation efficiency and hence the grade and D_o governs the level of the partition surface and hence recovery.

Table 32. Analysis of 13 Runs using the reconstructed binary feeds and partition surface model. The value of the exponent n was found to be very consistent across Runs 2-13.

Run	Balanced Data							Model				
	Feed (%Fe)	Product (%Fe)	Reject (%Fe)	Recovery (% Fe)	Solids (t/m2.h)	Solids (wt. %)	Feed (L/min)	Do (kg/m^3)	Exponent n	Ep (kg/m^3)	Product (% Fe)	Recovery (% Fe)
1	36.5	45.1	16.0	87.0	4.7	27	2	1868	0.46	727.9	45.1	87.1
2	37.2	64.6	17.2	73.2	10.0	26	6	3203	0.22	483.3	64.6	73.2
3	36.4	59.7	14.4	79.7	7.3	26	4	2880	0.26	534.6	59.6	79.7
4	36.0	60.7	19.3	67.8	9.0	27	5	3211	0.24	632.4	60.7	67.8
5	36.9	60.4	19.0	70.7	9.0	27	5	3058	0.26	598.4	60.4	70.7
6	36.3	58.1	16.8	75.6	9.2	27	5	2916	0.27	614.2	58.1	75.6
7	36.8	61.2	26.8	48.2	14.4	36	5	3615	0.26	785.8	61.2	48.3
8	35.5	54.3	14.3	81.0	5.8	16	5	2574	0.32	535.7	54.3	81.2
9	37.3	61.3	18.8	71.4	8.6	26	5	3073	0.26	581.2	61.2	71.5
10	37.1	61.4	20.7	66.8	8.8	27	5	3130	0.27	605.5	61.3	66.8
11	36.3	63.6	19.9	65.7	9.9	27	5	3289	0.25	552.5	63.6	65.8
12	36.4	65.1	17.3	71.7	8.8	16	8	2979	0.29	372.3	65.1	71.6
13	36.9	65.6	17.0	72.9	8.7	17	8	3019	0.27	365.3	65.6	73.0

Given the strong consistency seen in the experiments described in Part I, which is also apparent from the very close agreement between the raw and balanced data, it is possible to have confidence in the data, although some level of conjecture must always be present. This means we can begin to routinely explore how the E_p varies with the specific experimental conditions. Figure 27 shows the reduction in the E_p as the feed flowrate was increased from 2, to 4, and then 6 L/min. Clearly, the reduction in the E_p with increasing flowrate is significant compared to the magnitude of the error bars. The basis for the error bars used in Figure 27, which denotes a standard deviation of 5%,

is outlined later with reference to Figure 28. The product grades were found to be 45.1% Fe, 59.7% Fe, and then 64.6% Fe, while the Fe recoveries declined. In this work the goal was to achieve an Fe grade of at least 65%, and ideally 67%, thus a modest loss in recovery was acceptable in targeting a high grade.

Figure 27. Model calculation of the E_p versus the feed flowrate used in Runs 1-3. It is evident the E_p declines significantly as the feed flow rate increases.

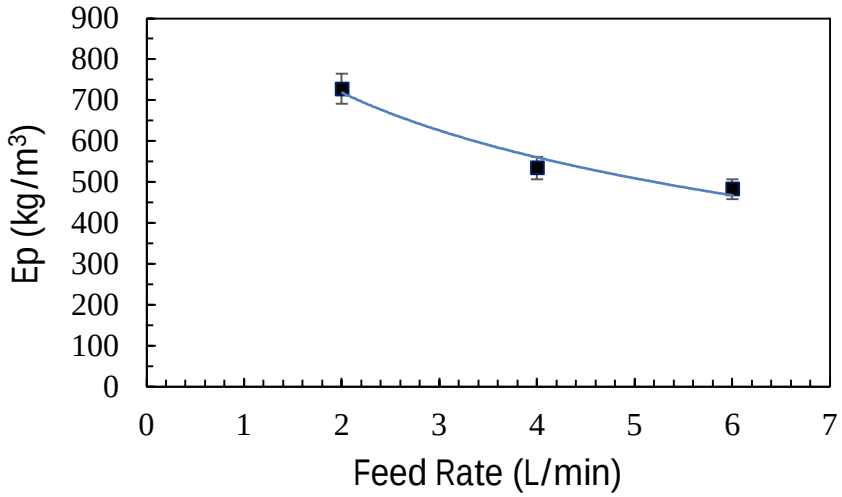

In the following series of experiments (4-10) the feed flow rate remained fixed at 5 L/min while a wide range of other modest changes were introduced. Figure 28 shows the reduction in the E_p due to the reduction in the feed weight % solids for the fixed flowrate of 5 L/min. Clearly, the strongest effect on the separation performance was due to changes in the feed weight % solids. An increase in the feed pulp density to 36% solids led to the E_p increasing to 786 kg/m^3, while a reduction in the feed pulp density to 16 wt. % solids led to an E_p of 536 kg/m^3. At the usual feed pulp density of 26%-27% solids for Runs 4, 5, 6, 9, and 10 the E_p had an average value of 606 kg/m^3 and standard deviation of only 28 kg/m^3. Based on these data we can conclude the standard deviation of the error in the E_p should be less than 5%. Hence error bars of 5% have been assigned.

The series of experiments conducted at the fixed flowrate of 5 L/min, and fixed feed weight % solids, showed the fluidization rate and the density set point of the controller had relatively little effect on the E_p. The product grades averaged 60 +/-1%. Despite

all the changes, it was not possible to shift the product grade significantly at the feed flow rate of 5 L/min. Surprisingly, when the channel spacing was increased to z=3 mm the grade did shift to 63.6 wt% Fe, but the recovery fell significantly to 65.7%. To achieve parity in the recovery at ~70% the set point would need to decrease, which would in turn lead to a lowering of the grade.

Figure 28. Reduction in the E_p due to a decrease in the weight % solids. This improvement in the E_p is likely due to the significant reduction in the slimes viscosity. All the data involved a fixed feed flowrate of 5 L/min.

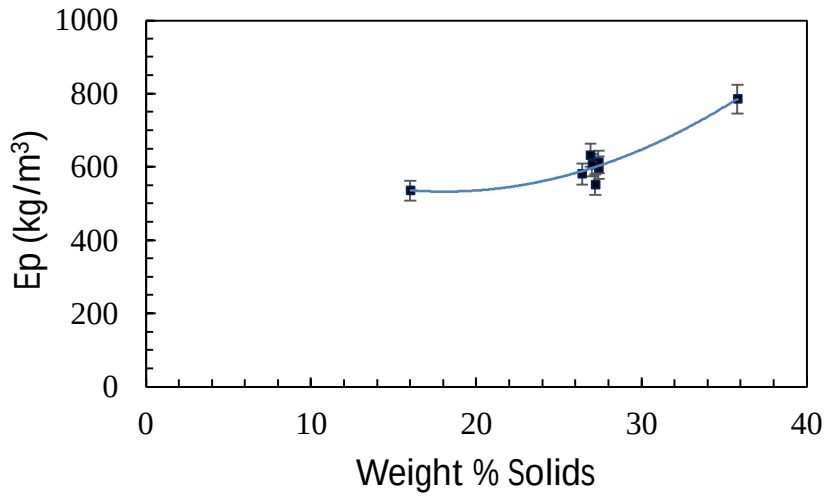

The decline in the E_p with pulp density is almost certainly due to the slimes viscosity as noted in Part I (Rodrigues et al, 2023). Figure 29 shows the E_p as a function of the slimes viscosity based on data from Part I at a shear rate of 63 s-1. The viscosity data were generated using suspensions from the Reflux Classifier overflow, formed from solids finer than 20 microns. There is no singular measurement that defines the viscosity during a separation, therefore the measured values used here only provide a form of characterisation of the experimental conditions. The viscosity increases exponentially with the wt% solids, as does the E_p. Thus, together the E_p and the viscosity correlate strongly, in fact appear to be linear. Interestingly, the E_p corresponding to the viscosity of water is close in value to the result at 16 wt% solids, meaning dilution has been successful in largely removing the effects of the slimes viscosity. At a feed pulp density of 26% solids the effect of slimes viscosity is modest, but at 36% solids there is a very large impact, with the recovery falling to only 48%. At

the lowest pulp density of 16% solids the grade fell to 54.3% while the recovery increased to a very high level of 81%. With this high recovery, it was anticipated that a strong performance would be possible by maintain the pulp density at 16 wt% solids and increasing the flowrate as shown later.

Figure 29. Correlation between the E_p and the slimes viscosity data from Rodrigues et al (2023). The data are based on a fixed flow rate of 5 L/min and (i) an E_p of 536 kg/m^3 at 16% solids (ii) an average E_p of 606 kg/m^3 at 26% solids and (iii) an Ep of 786 kg/m^3 at 36% solids. The viscosity values are 1.7, 4.8 and 13.7 mPas respectively at a shear rate of 63 s-1. These values are based on the feed concentrations, but it is acknowledged the actual concentration of the 0-20 micron portion of the suspensions within the inclined channels would have been lower.

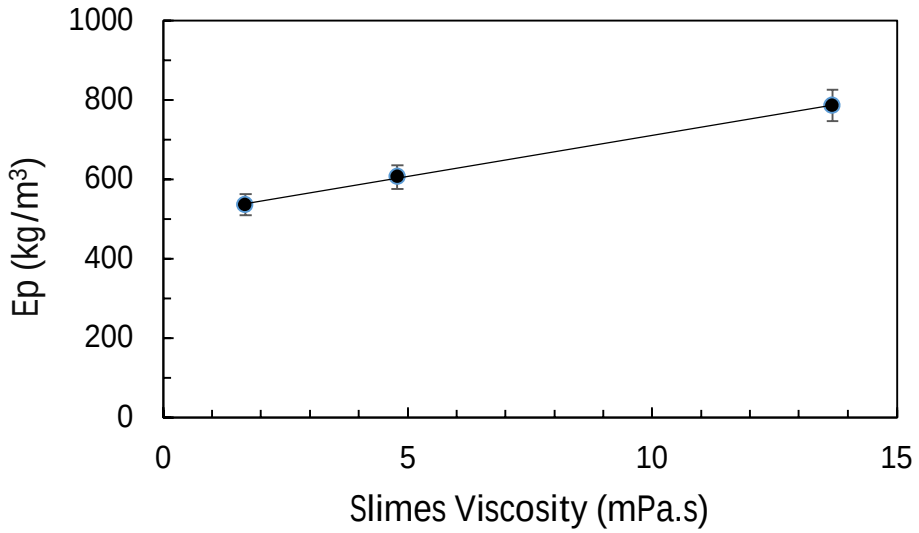

The combination of a further increase in the feed flow rate to 8 L/min, combined with a reduction in the feed pulp density, had the largest effect on improving the separation performance, as shown in Figure 30. Run 2, with a feed flowrate of 6 L/min, produced a step change reduction in the E_p. While this result in isolation might be questionable, in association with the larger reductions in E_p at a flowrate of 8 L/min appears to confirm the trend. Runs 11 and 12 involved a channel spacing of z=3 mm. Run 11 had a feed pulp density of 27% solids and feed flow rate of 5 L/min, resulting in a Fe grade of 63.6% and recovery of 65.7%. Run 12 had a pulp density of 15.9% solids and flowrate of 8 L/min. Here the Fe grade increased to 65.1% and the recovery increased to 71.7%,

a dramatic improvement. Moreover, the E_p fell from 552 to 372 kg/m^3. Again, this E_p=372 kg/m^3 is similar to the result obtained by Galvin et al (2020) for chromite. Here, the deslimed feed was also processed using an inclined channel spacing of z=3 mm, and the reported E_p based on the sink-float method was 325 kg/m^3.

Figure 30. Reduction in the E_p due to the combined effects of increasing the feed flow rate to 6 and then 8 L/min and reducing the feed pulp density. Interestingly this combination of a lower feed concentration and higher flowrate helps to preserve the solids processing rate.

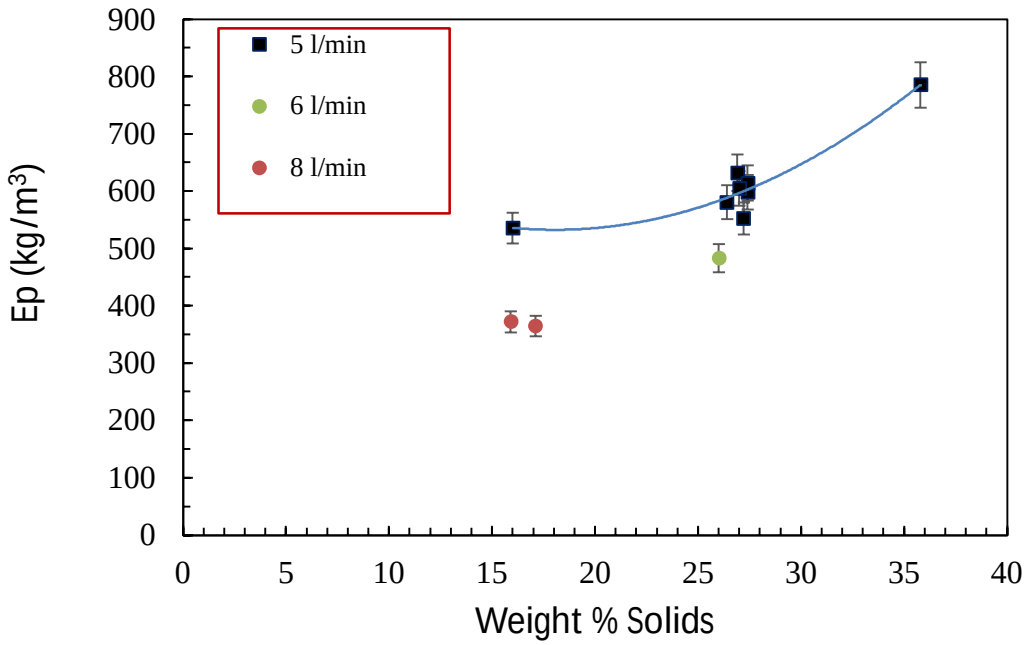

At this point we return to Run 13 which involved the narrower channel spacing of z=1.8 mm, a low feed pulp density of 17.1% solids and a feed flow rate of 8 L/min. In this case the product Fe grade was higher at 65.6% and the Fe recovery also higher at 72.9%. Clearly, the strong improvement in Run 12 over Run 11 was due to the lower pulp density and higher flow rate, and not due to the wider channel spacing of 3 mm, given Run 13 was also a stronger performer with the narrower channel spacing of z=1.8 mm. In this case the E_p was lower again at 365 kg/m^3.

In the limit as the feed solids concentration decreases, the effects of the slimes viscosity declines. We have previously investigated the effects of slimes viscosity (Carpenter et al, 2019) on the performance of the Reflux Classifier and observed its effect. It is therefore apparent that the lower feed pulp density case is similar to a deslimed feed where the E_p for the z=3 mm channels is approximately 372 kg/m^3, and for z=1.8 mm channels the E_p is 365 kg/m^3. But both results require a strong feed flowrate of 8 L/min, and hence a sufficient velocity through the system of inclined channels. We have previously reported on the mechanism of shear induced inertial lift (King and Leighton, 1997; Galvin and Liu, 2011). Here, coarse gangue particles experience shear induced inertial lift from the inclined surfaces, which leads to powerful entrainment of the silicates to the overflow. Basically, the higher volumetric flowrates result in more of the coarse gangue particles reporting to the overflow, hence a strong improvement in the Fe grade. This strong improvement in grade permits an improvement in Fe recovery across the board, however, there is a loss in Fe recovery at the finest particle sizes due to the higher flowrate. This means that at much higher flowrates the recovery of the finest portion of the feed will start to decline, impacting on the overall recovery. The improvement in the grade due to rejection of the coarse silicates could then be undermined by the loss of high-grade hematite at the finest sizes.

Figure 31 shows the grade-recovery curves generated directly from the model, based on the feed data from Run 13. The full curve is based on a fixed E_p of 365 kg/m^3, corresponding to the ideal operating conditions in Run 13. The filled-red data point denotes the result from Run 13. With the E_p fixed, and n=0.27, the entire curve is formed by simply varying Do. This approach, which provides a measure of the best separation performance, can be applied to alternative feeds. The dash curve corresponds to an E_p of 550 kg/m^3, typical of the other operating conditions investigated. The unfilled symbols correspond to Runs 1-12. As the flowrate is increased and pulp density reduced, operation moves from the dash curve to the full curve.

Figure 31. The grade-recovery curve is shown for an E_p of 365 and 550 kg/m^3, with n=0.27, and with data points shown from each of the experiments. This result illustrates the importance of reducing the value of the E_p.

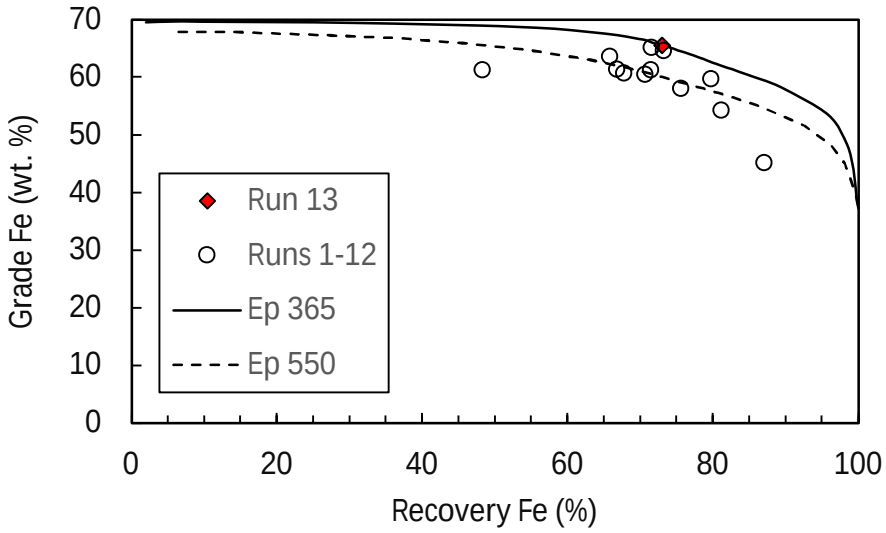

4.6. Conclusions

A comprehensive series of experiments was conducted using the Reflux Classifier on an itabirite feed. This work deduced the underpinning partition surfaces from relatively basic information on the Fe assays obtained as a function of the particle size. The feed data were converted into a simple binary description, quantified in terms of the particle density. This approach then provided a basis for applying the partition surface to the feed to calculate a separation. Data from the experiments were used to deduce the partition surface. The exponent, n, which describes the variation in the separation density with particle size was found to be approximately 0.26, very close to the value of 0.28 reported previously. With this consistency in the value of n, it was possible to also deduce the other model parameters, the value of D_o and the E_p. The value of D_o is concerned with the general level of the separation density and hence recovery. Thus, the work described in this paper provided strong measures of the changes in the E_p with key variables, the feed flow rate, and the feed weight % solids, the latter of which impacts the slimes viscosity. The primary conclusion is that the E_p is minimized by increasing the feed flow rate beyond 5 L/min, ideally to about 8 L/min, while also

reducing the feed concentration to a level sufficient to remove the effect of the slimes viscosity. (It is noted the standard volumetric feed flux of 5 L/min corresponds to a volume flux of 30 $m^3/(m^2.h)$.) The lowest E_p achieved for this feed was 365 kg/m^3. This work should prove useful in predicting the best possible grade recovery curve for new feeds, simply by setting the E_p to this lowest value, and then varying the value of D_o, with n=0.27.

4.7. Appendix A

Table 33. Grade and recovery versus particle size showing experimental data and model data. Values of n, E_p, and D_o in the Microsoft Solver Routine were varied so as to drive a close match between the experimental and model results. Remarkably, the average value of n was nearly constant across Runs 1-12 with an average value of n=0.26+/-0.02, meaning the underpinning variation in the D_{50} with particle size was nearly constant. The E_p accounted for the separation efficiency, governing the product grade at a given recovery, while D_o provided the agreement in the overall recovery.

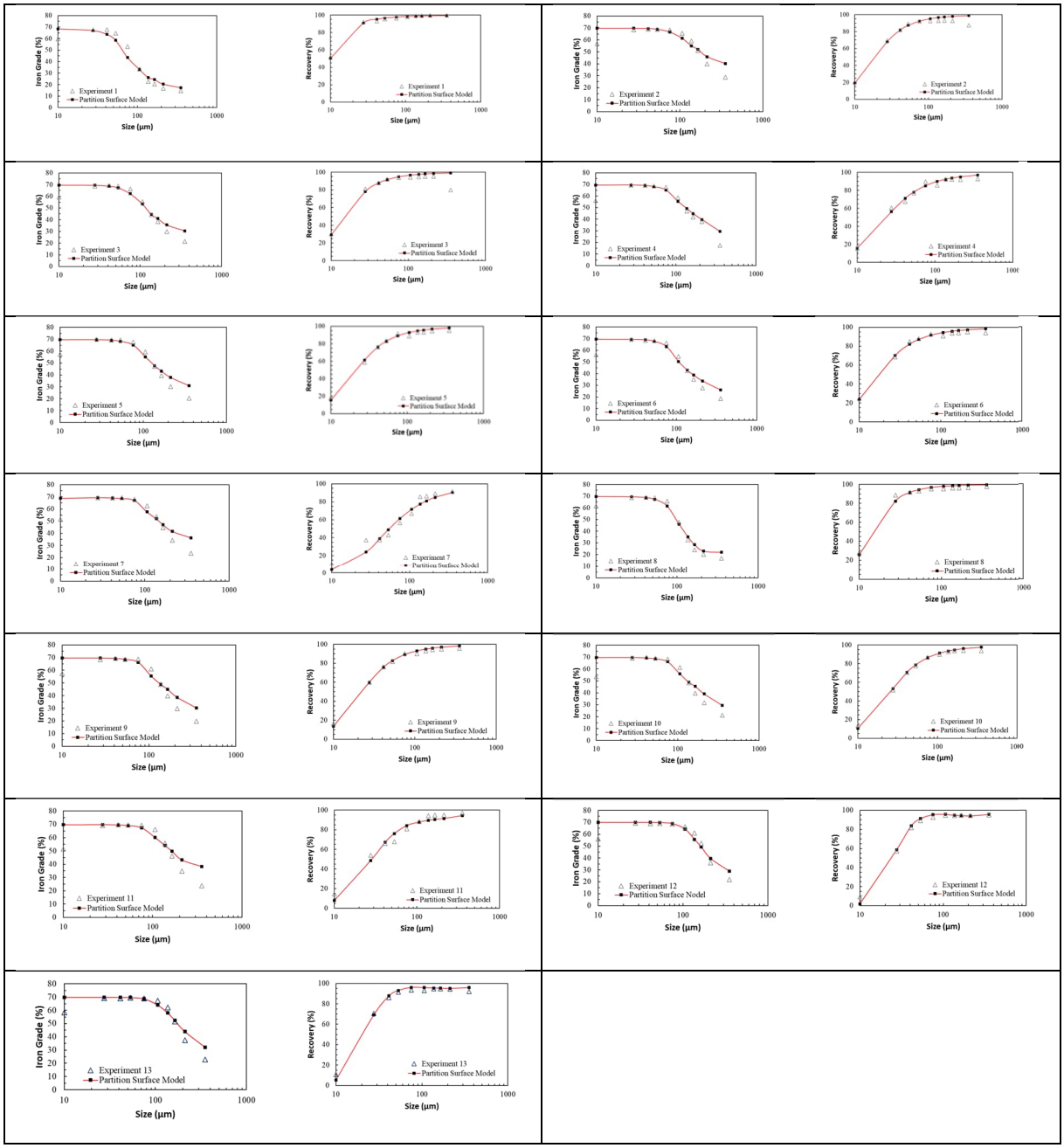

5. Transforming Iron Ore Processing – Simplifying the Comminution and Replacing Reverse Flotation with Magnetic and Gravity Separation[3]

[3]Rodrigues, A.F.V., Delboni Junior., H., Silva, K., Zhou, J., Galvin, K.P., Filippov, L.O., 2023. Miner. Eng. 199, 108112. https://doi.org/10.1016/j.mineng.2023.108112

5.1. Abstract

Much of the remaining iron ore resources in Brazil consist of low-grade itabirite ores. Accordingly, a typical beneficiation circuit includes a four-staged crushing/screening plant, followed by grinding in a closed-circuit ball mill, desliming in hydrocyclones and final ore mineral concentration via multistage reverse flotation and thickening of the final product. With the need for decarbonisation in the iron and steelmaking industry, there is a growing demand for high grade iron ore concentrate at more than 67% Fe. In the context of declining ore grades, there is an increasing need for a more effective circuit for beneficiating the itabirite ore. A proposed flowsheet consisting of a primary crushing stage, SAG mill, primary concentration using a VPHGMS magnetic separator, and a final concentration stage using the Reflux Classifier was investigated. The work demonstrated the significant reduction in energy consumption, and the potential for achieving high Fe grade of more than 67%, with high recovery, and in turn considerable process simplification. The new circuit would eliminate secondary to quaternary crushing, desliming stages, complex flotation circuits, product thickening and the flotation reagent plant. Further project assessments indicated an 8% smaller footprint, and 5% CAPEX and 42% OPEX reductions compared with the conventional circuit. These improvements would lead to a 50% higher Net Present Value.

5.2. Introduction

In ironmaking, it is essential to minimize and control the content of silica and alumina, the primary contributors to slag production. With increasing global interest in decarbonization of the industry, there is likely to be even greater interest in minimizing the production of slag, with a transition away from the use of blast furnaces, which utilize lower grade iron ore, to alternative methods of direct reduction, which require

higher grades of iron ore. It is noted that pure hematite (Fe_2O_3) has an iron content of 69.9%. In general, a pellet feed is classified as suitable for direct reduction when the iron content is higher than 67% or suitable for the blast furnace when lower than 67% (Morris, 2001). Morris (2001) has also noted that the high-grade pellets already attract a premium price due to the lower level of energy consumption in ironmaking and associated emissions. Clearly, new approaches in iron ore beneficiation will play a critical role in transitioning the global industry in the direction of so-called “green steel”.

In the recent past, iron ore resources from Brazil consisted of relatively high-grade iron ore, commonly processed via multi-stage crushing/screening, gravimetric concentration, magnetic separation, and reverse flotation. However, the high-grade iron ore reserves are in decline, resulting in the need to process the lower grade itabirite iron ores. Current methods of processing these itabirite ores involve high capital and operational costs (Segura-Salazar et al., 2018). Quartz is the primary gangue mineral (Hagemann et al., 2016), with the silica content often as high as 40%.

Conventional circuits seek particle size distributions finer than 0.15 mm for achieving adequate liberation of the itabirite ores (Rodrigues, 2014; França et al., 2020). Then, desliming is applied to remove the ultrafine silica below 20 microns in preparation for reverse flotation. Reverse cationic flotation, which involves the flotation of the gangue mineral, is the most widely used method of fine iron ore beneficiation (Filippov et al, 2014). Amines are employed as quartz collectors, while gelatinized corn starch is used as an iron oxide depressant (Araujo et al., 2005). Amines also act as a frother (Filippov et al., 2014). Flotation is performed in circuits consisting of mechanical cells, columns, or a combination of the two (Lima et al., 2016). High grade iron ore then emerges from the underflow stream of the cells, but at a low concentration of solids. Product thickening is therefore required ahead of the final dewatering stage.

Rodrigues et al. (2021) showed that autogenous or semi-autogenous grinding (AG or SAG) would lead to significant simplifications to Brazilian industrial iron ore plants. It was demonstrated that single-stage AG/SAG milling is technically feasible for itabirite grinding and is less complex and more efficient in energy consumption compared to traditional four-staged crushing and grinding circuits (Rodrigues et al., 2021). Lima et

al. (2013) compared the capital expenditure (CAPEX) and operational expenditure (OPEX) of semi-autogenous grinding followed by ball milling (SAB) and traditional multi-stages crushing/screening followed by ball milling (CB) circuit configurations, the former comprising primary crushing, SAG and ball milling, while the latter included a four-staged crushing plant followed by ball milling. The authors demonstrated not only the lower CAPEX and OPEX associated with the SAB circuit, but also that the difference in both CAPEX and OPEX are more favourable to SAB as ore hardness increases.

Dai et al. (2000) studied quartz recovery in the iron ore reverse flotation as a function of particle size. The authors concluded that quartz recovery decreases with increasing particle size due to the tendency for coarse particle detachment in flotation (Fornasiero and Filippov, 2017). This indicates that coarser grinding is detrimental to the performance of the current flotation route, as adopted in industrial operations for itabirite processing (Lima et al., 2020). Also, fine grinding has a negative impact on reverse flotation of iron ores due to high entrainment of the ultrafine hematite particles into the froth (Lima et al., 2012, 2016; Filippov et al., 2021) and due to the low collision probability of fine quartz particles with air bubbles (Fornasiero and Filippov, 2017, Farrokhpay et al., 2021). The desliming removes the portion below 10 μm while the particles larger than 150 μm can be up to 5% to 10% of the feed (Filippov et al., 2014: Lima et al., 2020).

Finkie and Delboni Jr. (2004) demonstrated the effect of particle density on the classification of the feeds in hydrocyclones. Accordingly, the separation size obtained for the higher density mineral (hematite) was ~3.5 times smaller than the separation size obtained for the lower density mineral (quartz). Thus, the application of hydrocyclones leads to finer size distributions for the hematite particles compared with quartz particles. Again, this can have a negative impact on the flotation performance, while increasing the iron losses in the desliming stages (Lima et al., 2020).

It is evident there are many inefficiencies in the conventional circuit used to beneficiate itabirite ores, in particular the fine grinding, desliming, flotation and the need for product thickening. New advances in crushing and grinding, and advances in magnetic

separation and gravity separation were therefore considered. Xiong et al. (2015) investigated the use of the Vertically Pulsating High-Gradient Magnetic Separator – VPHGMS for primary concentration of iron minerals directly after grinding. This approach offered a higher iron recovery, and significant flowsheet simplification by excluding the current desliming stage. Further investigations carried out by Pinto (2019) with VPHGMS achieved a 66% Fe metallurgical recovery and 64% Fe concentrate grade from the slimes-fractions (80% passing 16 µm).

Galvin and co-workers developed an innovative technology known as a Reflux Classifier (Galvin, 2004; 2021), used predominantly in gravity separation. This technology consists of a system of parallel inclined channels above a conventional fluidized bed. The entering feed is conveyed into the system of inclined channels. Here, the denser particles segregate towards the upward facing inclined surfaces and slide downwards, while the lower density particles are conveyed upwards to the overflow. A high shear rate develops within closely spaced channels, which in turn promote inertial lift of relatively large quartz particles. These particles are then conveyed efficiently to the overflow. The high-density particles segregate downwards towards the lower fluidized bed. When the fluidized bed density exceeds the density set point, the concentrate discharges into the underflow stream, in principle at very high pulp density. Amariei et al. (2014) used a Reflux Classifier to beneficiate an iron ore feed finer than 0.15 mm with an Fe grade of only 30%, achieving an Fe recovery of ~81% and Fe grade of 68.4%. With a second finer feed containing 42.6% Fe, they achieved an Fe recovery of ~ 89.6% and concentrate with an Fe grade of 69.8%.

The present work has identified an entirely new process circuit covering the crushing and grinding, and iron ore beneficiation, building on the above developments. In principle, the approach is vastly simpler, more environmentally sustainable, and cost effective than the conventional circuit, hence may have very significant implications globally for the beneficiation of fine iron ore. Following the comminution, a single stage of either gravity separation in a Reflux Classifier or single stage of magnetic separation in combination with a Reflux Classifier could be used to deliver the final concentrate. There would be no need for the initial desliming stage, which usually involves hundreds of cyclones, and there would be no need for flotation chemicals, reverse flotation, or

product thickeners. This is the first investigation of the potential for applying this new circuit, incorporating direct investigations of the iron ore feed using these alternative technologies.

5.3. Circuit Configurations

Figure 32 shows a typical flow sheet of a conventional high capacity itabirite iron ore processing plant in Brazil. As previously discussed, it comprises a multi-staged crushing plant followed by grinding in ball mills and desliming stages, together with concentration carried out by reverse flotation. In some plants magnetic separation is also included in combination with flotation as shown in the same figure. Thickening and filtration are conducted on both concentrate and tailings.

A proposed disruptive circuit aimed at reducing capital expenditure (CAPEX) and operational expenditure (OPEX) is shown in Figure 33. The circuit consists of a crushing step, SAG milling, pre concentration using VPHGMS and final concentration using the Reflux Classifier.

Figure 32. Conventional itabirite iron ore circuit.

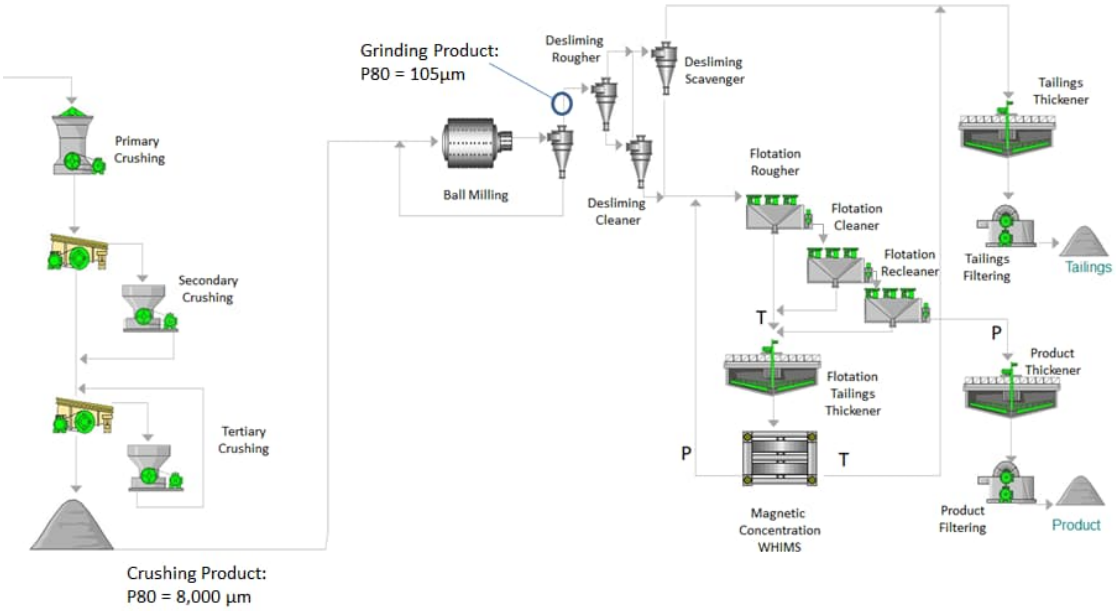

Figure 33. Proposed disruptive itabirite iron ore circuit.

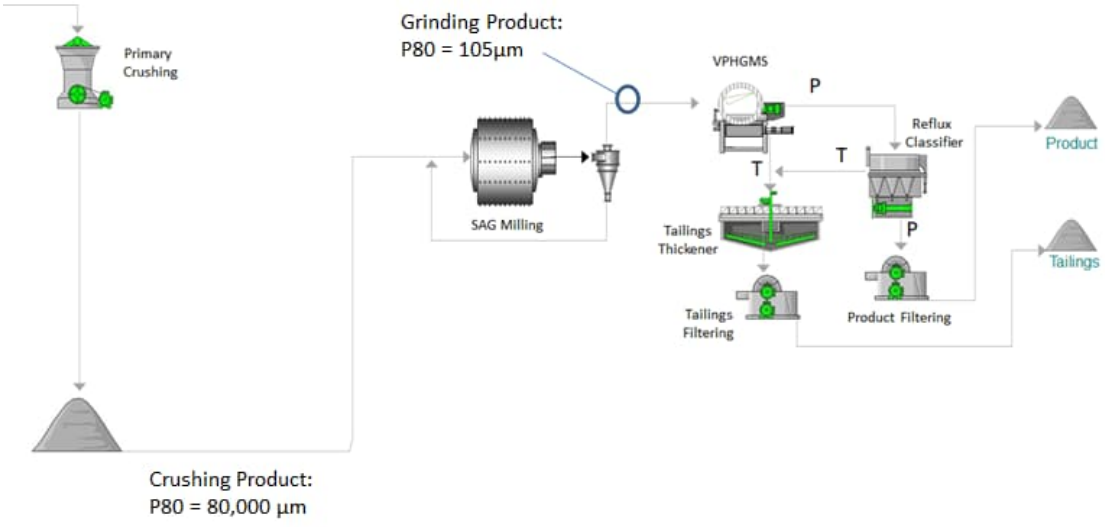

Comparing the two circuits, the disruptive circuit eliminates a series of unit operations such as the secondary and tertiary crushing, desliming, reverse flotation and concentrate thickening, as well as the entire flotation reagent plant. Here, SAG milling replaces secondary and tertiary crushing stages together, which includes not only various crushers and screens, but also handling equipment and devices such as feeders, conveyor belts, silos, chutes, and associated instrumentation. Despite the SAG milling being a well-known comminution technology for most minerals, this has never been used for comminution of itabirite ores. It is worth noting that the comminution proposed is a single stage SAG mill, which works as part of the crushing and ball milling. The combination of the VPHGMS and Reflux Classifier delivers process intensification, reducing the number of stages, as compared with the more conventional rougher, scavenger and cleaner flotation circuits. The new circuit also eliminates the need for the product concentrate thickener.

5.4. Process development

5.4.1. Comminution tests

Itabirite iron ore sample for comminution tests was obtained from a mine of a selected Vale industrial operation located in the Iron Quadrangle state of Minas Gerais, Brazil. Samples containing a total of 625 tons were collected for both bench-scale and pilot plant tests. The former sample was used for assessing energy consumption in ball milling while the latter for determining the SAG milling energy consumption.

Comminution properties were determined according to the Bond ball mill work index (BWi), Bond crushability work index (CWi), JK Drop Weight Tests (DWT) and JK Abrasion test (Napier- Munn et al., 1996). The BWi was determined following the standard test, using a 150 µm sieve as follows:

$$W = 10Wi\,(1/\sqrt{P_{80}} - 1/\sqrt{F_{80}}) \quad (7)$$

where W = specific energy required (kWh/ton), Wi = work index (kWh/ton), and P_{80} is the particle size below which 80% of the product passes.

The DWT consists of dropping a weight under gravity to crush individual particles placed on a steel anvil (Napier-Munn et al., 1996). Important parameters extracted from the DWT include the t_n values, where t is defined as the percentage passing each nth fraction of the original particle size. The value of tn that is most often used is t_{10} which can be described as the percentage passing a screen that is one tenth of the original particle size. The breakage index (t_{10}) is related to the specific comminution energy as follows:

$$t_{10} = A\,(1 - e^{-b\,E_{cs}}) \quad (8)$$

where E_{cs} is the specific comminution energy (kWh/t), t_{10} the percentage passing one tenth of the initial mean particle size tested, and A and b are ore impact breakage parameters. The product A*b is the amenability of the ore to breakage by impact.

SAG milling properties were determined in a comprehensive pilot-scale plant campaign carried out in the Centro de Investigacion Minera y Metalurgica (CIMM) installations in Chile. The circuit includes a 1.83 m diameter by 0.61 m length SAG mill and a spiral classifier, the latter used to close the circuit with the SAG mill. The SAG mill operated with a grate opening of 12-14mm and a trommel aperture of 12mm. Figure 34 shows the circuit configuration. The pulp density of the solids in the feed to the SAG mill was maintained at 78 ± 2% wt%. The test involved 4% of the ball filling and achieved 27% of total filling (balls + ore). Detailed experimental results are fully described elsewhere (Rodrigues, 2014) and by Rodrigues et al. (2021).

Figure 34. Circuit configuration of the pilot single stage SAG mill including the spiral classifier (Rodrigues, 2014)

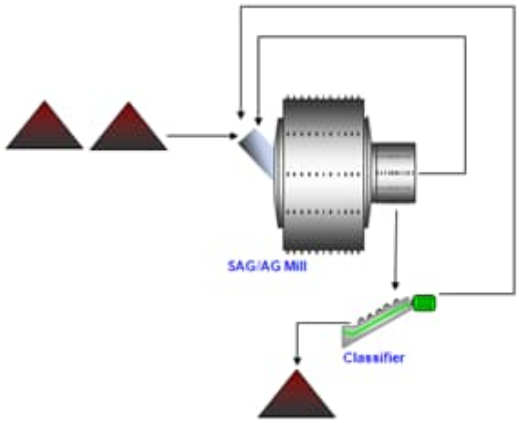

5.4.2. Beneficiation experiments

Approximately 3000 kg of iron ore was sampled at the plant via the cyclone overflow following the grinding circuit, and prior to the desliming. This sample was used for running the magnetic separator and Reflux Classifier experiments in accordance with . It is appreciated that run of mine ore can vary significantly over time (Filippov et al, 2021), thus it was only important that the feed for this work be typical of the run-of-mine operation. Here, the mineralogy of interest is largely binary in nature, consisting of similar portions of well-liberated low-density gangue minerals such as quartz and high-density hematite. The assays obtained for this sample are consistent with typical values from the mine.

Figure 35. Source of feed used for the VPHGMS magnetic separator and the Reflux Classifier.

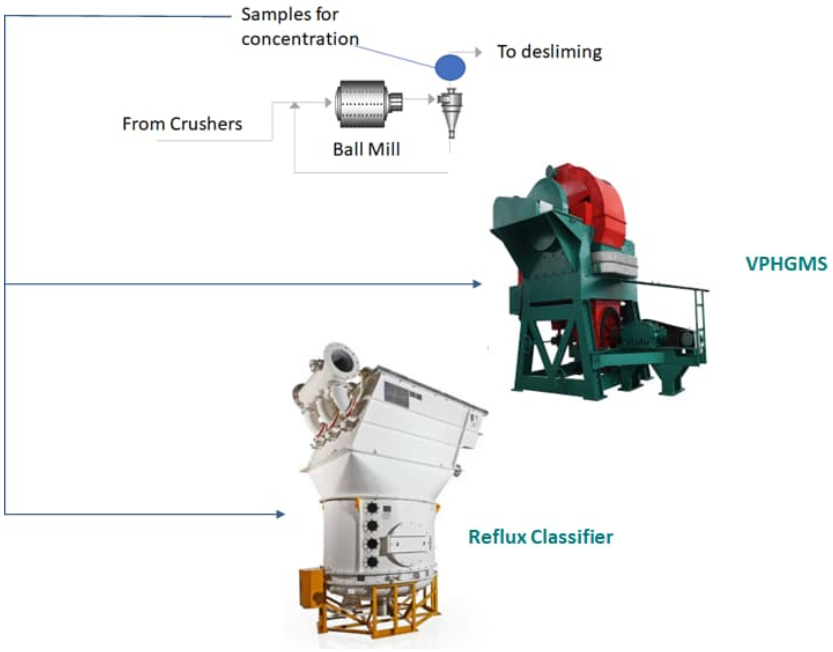

The magnetic concentration properties were determined using pilot-scale VPHGMS 500 mm ring diameter equipment. The conditions are shown in Table 34 and Figure 36 shows a schematic and an image of the VPHGMS separator.

Table 34. Magnetic concentration parameters

Pulsation (per min)	Ring Revolution (rpm)	Magnetic Field (Gauss)	Flowrate (l/h)	Solids (%)
300	1.0	14.000	200	35

Figure 36. Schematic representation of the VPHGMS (a) and image of the pilot-scale VPHGMS separator (b)

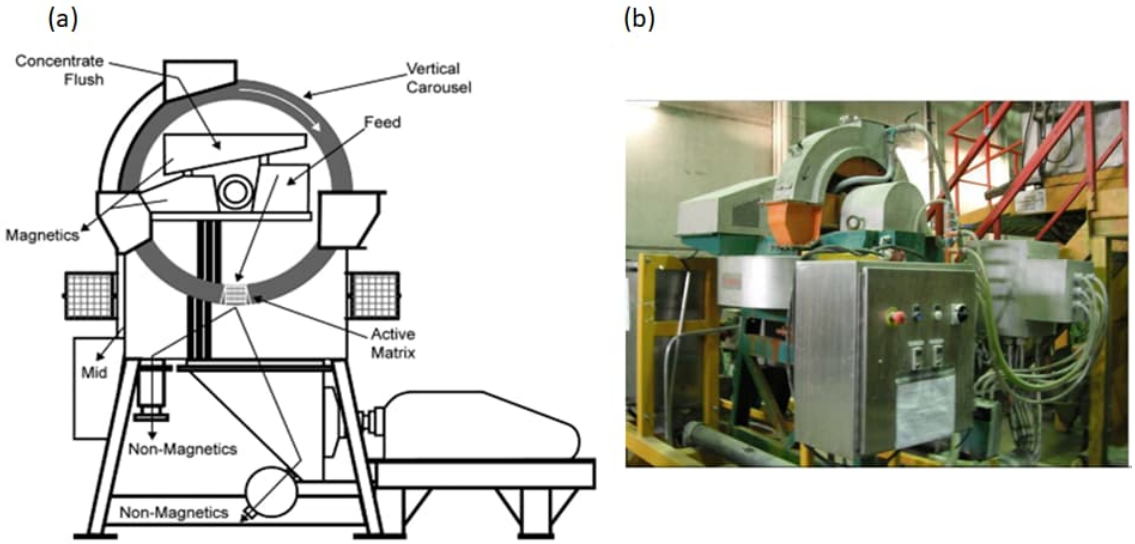

The gravity separation experiments were conducted using a pilot-scale Reflux Classifier shown in Figure 37. The RC100 had a 0.1m x 0.1m cross-section, with a 1 m high vertical section, and 1 m long inclined section containing parallel inclined channels with a close-spacing of 1.8 mm. A supplementary file to this paper describes the considerable care taken in the methodology to minimize errors in the experiments. An error analysis is also provided later in the paper to quantify the uncertainty in the final grades and recovery. The conditions used in the Reflux Classifier experiment are shown in Table 35.

Table 35. Reflux Classifier parameters

Channel (mm)	Feedrate ($t/m^2/h$)	Flowrate (L/h)	Pulp Density (wt %)
1.8	9.5	5.8	24

Figure 37. Schematic representation of the Reflux Classifier (a) and image of the pilot-scale Reflux Classifier (b)

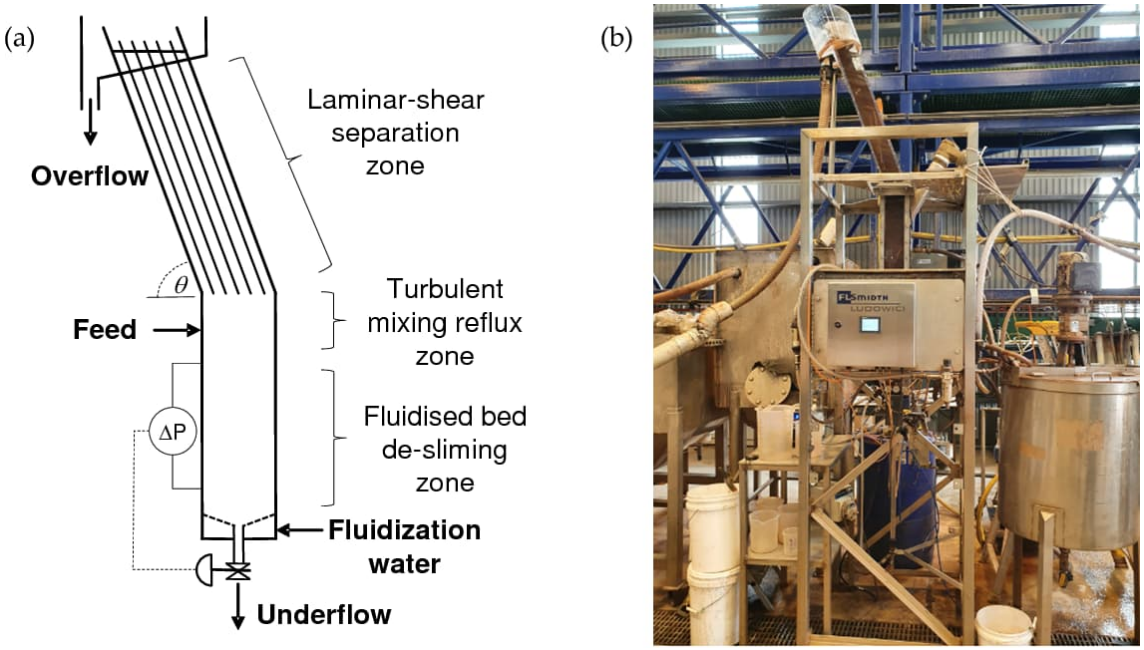

In order to investigate new synergy between the two physical separations, itabirite iron ore concentrate produced from the VPHGMS magnetic separator was also re-processed using the Reflux Classifier to achieve an even higher grade. Approximately 1,500 kg was used for the purpose of assessing the alternative circuit shown in Figure 38. Here the VPHGMS magnetic separator product is fed to the Reflux Classifier. In Run A the feed slurry had a pulp density of 18% solids, and was supplied at a flow rate of 8.8 L/min, corresponding to a solids throughput of 9 t/m^2/h. In Run B, to maximize recovery, the feed rate was reduced to 5.0 L/min, corresponding to a solids throughput of 5.3 t/m^2/h, the set point lowered to 1800 kg/m^3, while the fluidization rate was lowered very slightly. Other conditions are listed in Table 36.

Table 36. Reflux Classifier settings used to re-process the concentrate from the VPHGMS magnetic separator.

Run	Channel (mm)	Solids Flux ($t/m^2/h$)	Flowrate (L/h)	Pulp Density (wt %)	Set Point (kg/m^3)	Fluidization Rate (L/min)
A	1.8	9.0	8.8	18	2100	0.07
B	1.8	5.3	5.0	18	1800	0.06

Figure 38. Re-processing the concentrate from the VPHGMS magnetic separator using the Reflux Classifier.

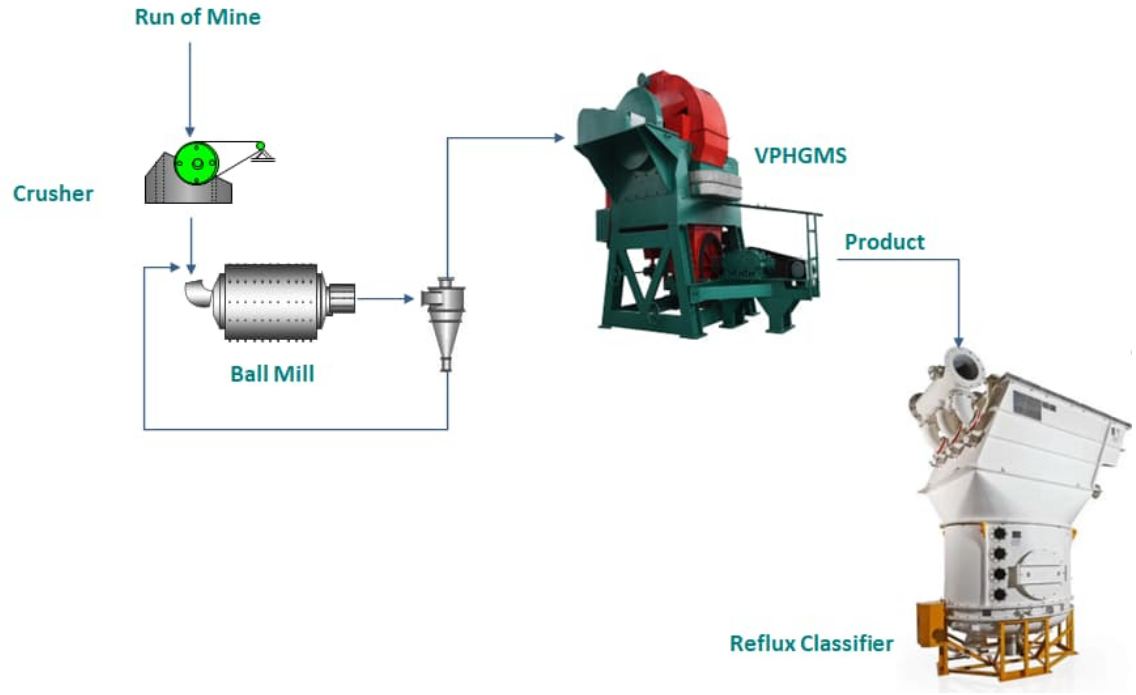

5.5. Results and Discussions

5.5.1. Comminution results

Table 37 shows a summary of the comminution test results. The data have been plotted in the diagram proposed by Bueno and Lane (2011), which originally consisted of sets of A*b (DWT) and BWi from 134 SAG/AG pilot plant samples. Figure 39 compares the original results from that work to the results of the four itabirite samples, showing the itabirite samples are much softer than any of the former.

Table 37. Ball milling test results

JK Abrasion ta	JK DWT			Bond crushing CWi (kWh/t)	Bond Ball mill BWi (kWh/t)*
	A	b	A*b		
3.42	58.8	4.51	265	6.4	6.2

* Calculated for 150 µm

Figure 39. Values of BWi and A*b from 134 tests in pilot-scale AG/SAG mill (Bueno and Lane, 2011)

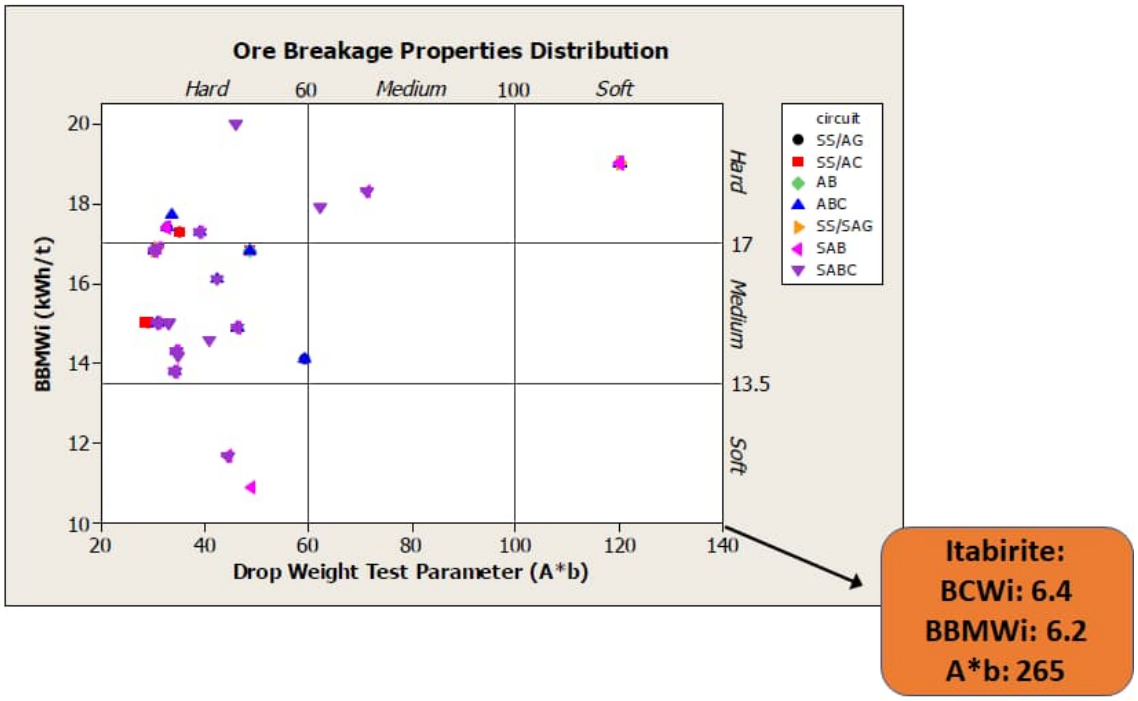

Figure 40 shows the size distributions derived from the pilot SAG mill pilot tests. Table 38 summarizes the mass balance data calculated for the same test. Table 38 also shows an energy consumption of 3.34 kWh/t corresponding to 8.5% retained at 0.15 mm (P_{80} 108µm) in the SAG milling test. Conversely, based on Bond equations and using the Bond crushing CWi and Bond Ball Mill BWi, it is possible to calculate the energy required to achieve the same product as the single stage SAG mill test. Table 39 shows the energy required for the conventional circuit with crushing and ball milling versus the proposed circuit with only a single stage SAG mill. It is evident the single stage SAG mill reduces the energy required for comminution by 41%.

Figure 40. Size distributions resulting from the pilot-SAG test

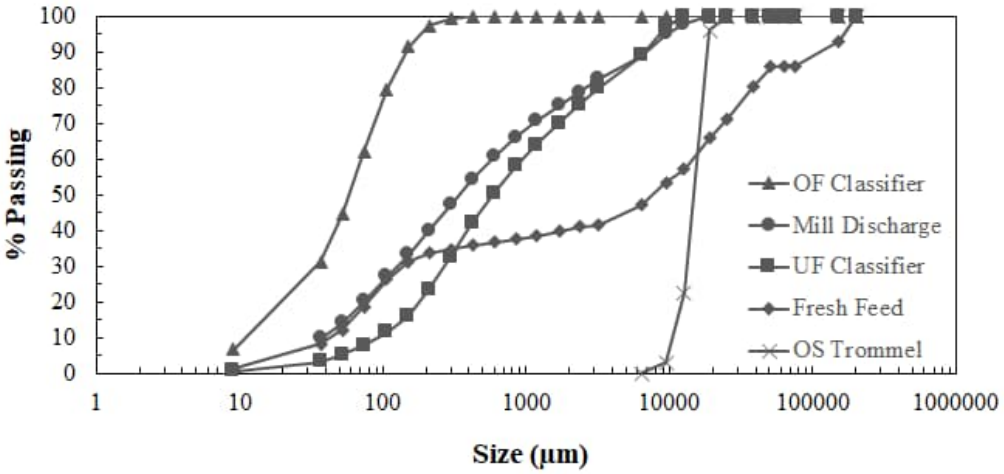

Table 38. Mass balance of the single stage SAG milling pilot test.

Parameter	Fresh Feed	SAG Mill Discharge	Trommel O/S	Classifier U/F	Classifier O/F	Circulating Load	Energy (kWh/t)
Solids flow rate (t/h)	4.13	17.73	0.52	13.08	4.13		
Pulp flow rate (l/h)	1,279	9,732	152	5,778	7,707	316%	3.34
%+0.15 (mm)	68.7	66.8	100	83.9	8.5		
80% Passing (µm)	37,777	2,639	18,103	3,226	108		

Table 39. Energy required crusher + ball mill versus single stage SAG mill.

Circuit	Specific Energy (kWh/t)
Crusher + Ball mill*	5.66 (calculated with BCWi and BBMWi)
Single stage SAG mill	3.34 (obtained from the SAG pilot test)

*Crushing: F_{80}: 37,777 µm; P_{80}: 8,000 µm / Ball Mill: F_{80}: 8,000 µm; P_{80}: 108 µm

5.5.2. Beneficiation experiments

Table 40 and Table 41 provide details on the feed used in the beneficiation experiments, including the assays by size and mineralogy. It is evident the primary components are hematite (56.8%) and quartz (41.4%), ideal for the physical separation. The sample was riffled and sent for beneficiation by VPHGMS magnetic separation and gravity separation using the Reflux Classifier.

Table 40. Assays by size of the samples used in beneficiation experiments.

Size	Retained	Assays (%)								
(µm)	(%)	Fe	SiO_2	P	Al_2O_3	Mn	TiO_2	CaO	MgO	LOI
+210	5.22	2.85	95.17	0.010	0.38	0.019	0.014	0.010	0.063	0.25
-210 +150	9.02	5.45	91.08	0.010	0.22	0.014	0.022	0.010	0.040	0.20
-150 +106	11.09	13.49	79.05	0.010	0.21	0.014	0.016	0.010	0.028	0.12
-106 +75	14.13	32.66	53.15	0.010	0.22	0.017	0.018	0.010	0.049	0.14
-75 +45	13.04	53.00	23.89	0.010	0.23	0.016	0.025	0.010	0.102	0.14
-45	47.50	57.23	17.02	0.011	0.45	0.023	0.036	0.010	0.099	0.24
Global	100.00	40.38	40.28	0.013	0.63	0.038	0.051	0.010	0.038	0.44

Table 41. Mineralogy of the samples used in beneficiation experiments.

Hematite	Quartz	Goethite	Kaolinite	Others	Liberated Quartz
56.76%	41.43%	0.80%	0.09%	0.93%	98.8%

Table 42 shows the overall results obtained using the VPHGMS magnetic separator. Details on the feed assays as a function of the particle size are given in Appendix A. The feed, which had an Fe grade of 42.6%, was concentrated to a final Fe grade of 64.9%. Importantly, the VPHGMS achieved a remarkably low tailings grade of 7.3% Fe, due to its efficiency in rejecting the coarse quartz. The solids yield, based on the three Fe assays, was 61.3% and the Fe recovery 93.4%. Unfortunately, the concentrate grade of 64.9% was less than the target of 67%, the threshold for a premium product suitable for direct reduction.

Table 42. Data obtained for the pilot-VPHGMS test on low grade itabirite ore

Flow	Mass (%)	Fe (%)	SiO_2 (%)	Al_2O_3 (%)	P (%)
Feed	100.0	42.60	37.77	0.71	0.020
Concentrate	61	64.93	6.55	0.43	0.018
Tailings	39	7.28	87.07	0.95	0.026

Table 43 shows the overall results of the experiment conducted using the Reflux Classifier. In this case, the Reflux Classifier achieved the target of 67.1% Fe in the concentrate, but with a lower Fe recovery of 83%. This lower recovery is due to the higher Fe grade of 13.4% in the tailings. The VPHGMS appears to be more effective than the Reflux Classifier in rejecting coarse quartz particles, which is essential for achieving a low tailings grade, while the Reflux Classifier appears to be more effective in upgrading the finer iron ore particles.

Table 43. Data from the Reflux Classifier test on low grade itabirite ore

Flow	Mass (%)	Fe (%)	Iron Recovery (%)
Feed	100.0	39.9	100.0
Concentrate	49.3	67.1	83.0
Tailings	50.7	13.4	17.0

5.5.3. Re-processing VPHGMS Concentrate using the Reflux Classifier

Table 44 shows the results obtained by re-processing the concentrate product from the VPHGMS magnetic separator using the Reflux Classifier. In Run A the Reflux Classifier achieved a very high concentrate grade of 68.5% Fe, however the Fe grade in the tailings was also relatively high at 56.8 % Fe, hence the recovery of the Fe was only 64.5%. The conditions for Run B were adjusted to increase the recovery. Here, the Reflux Classifier achieved a product grade of 66.3% Fe, just below the target grade of 67%, with a remarkably high recovery of 88.9%. These data suggest the target grade can be easily achieved, with a strong recovery. In effect, the VPHGMS provided an efficient method for removing the coarse quartz, while the Reflux Classifier provided an efficient way to deliver the final upgrade. Interestingly, the two-stage process appears to be equivalent to the single stage separation achieved using the Reflux Classifier, with a combined recovery of 0.889x93.4~83%, and a similar Fe grade close to 67%.

Table 44. Re-processing of the concentrate from the magnetic separator using the Reflux Classifier

Run	Feed Grade	Product Grade	Tailings Grade	Solids Yield	Fe Recovery	Fe Recovery Standard Deviation
	(%Fe)	(%Fe)	(%Fe)	(%)	(%)	%
A	63.8	68.5	56.8	60.1	64.5	5.0
B	63.1	66.3	45.5	84.6	88.9	2.4

5.5.4. Error Analysis

The supplementary provided with this paper outlines details of the methodology used to greatly reduce the uncertainty in the experimental data and provides additional information concerning the reproducibility. Detailed data from Run A on the re-processing of the concentrate from the magnetic separator using the Reflux Classifier is provided below, showing the assays as a function of the particle size for the feed, product, and tailings streams. Table 45 shows the balanced data set while Table 46 shows the corresponding raw data set. It is evident the balanced and raw data are very closely aligned, confirming steady state, and a high-quality data set.

The standard deviation of the errors in the assays between the raw and balanced values is only 0.8% of the numerical values, hence the accuracy in the final grades is typically ~+/-0.5%. However, the error in the recovery is governed by the numerical calculation, via the so-called two product formulae. It is well known (Wills and Finch, 2016) the recovery, R, is given by,

$$R = \frac{(G_F - G_T)}{(G_P - G_T)} \frac{G_P}{G_F} \quad (9)$$

where GF, GP, and GT are the Fe grades in the feed, product, and tailings streams respectively. A Monte Carlo analysis was applied to the grade values for Run A with an uncertainty of 0.8% applied to each grade value. A random number generator was used to independently form a probability distribution for each of the grades in Run A, and Equation 9 applied 5000 times to form a probability distribution for the recovery. The standard deviation in the recovery was found to be 8% of the recovery value, corresponding to an absolute error in the recovery of 5%. However, when applied to Run B the standard deviation in the recovery was 2.7% of the value, which is an error in the recovery of 2.4%. This lower error reflects the larger numerical difference between the product and tailings grades in the denominator of Equation 9. Thus, there is high confidence in the potential to reach the target iron grade, with high iron recovery.

Table 45. Balanced data set for re-processing of concentrate from the magnetic separator using the Reflux Classifier.

	Feed		Product		Tailings	
Sieve size (mm)	Mass (%)	Grade (%Fe)	Mass (%)	Grade (%Fe)	Mass (%)	Grade (%Fe)
0.180	0.8	48.4	1.3	52.6	0.2	6.7
0.150	1.1	53.0	1.5	59.8	0.3	5.0
0.125	1.5	52.7	2.2	61.3	0.6	4.4
0.090	6.1	52.6	8.1	64.8	3.1	4.2
0.063	15.4	58.9	21.3	68.6	6.5	10.4
0.045	17.4	65.4	24.4	69.7	6.9	42.5
0.038	5.5	65.9	7.1	69.3	3.0	53.9
0.020	27.7	68.0	26.4	70.0	29.7	65.3
-0.020	24.6	65.1	7.8	68.7	49.8	64.3
Overall	100	63.8	100	68.5	100	56.8

Table 46. Raw data set for re-processing of concentrate from the magnetic separator using the Reflux Classifier.

	Feed		Product		Tailings	
Sieve size (mm)	Mass (%)	Grade (%Fe)	Mass (%)	Grade (%Fe)	Mass (%)	Grade (%Fe)
0.180	1.0	48.7	1.1	52.3	0.2	6.7
0.150	1.2	52.7	1.5	60.1	0.3	5.0
0.125	1.6	52.9	2.0	61.1	0.6	4.3
0.090	6.1	52.9	7.5	64.3	3.3	4.2
0.063	15.2	58.6	21.4	68.4	5.9	10.4
0.045	17.5	65.1	23.5	69.4	6.5	42.5
0.038	4.5	65.4	10.4	69.7	3.1	54.1
0.020	28.5	67.3	24.9	69.8	29.4	65.3
-0.020	24.4	64.4	7.7	68.2	50.6	66.1
Overall	100	64.0	100	68.5	100	56.8

5.6. Project engineering and valuation

This paper has brought together three distinct parts in arriving at a new circuit for processing the low grade itabirite ores. To compare high level economics of both circuits, the two industrial plants were designed to deliver a stipulated pellet feed production of 14.0 Mtpa based on 55% mass recovery. The main equipment list is shown in Table 47. A significant reduction in the equipment inventory for the disruptive circuit is evident for the crushing stage, classification in the grinding and desliming stages, as well as in reverse flotation and thickening.

The new circuit led to an 8% reduction in the total land usage, from 30.3 Hectares to 28.0 Hectares. The new circuit had a 5% lower capital expenditure, however this increased to a 13% lower capital expenditure due to the smaller processing footprint and hence lower civil infrastructure. The disruptive circuit design had an operating cost 42% lower than for the conventional design, primarily due to the reduction in chemical reagents, and grinding media, and a lower energy consumption. This improvement in capital and operating costs led to a 50% increase in the Net Present Value, NPV.

Table 47. Equipment list for the two circuits.

Equipment	Quantity Conventional Circuit	Quantity Disruptive Circuit
Crushing		
Primary Crusher	1	1
Secondary Crusher	2	
Tertiary Crusher	6	
Secondary Screening	2	
Tertiary Screening	6	
Grinding		
Ball Mill (Ø28')	2	
SAG (Ø40')		2
Classification		
Grinding Circuit	40	40
Hydrocyclones in Thickening		
Pellet Feed	18	
Magnetic Product	18	
Magnetic Tailings	44	
Tailings		80
Hydrocyclones in Desliming		
First Stage	32	
Second Stage	80	
Third Stage	768	
Magnetic Concentration		
Magnetic Concentrator	4	
VPHGMS		8
Flotation		
Conditioner	1	
Rougher column	4 x 200m^3	
Cleaner column	6 x 200m^3	
Recleaner column	6 x 200m^3	
Reflux Classifier		
Reflux Classifier		16 x 60m^3
Solid-Liquid Separation		
Pellet Feed Thickener	1	
Tailings Thickener	1	1
Pellet Feed Filtering	12	12
Tailings Filtering	10	10

5.7. Conclusions

The conventional circuit applied to the beneficiation of low grade itabirite ores usually involve multiple stages of crushing and grinding, classification, then desliming, reverse flotation, and product thickening. Considerable process intensification and simplification can be achieved by introducing autogenous forms of crushing and grinding via a SAG mill, and physical beneficiation via VPHGMS magnetic separation and gravity separation in a Reflux Classifier. This study examined a novel and disruptive circuit demonstrating a reduction in energy consumption, and the potential for single stage beneficiation, as well as synergy by combining approaches. It is concluded that high grade iron ore concentrate can be produced for direct reduction in iron and steelmaking, with high recovery and a smaller footprint.

These approaches were combined in an industrial circuit flowsheet and compared with conventional itabirite iron ore processing, as currently carried out by Vale. The results indicated significant reduction in equipment, with the CAPEX and OPEX reductions 5% and 42%. respectively. The NPV calculated for the disruptive circuit was 50% higher than for the conventional circuit.

5.8. APPENDIX A

Table 48 shows the assays as a function of the particle size in the feed to the VPHGMS magnetic separator. SiO_2 grade decreases from coarse to fine size fractions, while the opposite is observed for Fe grades.

Table 48. Assays by size of the feed to the pilot-VPHGMS magnetic separator

Size	Retained	Passing	Assays (%)				
(mm)	(%)	(%)	Fe	SiO_2	P	Al2O3	LOI
0.210	3.10	96.90	4.50	92.99	0.010	0.41	0.10
0.150	7.78	89.12	6.01	89.81	0.012	0.24	0.26
0.106	9.21	79.92	14.38	79.19	0.010	0.21	0.11
0.075	13.47	66.44	32.61	52.89	0.010	0.22	0.16
0.045	21.59	44.85	50.62	27.63	0.012	0.22	0.12
0.037	5.58	39.28					
0.025	10.94	28.34					
0.015	10.53	17.80	56.51	16.77	0.032	1.29	0.70
0.010	5.45	12.35					
-0.010	12.35	0					
Overall	100		42.60	37.77	0.020	0.71	0.39

Figure 41 shows the size distributions from the VPHGMS pilot test. The removal of the coarse quartz from the feed leads to a much finer concentrate.

Figure 41. Size distributions from the pilot-VPHGMS test

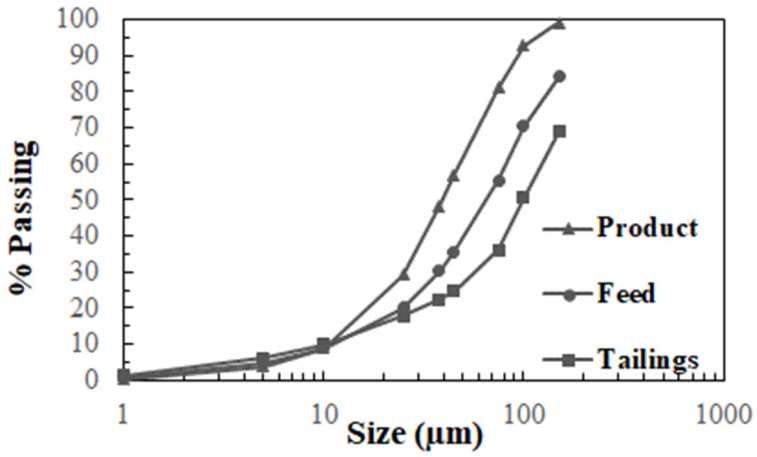

Table 49 shows the assays by size for the feed to the Reflux Classifier. Again, the SiO_2 grades decrease from coarse to fine size fractions while the reverse is evident for the Fe grades.

Table 49. Assays by size for the feed to the pilot-Reflux Classifier test.

Size (mm)	Retained (%)	Passing (%)	Fe (%)
0.250	1.4	98.6	1.51
0.180	4.5	94.2	2.36
0.150	5.2	88.9	4.72
0.125	4.2	84.7	8.88
0.090	12.8	71.9	20.70
0.063	20.0	51.9	45.78
0.045	17.0	34.9	57.82
0.038	5.3	29.6	59.00
0.020	12.1	17.5	60.13
-0.020	17.5	0.0	49.98
Overall			39.90

Figure 42 shows the particle size distributions for the three process streams of the Reflux Classifier. Again, the product concentrate is much finer than the feed, however the concentrate contains less of the ultrafines.

Figure 42. Size distributions of the three process streams of the pilot scale Reflux Classifier

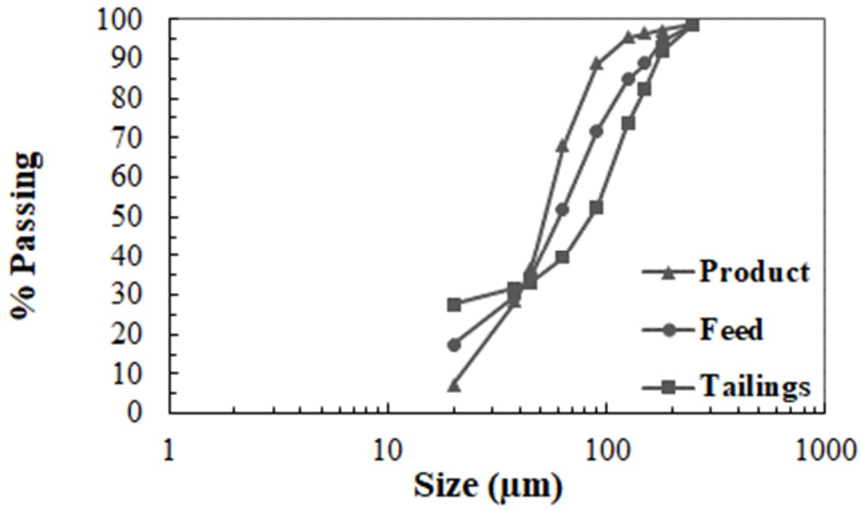

6. GENERAL CONCLUSIONS

The conventional circuit currently used for the beneficiation of low grade itabirite ores usually involves multiple stages of crushing and grinding, classification, desliming, reverse flotation, and product thickening. Considerable process intensification and simplification can be achieved by introducing autogenous forms of crushing and grinding via a SAG/AG mill, as well as physical beneficiation via VPHGMS magnetic separation and gravity separation in a Reflux Classifier. This study examined a novel and disruptive circuit demonstrating a reduction in energy consumption, and the potential for single stage beneficiation, as well as synergy by combining approaches. It is concluded that high grade iron ore concentrate can be produced for direct reduction in iron and steelmaking using this novel circuit configuration, with high recovery and a smaller footprint.

The results of the comminution pilot test study showed that AG/SAG milling is technically feasible and generally an attractive alternative from the standpoint of energy efficiency, for grinding of itabirites. The closed single-stage tests circuit were the most attractive in terms of grinding efficiency. However, it is highly recommended care is taken on mill discharge design in order to avoid slurry pooling.

This work showed the clear potential of the Reflux Classifier gravity separator to replace reverse flotation, resulting in a significant reduction in the complexity, cost, and environmental impact of the beneficiation circuit. The best overall results were obtained by increasing the volumetric feed rate to 8 L/min, 9t/m^2/h and lowering the feed pulp density to 17 wt% solids.

The deduction of the underlying partition surface from relatively basic feed information on the Fe assays obtained as a function of the particle size provided confidence in the application of the partition surface to predict similar dense mineral separations, and stronger insights into the mechanisms responsible for the separation.

The tests of re-processing the concentrate product from the VPHGMS magnetic separator using gravity separation in Reflux Classifier achieved a very high concentrate grade of 68.5% Fe. It was shown that the VPHGMS provides an efficient method for removing the coarse quartz and generate tailings with very low iron grade, while the Reflux Classifier provided an efficient way to deliver the final upgrade. These approaches were combined in a novel industrial circuit flowsheet as compared with conventional itabirite iron ore processing. The results indicated significant reduction in equipment, with the CAPEX and OPEX reductions and 8% smaller footprint.

7. REFERENCES

Amariei, D., Michaud, D., Paquet, G., and Linday, M., 2014. The Use of the Reflux Classifier for Iron Ores: Assessment of Fine Particles Recovery at Pilot Scale. Minerals Engineering, 62, 66-73.

Araujo, A.C., Viana, P.R.M., Peres, A.E.C., 2005. Reagents in iron ores flotation. Miner. Eng., 18, 219-224, 10.1016/j.mineng.2004.08.023.

Ballantyne, G.R., Peukert, W., Powell, M.S., 2015, Size specific energy (SSE) – Energy required to generate minus 75 micron material, Int. J. Miner. Process. 136, 2-6, http://dx.doi.org/10.1016/j.minpro.2014.09.010.

Bradshaw, D.J., 2014. The role of 'process mineralogy' in improving the process performance of complex sulphide ores, Keynote Paper, proc. XXVII Int. Min. Proc. Conf., Santiago, Chile, October 2014.

Bueno, M., Lane, G. 2011, A review of 10 years of AG/SAG pilot trials, Proc. 5th Int. Conf. on Semi-Autogenous and High-Pressure Grinding Technology, Canadian Institute of Mining and Metallurgy (CIM), Vancouver, BC, Canada, pp. 1-16.

Bueno, M., Niva, E., Powell, M.S., Adolfsson, G, Kojovic, T., Henriksson, M., Worth, J., Partapuoli, Å., Wikström, P., Shi, F., Tano, K., Fredriksson, A., 2011a. The dominance of the competent, Proc. 5th Int. Conf. on Semi-Autogenous and High-Pressure Grinding Technology, Canadian Institute of Mining and Metallurgy (CIM), Vancouver, BC, Canada, pp. 1-12.

Bueno, M. Powell, M.S., Kojovic, T, Shi, F. Sweet, J., Philips, D., Durant, B., Plint, N., 2011b. Multi-component autogenous pilot trials, Proc. 5th Int. Conf. on Semi-Autogenous and High-Pressure Grinding Technology, Canadian Institute of Mining and Metallurgy (CIM), Vancouver, BC, Canada.

Bueno, M.P., Kojovic, T., Powell, M.S., Shi, F., 2012, Multi-Component AG/SAG Mill Model, Miner. Eng. 43–44, 12–21, http://dx.doi.org/10.1016/j.mineng.2012.06.011.

Carpenter, J.L., Zhou, J., Iveson, S.M., Galvin, K.P., 2019. Gravity separation in the Reflux Classifier in the presence of slimes, 143, 105941.

Collins, A. R., 2016. Classification of Multi-Component Feeds in a Hydrocyclone. 179 pp. Thesis (PhD) – The University of Queensland, Australia.

Crompton, L. J., Islam, M. T., and Galvin, K. P., 2022. Investigation of Internal Classification in Coarse Particle Flotation of Chalcopyrite Using the CoarseAIR^{TM}. Minerals, 12(6). doi:10.3390/min12060783

Dahe, X., 2003. Slon magnetic separator applied to upgrading the iron concentrate. Physical Separation in Science and Engineering. 12(2), 63–69

Dai. Z., Fornaziero, D., Ralston, J., 2000. Particle-bubble collision models – a review. In: Advances in Colloid and Interface Science.

Farrokhpay, S., Filippov, L., Fornasiero, D., 2021 Flotation of fine farticles: A review. Mineral Processing and Extractive Metallurgy Review, 42 (7), 473-483. doi.org/10.1080/08827508.2020.1793140

Filippov, L.O., Severov, V., Filippova, I.V., 2014. An overview of the beneficiation of iron ores via reverse cationic flotation. Int. J. Miner. Process. 127, 62–69. doi:10.1016/j.minpro.2014.01.002.

Filippov, LO., Silva, K., Piçarra, A., Lima, N., Santos, I., Bicalho, L., IV Filippova, Peres, A., 2021. Iron ore slimes flotation tests using column and amidoamine collector without depressant. Minerals 11 (7). 699

Finkie, R. L., Delboni, Junior, H., 2004. Influência da densidade das partículas no desempenho de ciclone - estudo de caso. In: Encontro Nacional de Tratamento de Minérios e Metalurgia Extrativa. 20. Florianópolis. SC. Anais do 20. Entmme. Criciúma: Desktop Publishing/UNESC. 2004. v. 2. p. 193-200.

Fornasiero, D. and Filippov, L. O., 2017. Innovations in the flotation of fine and coarse particles. Journal of Physics: Conference Series. 879. 012002. doi :10.1088/1742-6596/879/1/012002.

França, J.R.O., Barrios, G.K.P., H.D.G. Turrer, L.M. Tavares, 2020. Comminution and liberation response of iron ore types in a low-grade deposit, Miner. Eng. 158, 106590.

Galvin, K.P., Compton, T., Firth, B.A., 1995. Quantification of the data improvement produced by optimised metallurgical plant mass balances. Miner. Eng. 8 (7), 739–752. https://doi.org/10.1016/0892-6875(95)00036-P.

Galvin, K.P., 2004. A Reflux Classifier. The University of Newcastle Research Associates Limited. United States Patent No. 6814241

Galvin, K. P., and Liu, H., 2011. Role of inertial lift in elutriating particles according to their density. Chemical Engineering Science, 66(16), 3687-3691. doi:10.1016/j.ces.2011.05.002

Galvin, K.P., Iveson, S.M., Zhou, J., Lowes, C.P., 2020. Influence of Inclined Channel Spacing on Dense Mineral Partition in a Reflux Classifier. Part I: Continuous Steady State 146 106112

Galvin. K.P., 2021. Process Intensification in the Separation of Fine Minerals. Chemical Engineering Science. 231. 116293

Galvin, K.P., and Iveson, S., 2022. New Challenges for Gravity Concentration and Classification of Fine Particles, Minerals Engineering, 190, 107888.

Gupta, A., Yan, D., 2016, Autogenous and semi-autogenous mills. In: Mineral Processing Design and Operations, 2nd ed., Elsevier, pp. 263-285, https://doi.org/10.1016/B978-0-444-63589-1.00009-5.

Hagemann, S.G., Angerer, T., Duuring, P., Rosière, C.A., Silva, R.C.F., Lobato, L., Hensler, A.S., Walde, D.H.G., 2016. BIF-hosted iron mineral system: A review, Ore Geology Reviews 76, 317-359.
http://dx.doi.org/10.1016/j.oregeorev.2015.11.004

Holappa, L., A General Vision for Reduction of Energy Consumption and CO2 Emissions from the Steel Industry, Metals 2020, 10(9), 1117; https://doi.org/10.3390/met10091117

King, M.R., Leighton, D.T., 1997. Measurement of the inertial lift on a moving sphere in contact with a plane wall in shear flow. Phys. Fluids 9 (5), 1248–1255.

Lima, N.P., Peres, A. E. C., Marques, M. L. S., 2012. Effect of slimes on iron ores flotation. Int. J. Min. Eng. Miner. Process, 1. 43–46

Lima, N. P., Rodrigues, A., Pinto, P. F., Delboni Jr. H., 2013. Comminution routes for poor itabirites from the iron quadrangle In: Simposio Brasileiro De Minerio De Ferro. 14.. 2013. São Paulo. Anais. São Paulo: ABM. 2013. 1 CD-ROM.

Lima, N., P. Pinto, T. C. S., Tavares, A. C., Sweet, J., 2016. The entrainment effect on the performance of iron ore reverse flotation. Minerals Engineering 96-97, 53-58, 2016.

Lima, N.P., Silva, K., Souza. T., Filippov, L., 2020. The characteristics of iron ore slimes and their influence on the flotation process. Minerals, 10(8). 675; https://doi.org/10.3390/min10080675

Moritomi, H., Iwase, T., Chiba, T., 1982. A comprehensive interpretation of solid layer inversion in liquid fluidized beds. *Chem*. *Engng Sci*., *37*(12), 1751Ð1757.

Moritomi, H., Yamagishi, T., Chiba, T., 1986. Prediction of complete mixing of liquid-fluidized binary solid particles. *Chem*. *Engng Sci*., *41*(2), 297Ð305.

Morris, A.E., 2001. Encyclopedia of Materials: Science and Technology.

Morrell, S., 2004, A new autogenous and semi-autogenous mill model for scale-up, design and optimisation, Miner. Eng. 17, 547-445.
https://doi.org/10.1016/j.mineng.2003.10.013

Napier-Munn, T.J., Morrel, S., Morrison, R.D., Kojovic, T., 1996. Mineral Comminution Circuits: Their Operation and Optimization, Julius Kruttschnitt Mineral Research Centre, Brisbane, Australia.

Padhi, M., Mangododdy, N., Sreenivas, T., Vakamalla, T. R., Mainza, A. N., 2019. Study on Multi-Component Particle Behaviour in a Hydrocyclone Classifier Using Experimental and Computational Fluid Dynamics Techniques, Separation and Purification Technology, 229, 115698.

Pinto, P. H. F., 2019. Aproveitamento de lamas de minério de ferro do Quadrilátero Ferrífero por concentração magnética de alta intensidade de campo magnético. 225 p. Thesis (PhD). Universidade de São Paulo. São Paulo.

Powell, M.S., Mainza, A.N., Hilden, M., Yahyaei, M., 2015. Full pre-crush to SAG mills – the case for changing this practice, Proc. 6th Int. Conf. on Semi-Autogenous and High-Pressure Grinding Technology, Canadian Institute of Mining and Metallurgy (CIM), Vancouver, BC, Canada.

Powell, M.S., Bozbay, C., Kanchibotla, S., Bonfils, B., Musuniri, A., Jokovic, V., Hilden, M., Young, J., Yalcin, E., 2019. Advanced mine-to-mill used to unlock SABC capacity at the Barrick Cortez mine, Proc. 7th Int. Autogenous and Semi-Autogenous Grinding and High Pressure Grinding Roll Technology, Canadian Institute of Mining and Metallurgy, Vancouver, BC, Canada.

Rodrigues, A.F.d.V., 2014, Grinding of Itabirite Iron Ore in Autogenous and Semi-Autogenous Mills, MPhil thesis, University of Queensland, Australia.
https://doi.org/10.14264/uql.2014.250

Rodrigues, A.F.d.V., Delboni Jr., H., Powell, M. S., Tavares, L. M., 2021. Comparing strategies for grinding itabirite iron ores in autogenous and semi-autogenous pilot-scale mills. Miner. Eng. 163. 106780.
https://doi.org/10.1016/j.mineng.2021.106780

Rodrigues, A.F.d.V., Delboni, H. Jr., Rodrigues, O.M.S, Zhou, J., Galvin, P.K., 2023. Gravity separation of fine itabirite iron ore using the Reflux Classifier – Part I – Investigation of continuous steady state separations across a wide range of parameters. Minerals Engineering, 201. 108187. https://doi.org/10.1016/j.mineng.2023.108187

Scott, I. A., and Napier-Munn, T. J., 1992. A dense medium cyclone model based on the pivot phenomenon. Trans. Inst. Min. Met., C61-C76.

Segura-Salazar, J., Souza, N., Tavares, L.M., 2018, A holistic pre-feasibility study of comminution routes for a low-grade Brazilian iron ore. Proc. 11th Int. Comminution Symp., MEI International, Cape Town, p. 1-11.

Siddal, B., Henderson, G., Putland, B., 1996. Factors influencing sizing of mills from drillcore samples, Proc. 2nd Int. Conf. Autogenous and Semi-Autogenous Technology, Vancouver, UBC, p. 463-480.

Siddal, B., Putland, B., 2007. Process design and implementation techniques for secondary crushing to increase milling capacity. SME Annual Meeting. Feb. 25-Feb. 28, 2007, Denver, CO, USA.

Starrett, J., and Galvin, K.P., 2023. Application of Inclined Channels in the Hydrodynamic Classification of Minerals by Particle Size, Minerals Engineering, 195, 108002
https://doi.org/10.1016/j.mineng.2023.108002

Tavares, L.M., da Silveira, M.A.W., 2008. Comparison of measures of rock crushability. Fine Particle Technology and Characterization (M. Yekeler, Ed.), Research Signpost, pp. 1-20.

Wills, B. A., and Finch, J. A., 2016. Wills' Mineral Processing: An Introduction to the Practical Aspects of Ore Treatment and Mineral Recovery (8th ed.). Elsevier. doi:10.1016/C2010-0-65478-2.

Xiong, D., Lu, L., Holmes R, J., 2015. Developments in the physical separation of iron ore: magnetic separation. In: Lu. L. Iron Ore. Elsevier. p. 283-307.